Report To Regional Response Team
Coastal Region II
Third Coast Guard District

A Climatological Oil Spill Planning Guide

No.1 The New York Bight

February 1980

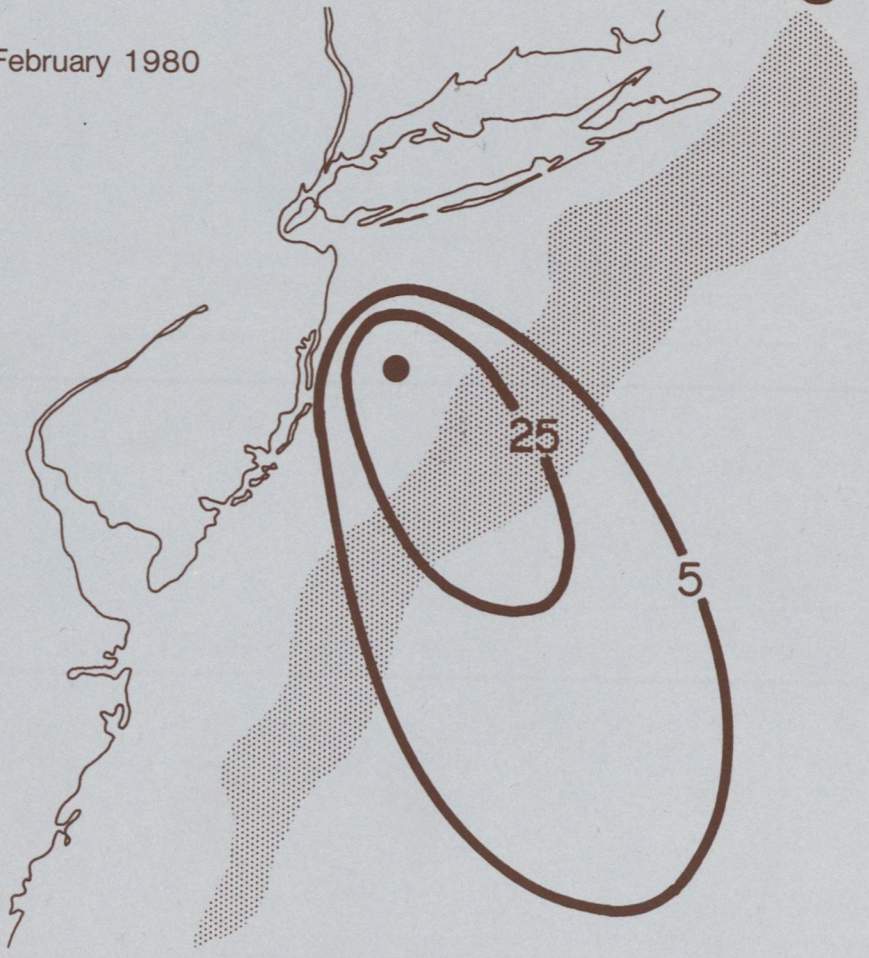

U.S. DEPARTMENT OF COMMERCE
National Oceanic and Atmospheric Administration
Environmental Data and Information Service

Report To Regional Response Team
Coastal Region II
Third Coast Guard District

A Climatological Oil Spill Planning Guide

No.1 The New York Bight

Compiled by: Joseph M. Bishop
Center for Environmental Assessment Services
Marine Environmental Assessment Division

Washington, D.C.
February 1980

U.S. DEPARTMENT OF COMMERCE
Philip M. Klutznick, Secretary

National Oceanic and Atmospheric Administration
Richard A. Frank, Administrator

Environmental Data and Information Service
Thomas D. Potter, Director

CONTENTS

1. INTRODUCTION

Oil spills are a major concern associated with both offshore oil production and movement of oil through the Mid-Atlantic Bight area. This report summarizes appropriate environmental data, discusses the movement of oil at sea, and attempts to predict the effects of oil spills for the New York Bight, a region lying between Montauk Point, N.Y., and Cape May, N.J. The concept that a report of this type should be available was initially developed during the grounding of the Argo Merchant. At that time, and even to the present, there is no source of key environmental data available related to oil spills for regional response planning. The objective of this study is to provide this information in a format that can be both understood and used by decision makers for oil spill contingency planning and for scientific support personnel during spills.

2. FATE OF OIL AT SEA

2.1 Introduction

Environmental factors determine the fate of oil spilled at sea. Initially, the oil starts to spread. This process is at first rapid but slows (except for some oil fractions) until after some hours a slick of semi-solid consistency is formed. Wind and waves tend to break up the slick into patches. These patches are eventually advected and diffused from the spill site. In general, the primary factors concerning oil fate, as illustrated in figure 1, are:

Spreading
Advection
Turbulent diffusion
Emulsion formation
Photochemical oxidation
Solution and dispersion
Microbiological action
Evaporation

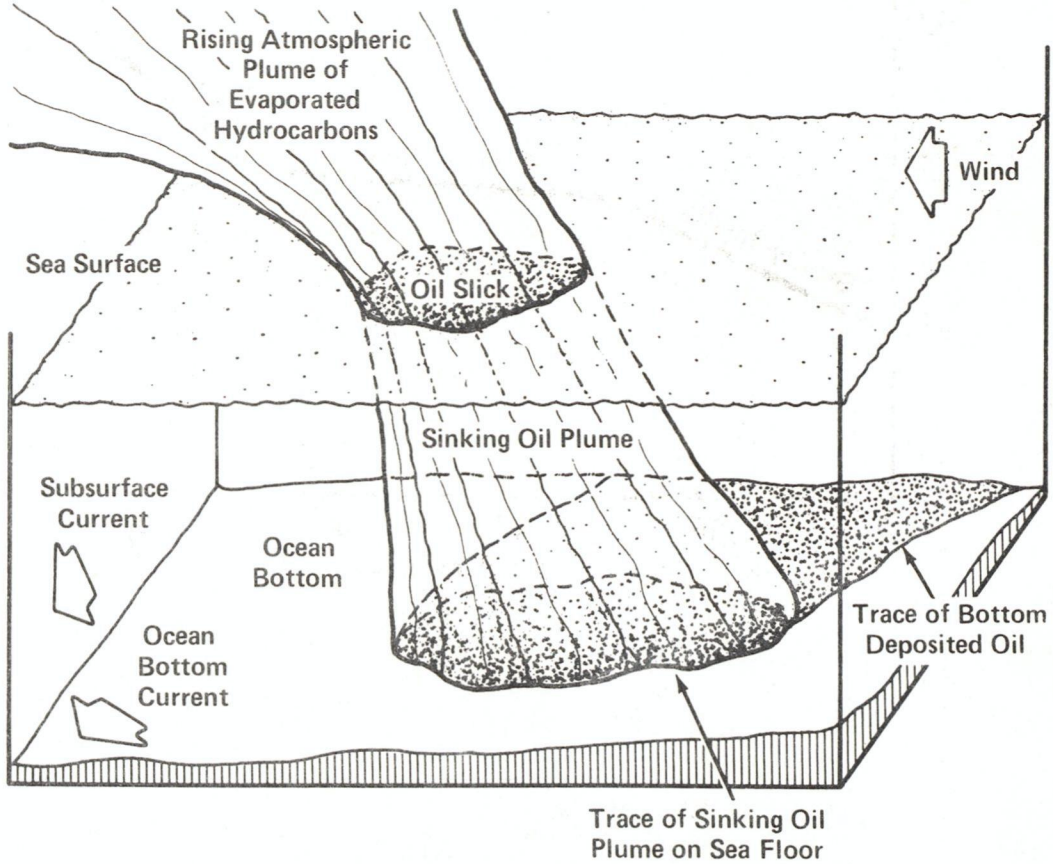

Figure 1. --Block diagram showing the fate of an oil slick (after Kolpack and Plutchak, 1976)

2.2 Spreading

Attempts to describe theoretically the spreading of an oil slick have been simple and are generally considered to be of limited practical value for use at sea. The commonly used Fay (1969) Theory states that oil spreads in three stages as shown in figure 2. This type of information might be useful in helping one make a decision on the amount of clean up resources required by giving estimates of spill size.

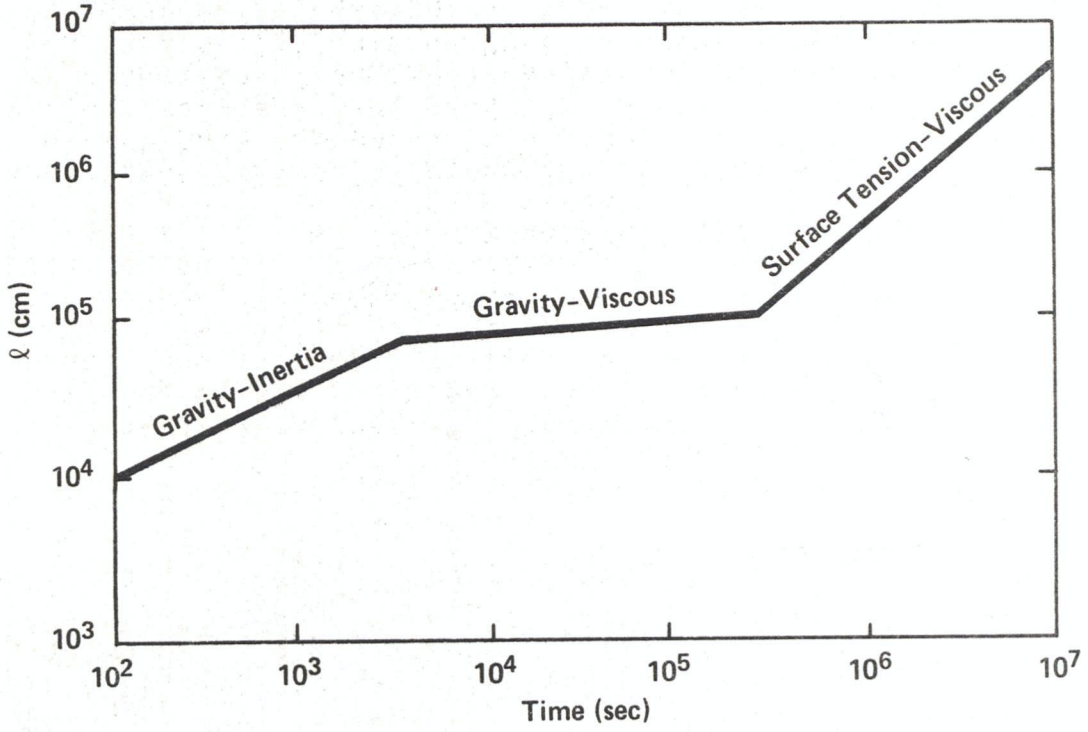

Figure 2.--The size (diameter) of an oil slick as a function of time for a 10,000 ton spill (after Fay, 1969)

2.3 Advection

The steady or residual movement of an oil slick is critical. To determine this advection one must first consider the appropriate averaging interval, because currents that occur at intervals equal to or less than that time may cause either no net movement (if they are periodic) or a diffusive effect (if they are random). In general, for oil spill advection estimates one usually uses the currents as depicted in an available atlas that have been averaged for periods on the order of a month for many years of observations. For this interval tidal currents are periodic and transient wind-driven currents have strong random nonadvective components. One must be careful here in that if the oil is, for example, near the coast both the tidal current and/or "random" wind-drift may drive the oil slicks on shore over a shorter than advective time scale.

2.4 Turbulent Diffusion

Under favorable environmental conditions oil slicks tend to break up into patches. These patches are generally advected with the mean current but they are also subjected to random eddies in the current field which spread the patches over a large area. The rate of lateral spreading of these patches can be roughly estimated using figure 3 over various time and space scales.

2.5 Emulsion Formation

In a short time after the spill the heavier fractions at times take on a highly viscous consistency caused by the formation of a water-in-oil emulsion termed "mousse" because of its color and consistency. In this form oil may persist for months and be advected to distant shorelines. An oil-in-water emulsion can also exist with the oil in suspension.

2.6 Photochemical Oxidation

The less volatile fractions of oil are hydrocarbons whose solubility in water is slight. Under the influence of sunlight, however, these fractions can react with atmospheric oxygen to produce more soluble compounds. This effect is small and could only become important when oil is spread in a thin film over a large area. Thus, photochemical oxidation may become a factor in breaking down slicks a few microns thick.

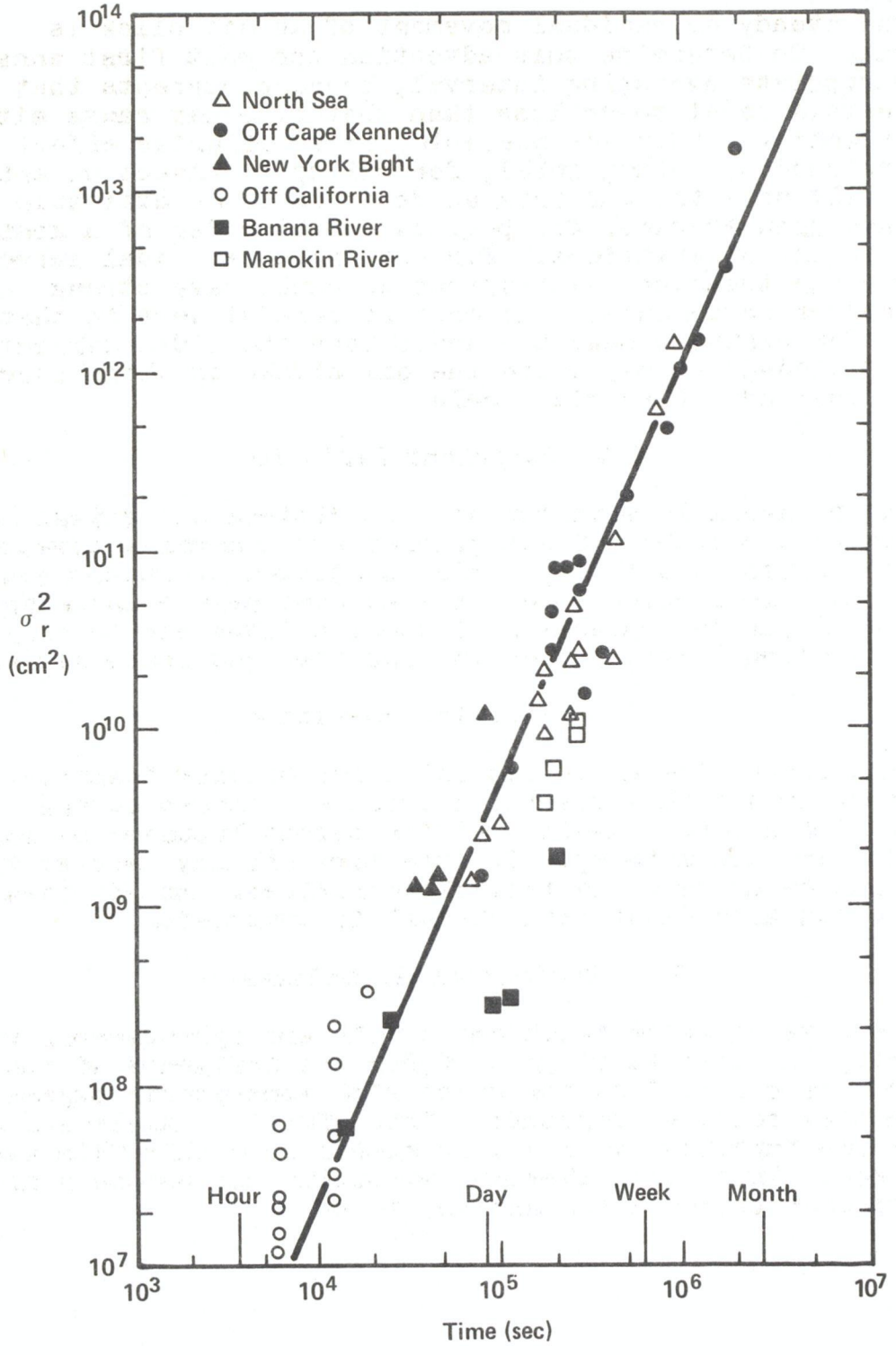

Figure 3.--Surface dye patch size, σ_r^2, as a function of time (after Okubo, 1962)

2.7 Solution and Dispersion

A certain amount of the oil slick may actually pass into solution in seawater. Although most probably a small effect, it may constitute a pollution hazard because this is the easiest state for interaction with marine organisms. Solubility decreases rapidly with molecular weight and is usually small when compared to the amount of oil dispersed as fine droplets. Dispersion and solubility are processes that move oil from the slick to the water column. Sea state (wave height) is the most important environmental parameter governing dispersion. This process could lead to concentrations of oil of 10 ppm to depths of a few meters below a slick. Dispersed oil can easily be ingested by marine organisms.

2.8 Microbiological Action

Many species of bacteria, molds, and yeasts, capable of attaching oil, exist in seawater. These organisms are more numerous in coastal waters. They use the hydrocarbons as an energy source, but their activity depends on a plentiful supply of nutrients. Under the most favorable conditions it seems that a period of months is required to remove a large portion of a slick.

2.9 Evaporation

A surface oil slick will lose mass due to surface evaporation (vaporation). The amount of loss is directly related to the carbon number of the oil fraction in question. It also depends on environmental factors such as wind speed and the amount of wind-wave whitecapping. For the slick as a whole, evaporation rates decline with time. Evaporation is usually predicted using the single step approach in which the evaporated fraction of the slick is removed as a step function.

2.10 Oil Spill Modeling

Knowledge of the movement of a surface oil slick is important to give warning of possible shoreline pollution and application of clean-up counter measures. Oil spill modeling techniques have been developed to predict the movement of an oil spill under actual or hypothetical conditions. Some of the commonly used modeling techniques include:

Oil fate models
Oil fate and effect models
Single event models
Climatological models
Risk assessment models

2.10.1 Oil Fate Models

The oil fate model is used to estimate the concentration, distribution, and residence time of various fractions of oil into various environmental sinks. An attempt is made to trace the pathways that oil takes as it comes into contact with the biota. The resulting computer calculations include all known processes and parameters and their variable reaction rates. This approach is probably the most advanced scientifically, but because of the detailed environmental data inputs required, has limited operational use.

2.10.2 Oil Fate and Effects Models

The oil fate and effect model is similar to the fate model. It extends this type of calculation by using the output of a fate model as input to a biological effect model. It also requires detailed environmental data but, in general, is less sophisticated in its physical and chemical parameterizations than the fate model. This is a useful research tool but to date is also not considered to be an operational tool that can be used under actual spill conditions.

2.10.3 Single Event Models

The single event model is probably the best tool decision makers have at their disposal for an actual spill, providing that limited environmental data is available to a modeling support group. It generally attempts to incorporate the most important physical processes such as advection, diffusion, and spreading. This type of model attempts to calculate future locations of oil based on input parameters such as wind conditions and the ambient current patterns, but it is limited by data inputs and thus calculated trajectories are only as good as the sometimes questionable inputs.

2.10.4 Climatological Models

The climatological modeling technique is based on archived environmental data. It uses first order calculations of currents to estimate oil advection. Usually advection is dominant over other environmental factors and thus results have been useful in such spills as that of the Argo Merchant. The "permanent" current (derived from available atlas presentations) and a transient wind-driven current (derived from local wind records using the 3 percent rule) are added to produce a trajectory. The trajectory is tracted in 3-hour intervals using a computer simulation from the hypothetical spill site. Additional trajectories are traced until relative risk diagrams can be drawn that indicate the major direction of oil movement and its spread

around this axis. The advantage of this calculation is that it can be done calmly before the spill occurs and kept available in, for example, an atlas for a specific location. The disadvantage is that it is an approximation under actual conditions that is only as good as the simple model assumptions. Also, this type of model is limited by the assumption that conditions at spill time are close to the climatological mean. This last approximation may not be a poor one if the distance to an impact point is large.

In section 3.11, relative risk diagrams are presented for the New York Bight using a climatological computer simulation as explained in Bishop (1976). These relative risk diagrams for summer and winter are considered appropriate for all regions in the New York Bight. The relative risk charts are moved to the position of the hypothetical spill and adjusted to the mean advection current axis. In this manner, one can estimate the relative risk of various regions to impact.

2.10.5 Risk Assessment Models

A risk assessment model combines the trajectory of oil movement with its biological and economic impact to arrive at a decision on the possible deployment of the available limited resources to reduce damage. It also can be used before the fact to make decisions about locating oil facilities.

Summer and winter risk assessment charts for the New York Bight were constructed by overlaying resource charts with the climatological relative risk diagrams (fig. 57-105). In general, winter spills tend seaward and possibly endanger offshore fishing resources, while summer spills tend to impact the south shore of Long Island more than any other region.

2.11 Rule of Thumb Techniques

Under certain circumstances, the person charged with making a timely decision that requires an estimate of the fate of spilled oil must act before qualified scientific advice can be rendered. In this case, climatological estimated trajectories might be helpful, but it seems a few common sense "rules of thumb" are needed to help in making decisions. Consider the following first-order approximations for advection.

In the absence of a strong permanent current, both empirical and theoretical studies have shown that an oil slick on the ocean surface travels at about 3 percent of the wind speed directed at a slight angle (about 15° to the right) of the downwind direction.

In regions where strong permanent currents exist, such as the Gulf Stream, available atlas presentations or satellite data should be consulted. In general, the Gulf Stream is visible on the IR photograph as a dark region about 100 km wide with the core about 30 km from the shoreward boundary. A peak current of about 150 cm/sec can be assumed for the core. The advection can be approximated as the vectoral sum of wind driven current and permanent current. If the oil spill is within a tidal excursion to the impact point, an estimate of tidal current may also be added to the current vector.

Another important operational consideration is the distance between impact and spill site and how this relates through various environmental processes to the time of impact. Figure 4 indicates these relationships by plotting the important environmental processes on a space-time chart. One need only estimate the distance to the impact points and the advection velocity toward impact. The diagram indicates impact time and the various physical processes of importance for those length and time scales. For example, a consideration of tidal currents is only needed at a distance of 10^3 to 10^4 m from spill to impact.

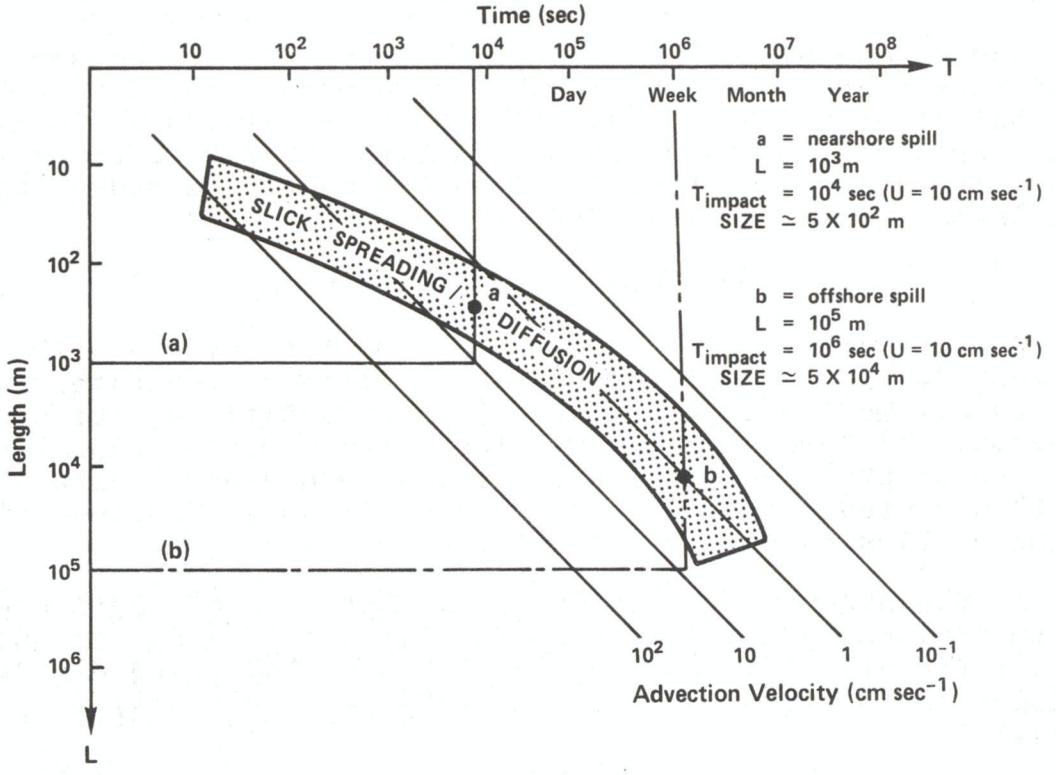

Figure 4.--Time-length scales connected with oil spills of various distance from shore (after Stolzenbach et. al., 1977)

3. ENVIRONMENTAL DATA

3.1 Surface Wind Field

An oil spill at sea is influenced by weather conditions. Surface wind conditions produce wind waves and wind-driven currents. Wind waves mix the oil both into the water column and horizontally. Also, in theory, wave height is related to a downwind wave driven current. Surface wind driven currents, in theory, flow at 45° to the right of the wind. The combined oil advection due to waves and wind-drift has been observed to be about 3 percent of the wind magnitude directed about 15° to the right of the wind. Other meteorological factors such as the movement and location of major weather systems and atmospheric fronts are important due to shifting wind conditions associated with such disturbances.

The surface wind field is of prime importance in judging the movement and thus the fate of oil spilled at sea. During the winter, the wind in the New York Bight, related to a most probable climatological pollutant trajectory, is from the WNW-NW at 5 to 10 kt. During the summer the mean wind is directed from the southwest at 3 to 4 kt. Figures 5 to 10 show calculated mean wind vectors for various regions during specific months. Based on this data, mean surface wind driven oil trajectories have a higher probability of moving offshore during the winter months, with the summer trajectories having a higher onshore tendency.

The mean wind field as presented can be explained by the winter dominance of the Icelandic Low pressure system (producing WNW-NW flow) and the summer dominance of the Bermuda high pressure system (producing SSW-SW flow).

The constancy of the surface wind in the New York Bight has been calculated by Williams and Godshall (1977). Winter and summer constancy (about 50 percent and 40 percent, respectively) is relatively high as compared to spring (about 15 percent) and fall (about 25 percent).

The above information concerning the mean wind and its constancy can be interpreted in terms of oil spill trajectory estimates in the following manner. In regions that are far enough from the impact point (for example, outside one tidal excursion), the most probable impact would occur more frequently along the mean wind direction. This type of climatological projection, based on wind-driven currents, is most accurate during seasons of high wind consistency and will be modified in the presence of the prevailing permanent current. The constancy can be interpreted in the context of the spread of oil spill trajectories starting from a common point. The climatological

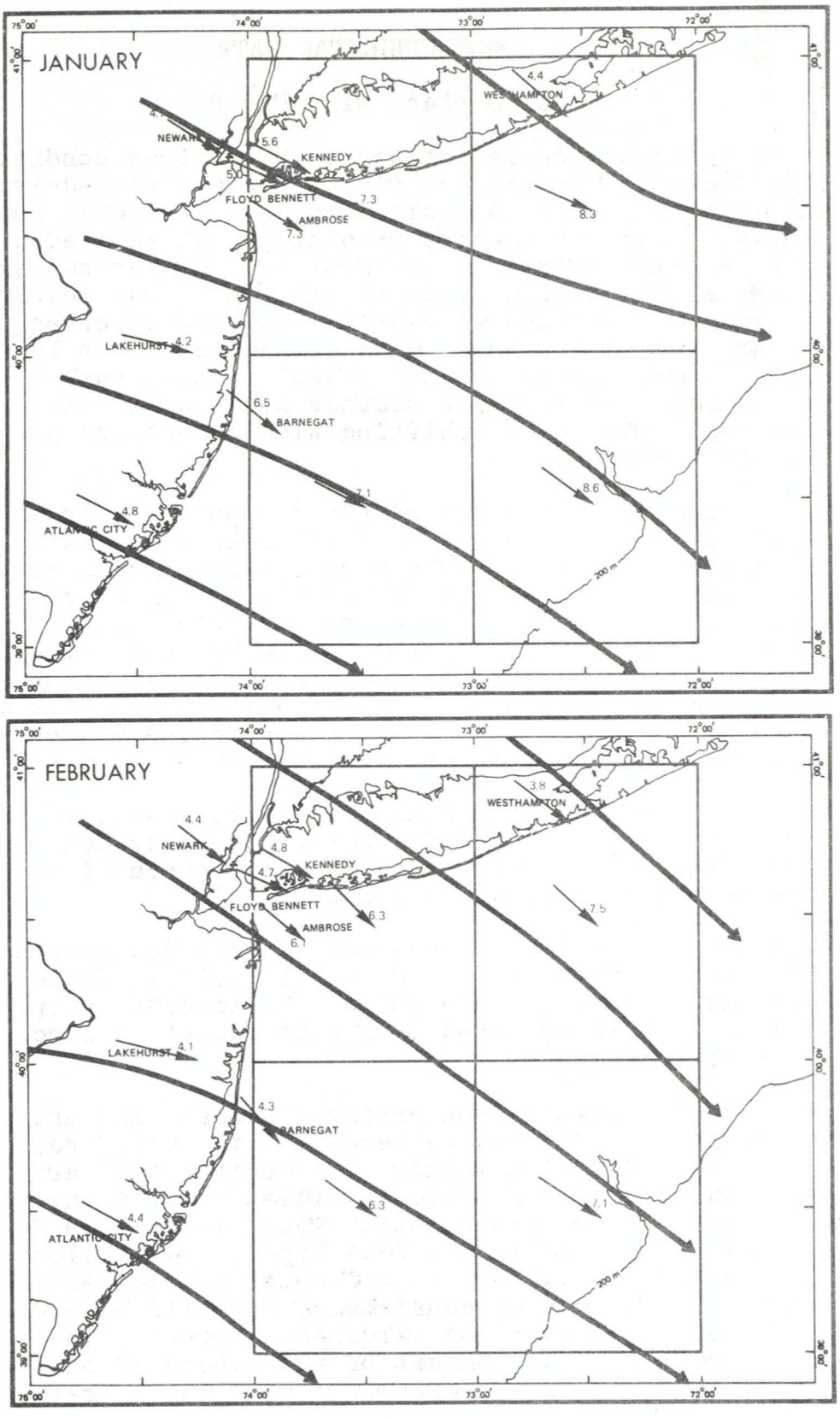

Figure 5.--Monthly mean wind vectors in knots (after Lettau, Bernhard, and Bower, 1976)

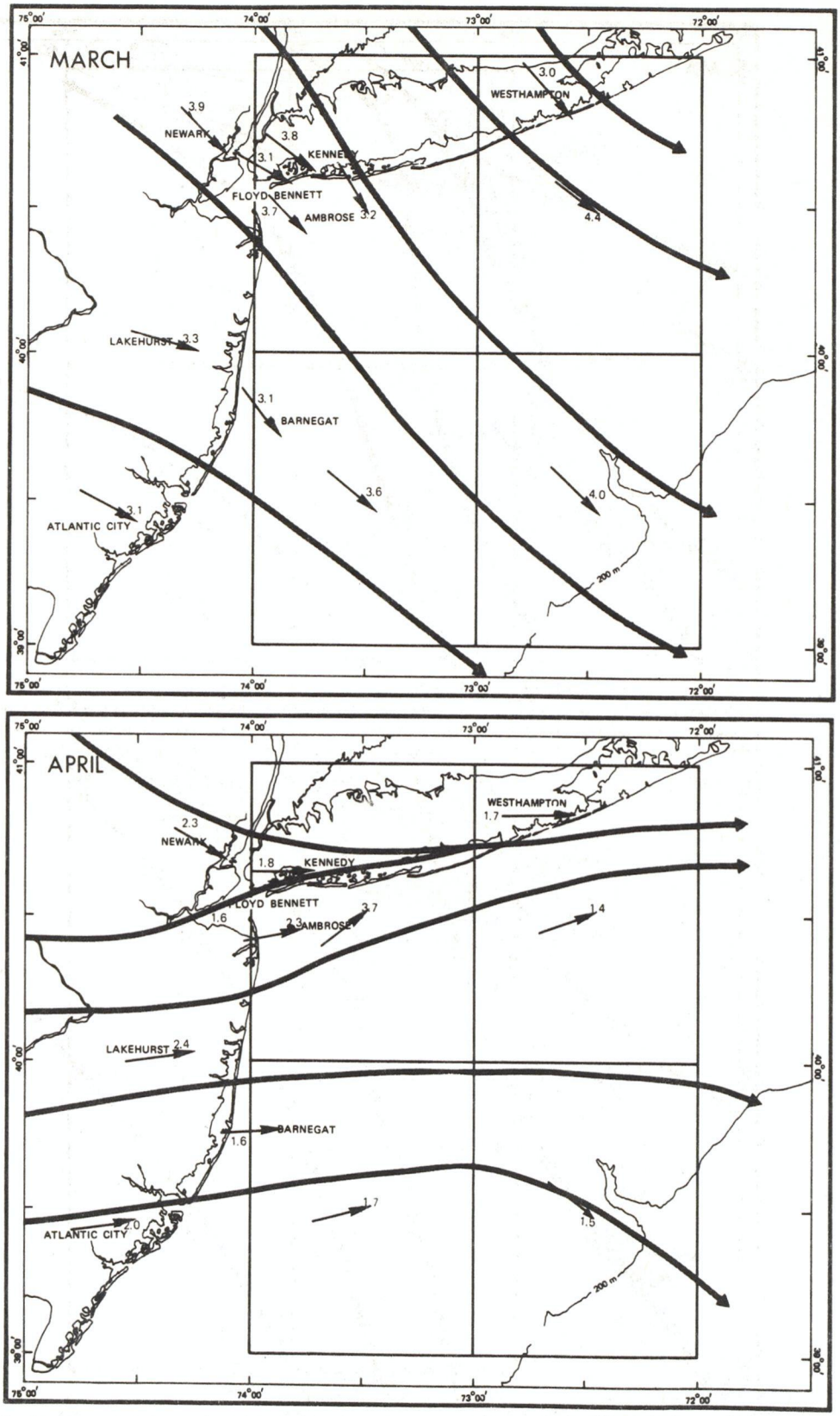

Figure 6.--Monthly mean wind vectors in knots (after Lettau, Bernhard, and Bower, 1976)

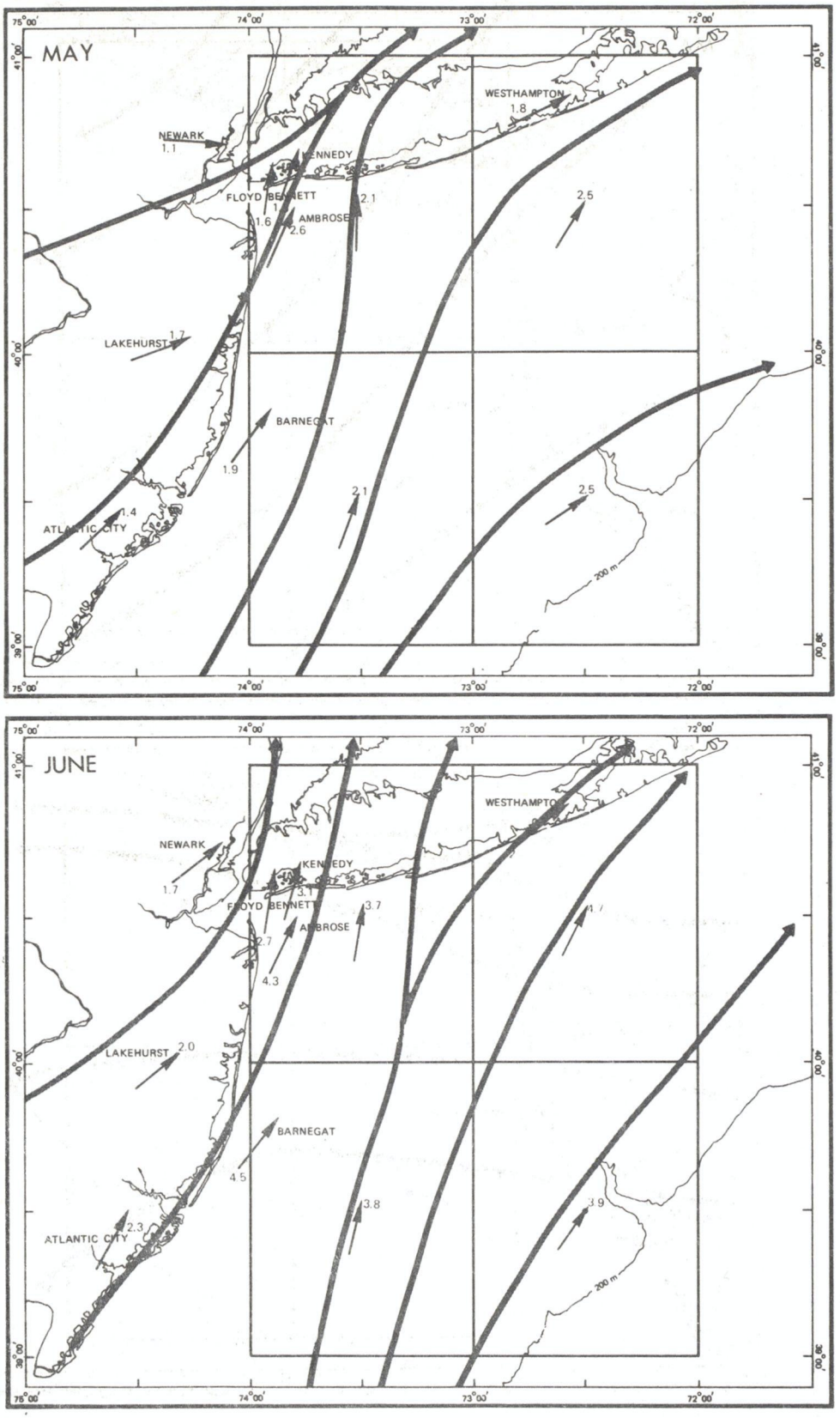

Figure 7.--Monthly mean wind vectors in knots (after Lettau, Bernhard, and Bower, 1976)

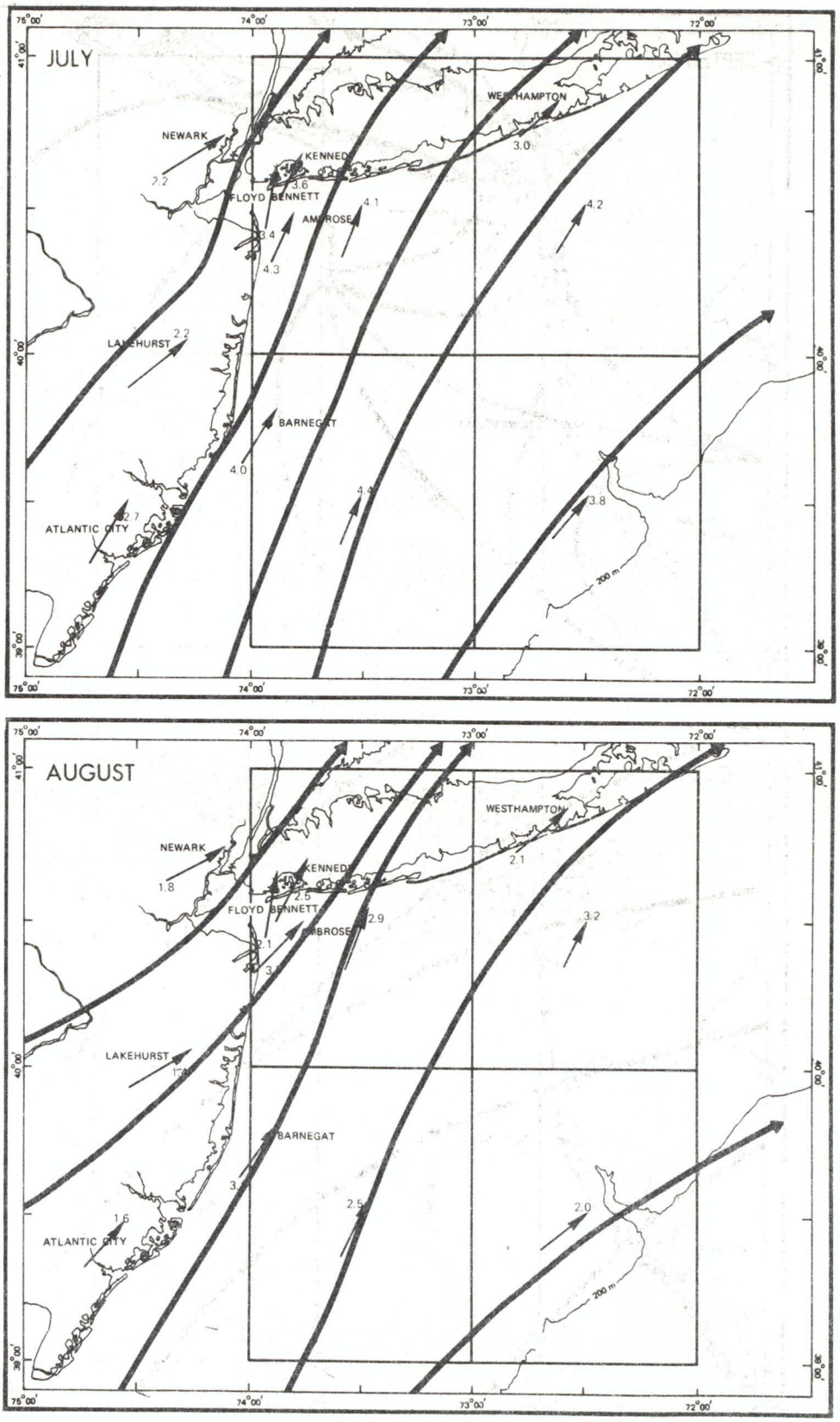

Figure 8.--Monthly mean wind vectors in knots (after Lettau, Bernhard, and Bower, 1976)

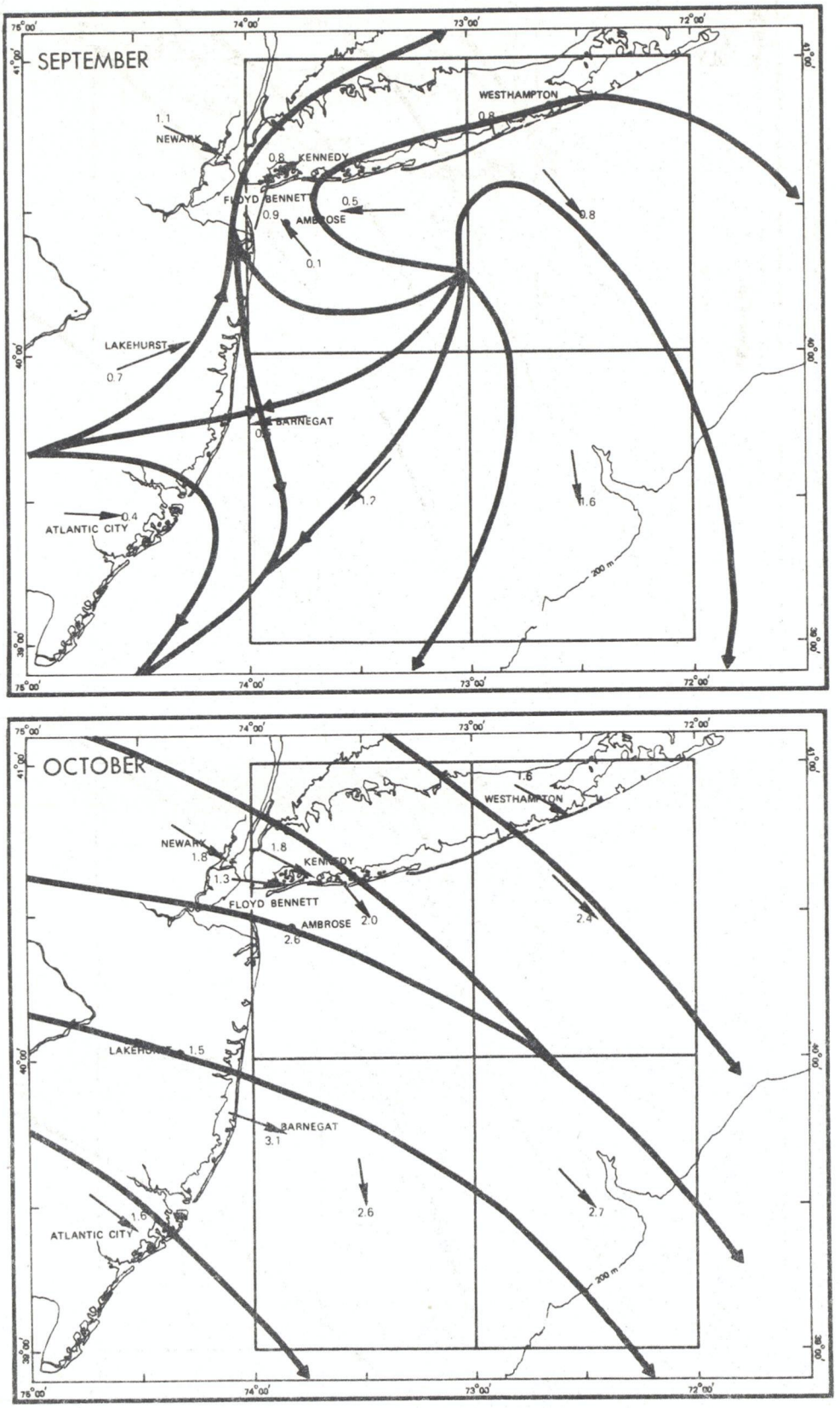

Figure 9.--Monthly mean wind vectors in knots (after Lettau, Bernhard, and Bower, 1976)

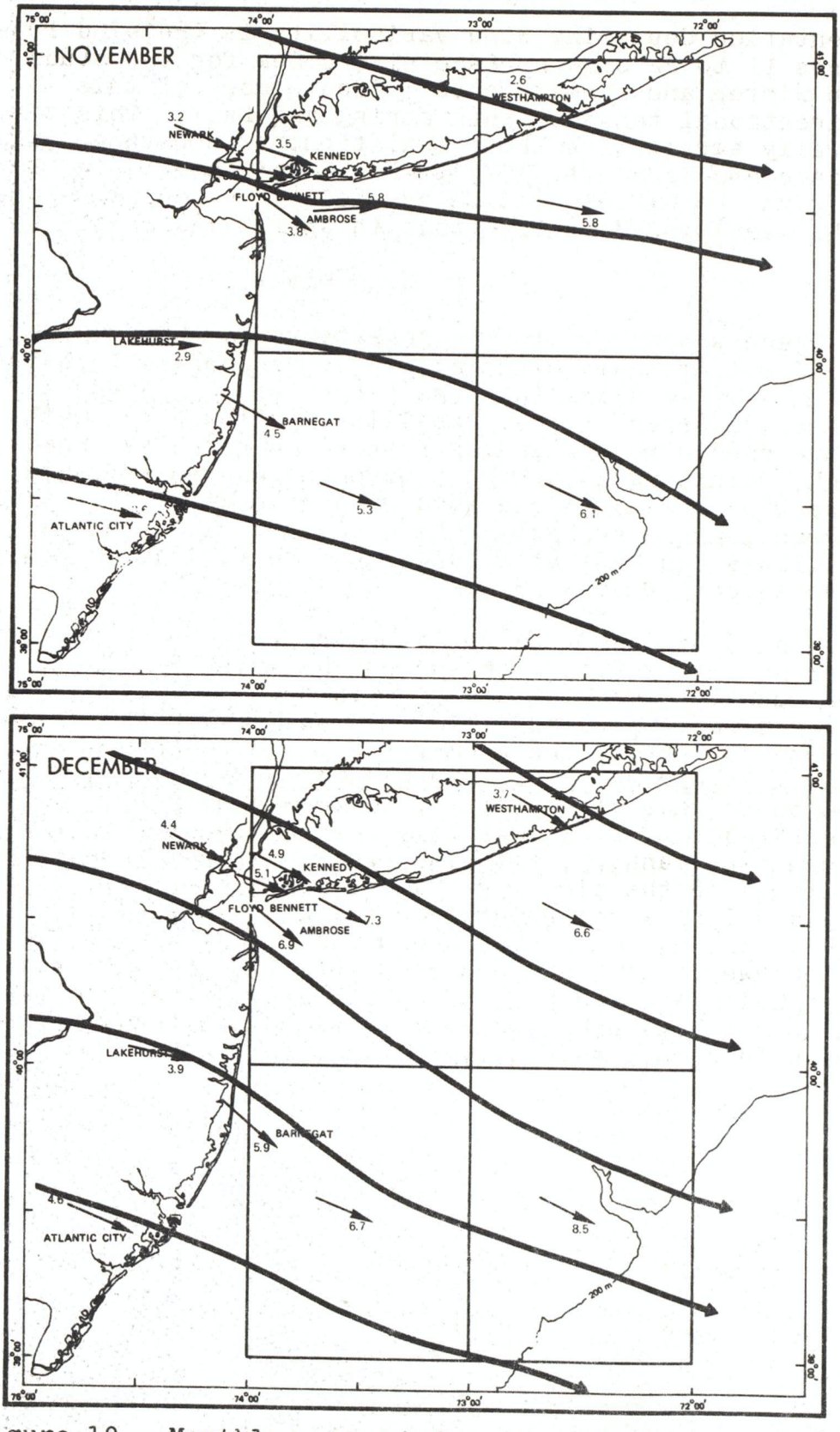

Figure 10.--Monthly mean wind vectors in knots (after Lettau, Bernhard, and Bower, 1976)

presentation depicting wind variability is the wind rose. Figures 11 to 22 show surface wind roses for the study region in which winter and summer roses indicate more of this unidirectional tendency than spring and fall. This tendency generally agrees with the calculations of constancy given by Williams and Godshall (1977). Hence, oil spills in winter and summer can be expected to be advected with a higher probability in the mean wind direction than in spring and fall.

3.2 Wind Waves

Ocean waves have important effects on the eventual fate of spilled oil at sea. Wind waves provide surface turbulence which mixes a surface slick into the water column. Also, due to exponential decay of wave particle velocity with depth, particles on wave crests move slightly forward compared to those at the trough, resulting in a slight wave-induced drift (about 1 percent of the wind speed) in the down wind direction. For the purpose of oceanographic analysis, the ocean area has been partitioned as in Williams and Godshall (1977) into various ocean regions as illustrated in figure 23.

Area 6 has a depth on the order of 50 m. Because of the coastline, it is fetch-limited to the west and north; thus, for a given duration, maximum waves would not be expected when the wind is from these directions. Monthly wave roses for winter (November to April) and summer (May to October) in this area are shown in figure 24. Seas are higher in winter, and the predominant wave direction for November and February is from west to northwest. The highest waves, from 6 to 7.5 m, are observed in December, January, and February, but for only a very small percentage of the time. For 30 percent of the time, the waves propagate from a westerly direction and are less than 1.5 m in height. In June and July, the waves are almost exclusively from the southwest and south and less than 1.5 m high. The winter and summer height-period histograms for area 6 indicate that waves as high as 9 m have been observed in winter, although rarely, whereas in summer the maximum is 5 m (fig. 25).

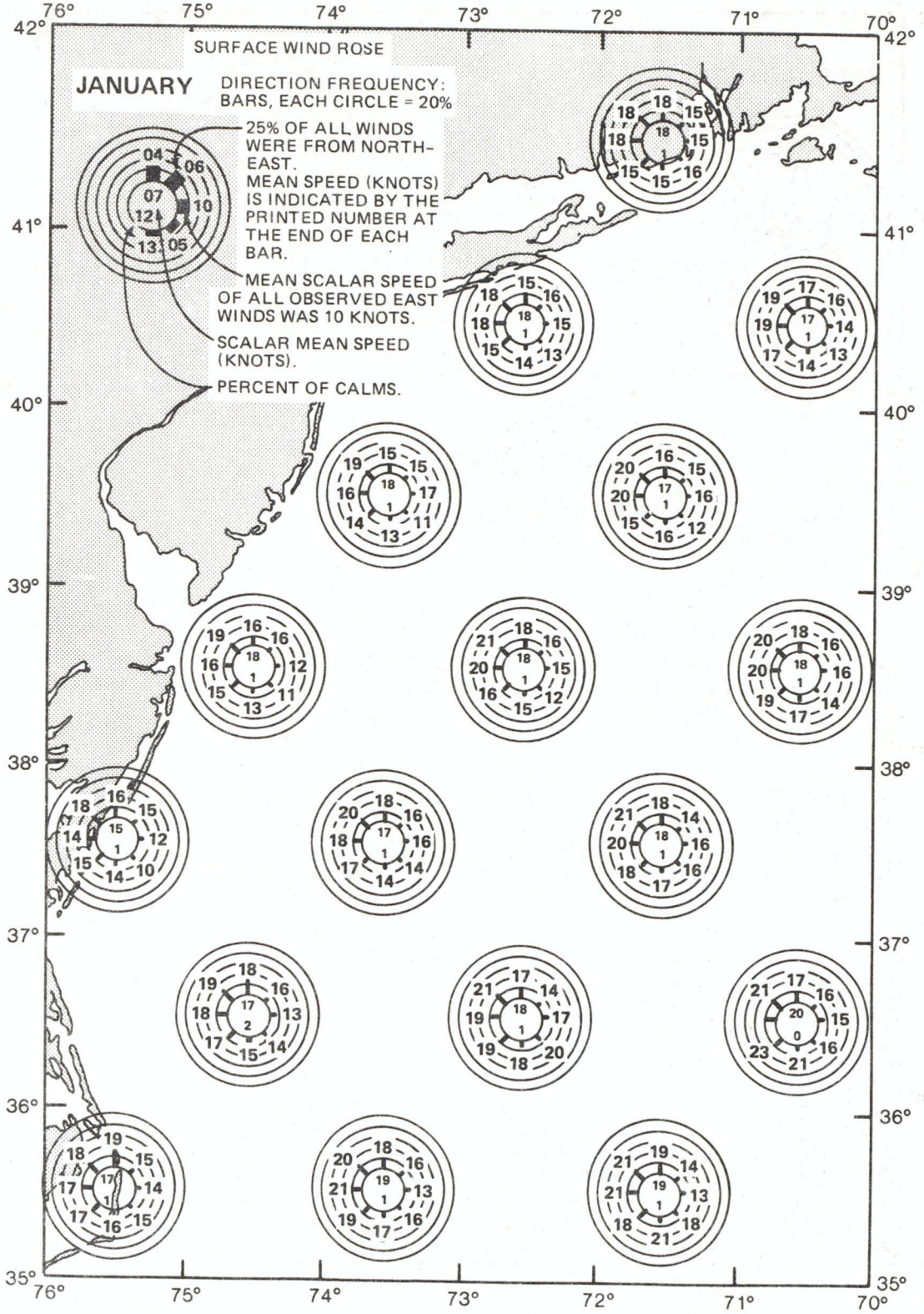

Figure 11.--Monthly surface wind roses for the New York Bight (after the Naval Weather Service Detachment, 1976)

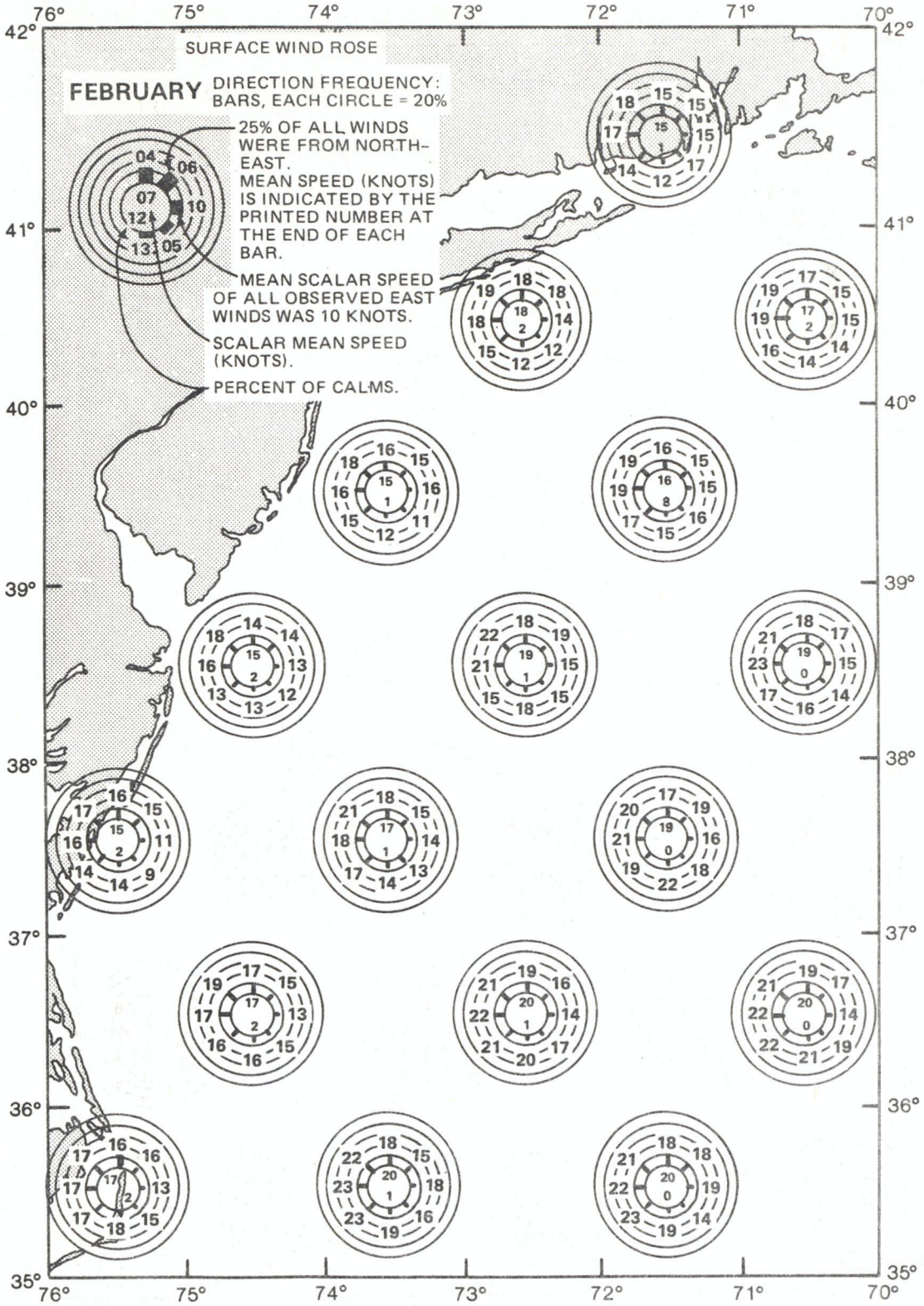

Figure 12.--Monthly surface wind roses for the New York Bight (after the Naval Weather Service Detachment, 1976)

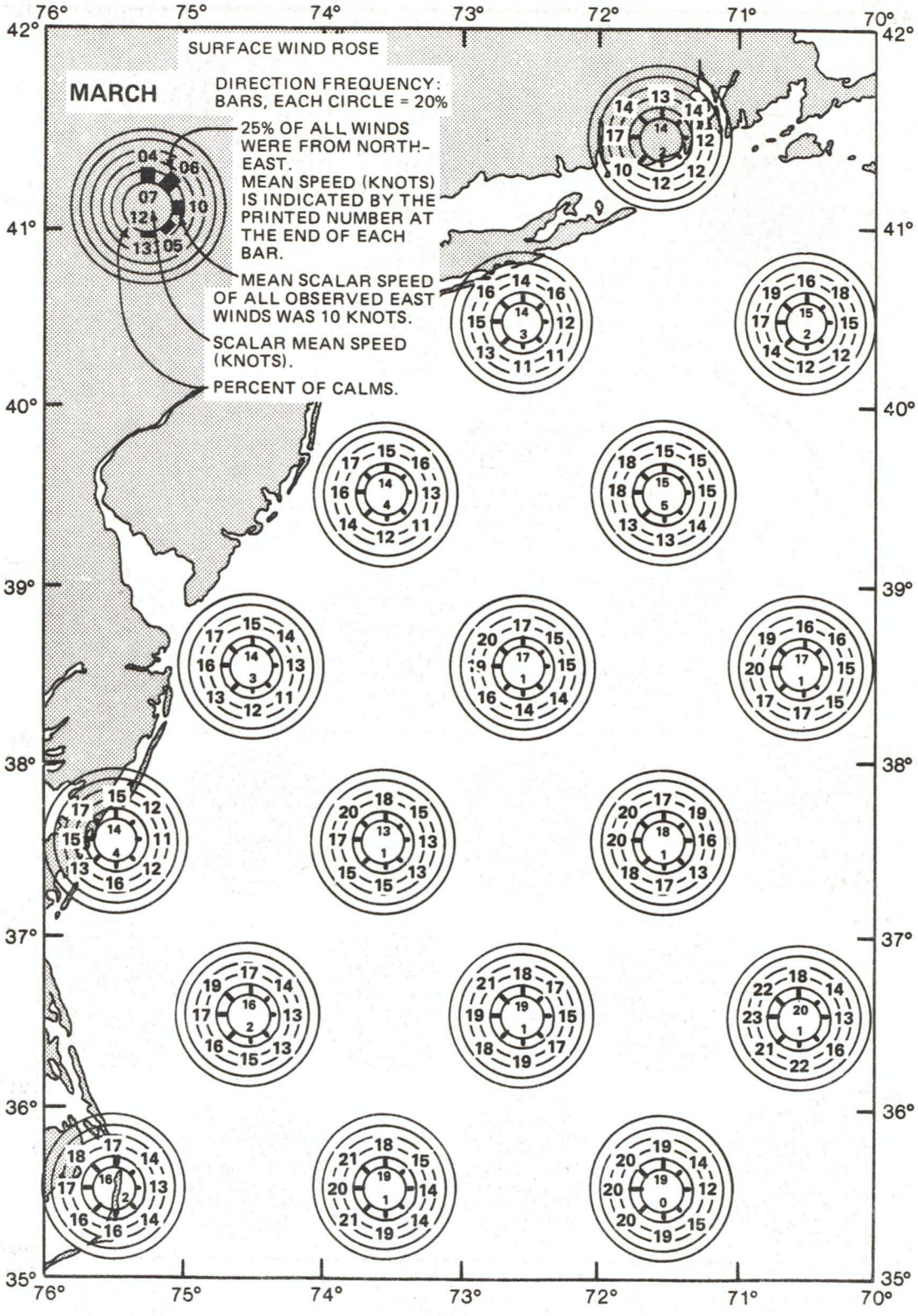

Figure 13.--Monthly surface wind roses for the New York Bight (after the Naval Weather Service Detachment, 1976)

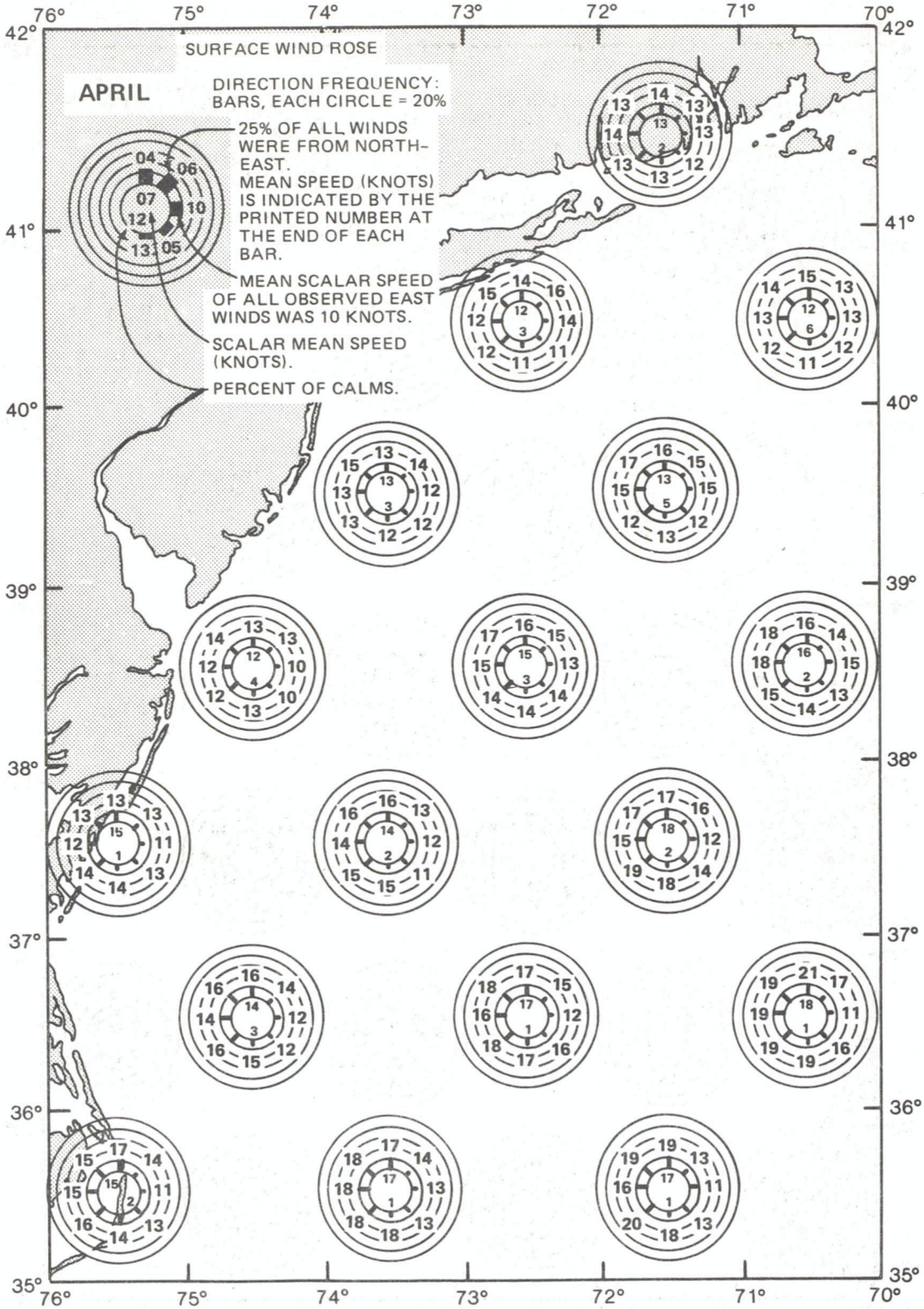

Figure 14.--Monthly surface wind roses for the New York Bight (after the Naval Weather Service Detachment, 1976)

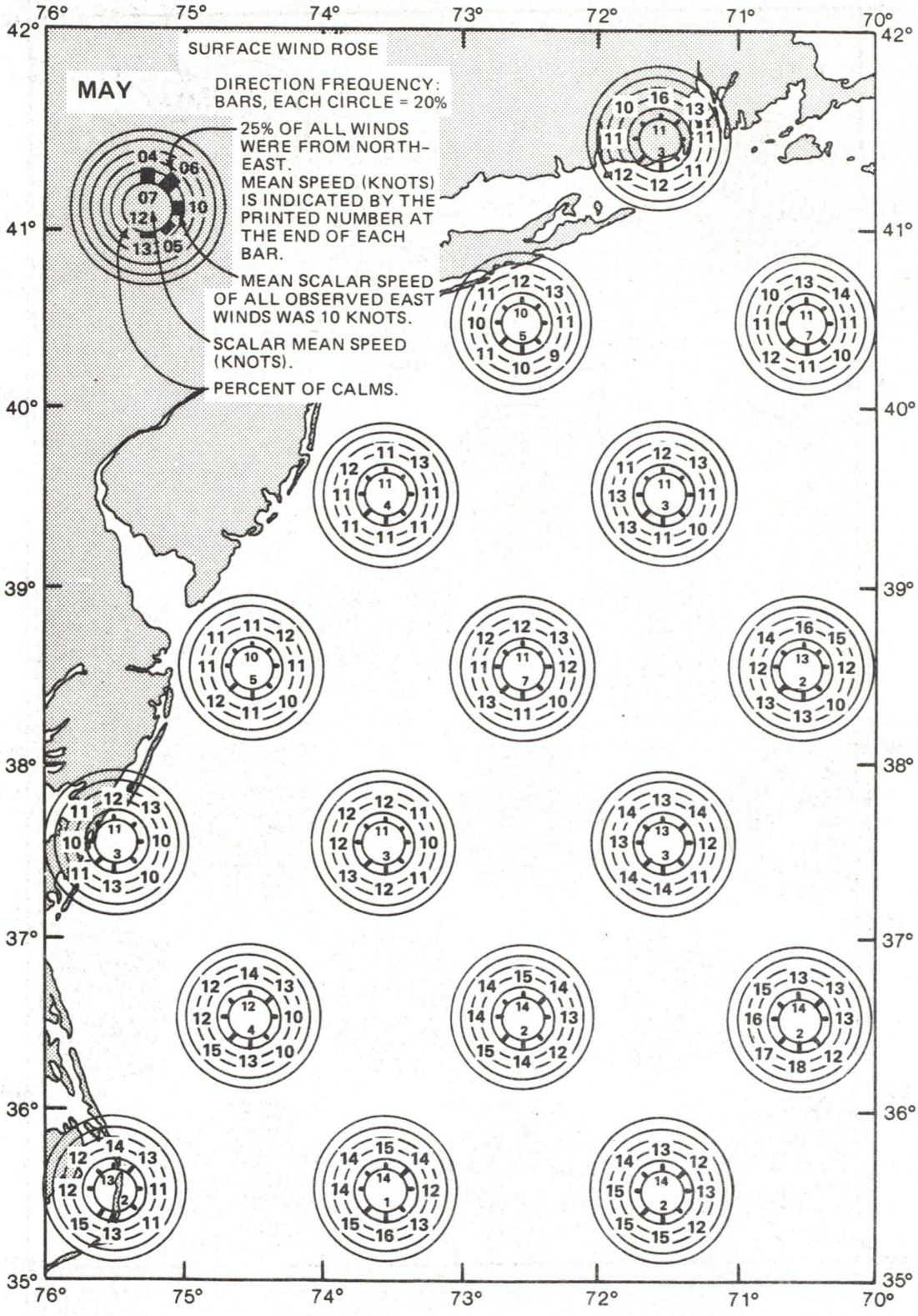

Figure 15.--Monthly surface wind roses for the New York Bight (after the Naval Weather Service Detachment, 1976)

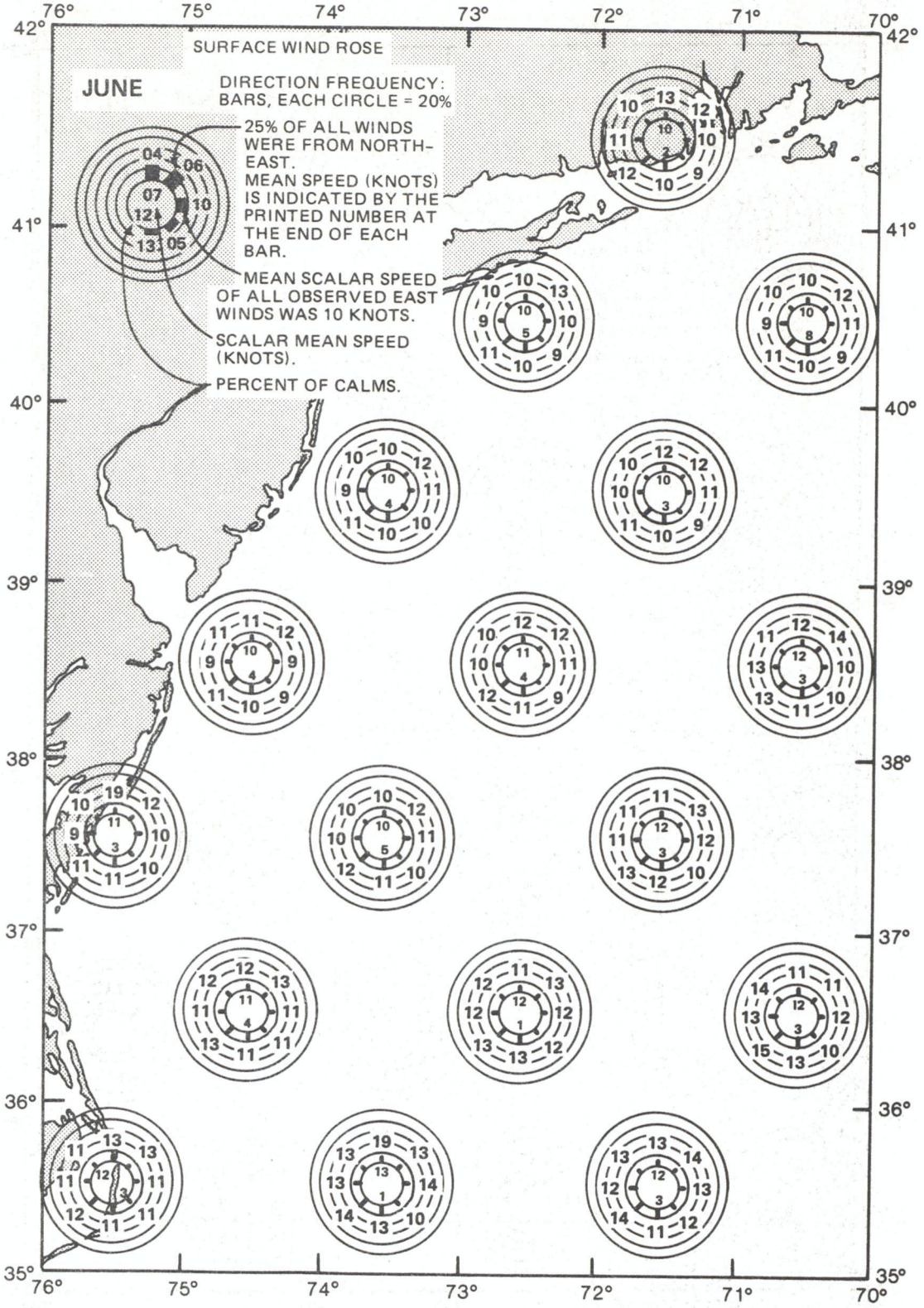

Figure 16.--Monthly surface wind roses for the New York Bight (after the Naval Weather Service Detachment, 1976)

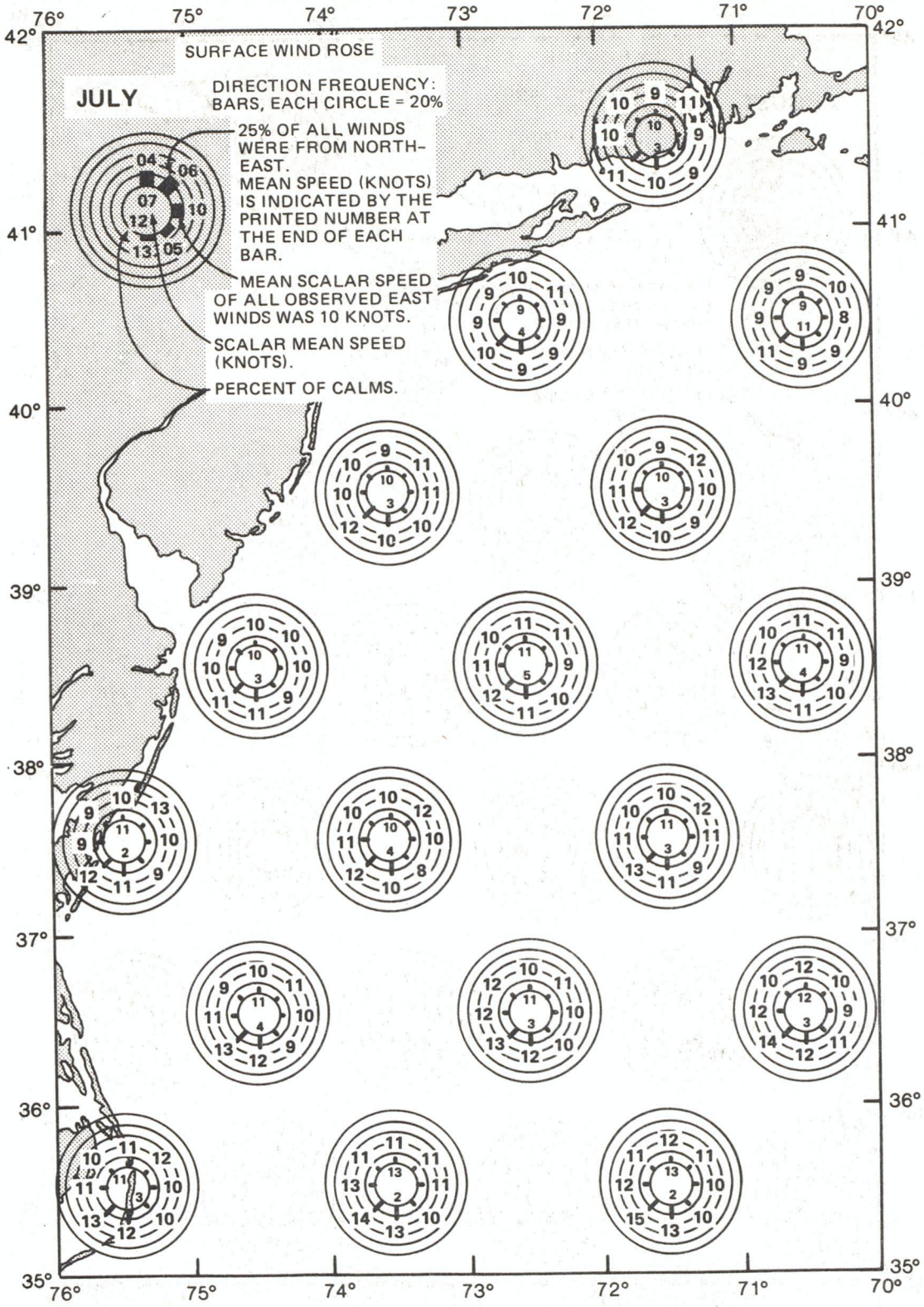

Figure 17.--Monthly surface wind roses for the New York Bight (after the Naval Weather Service Detachment, 1976)

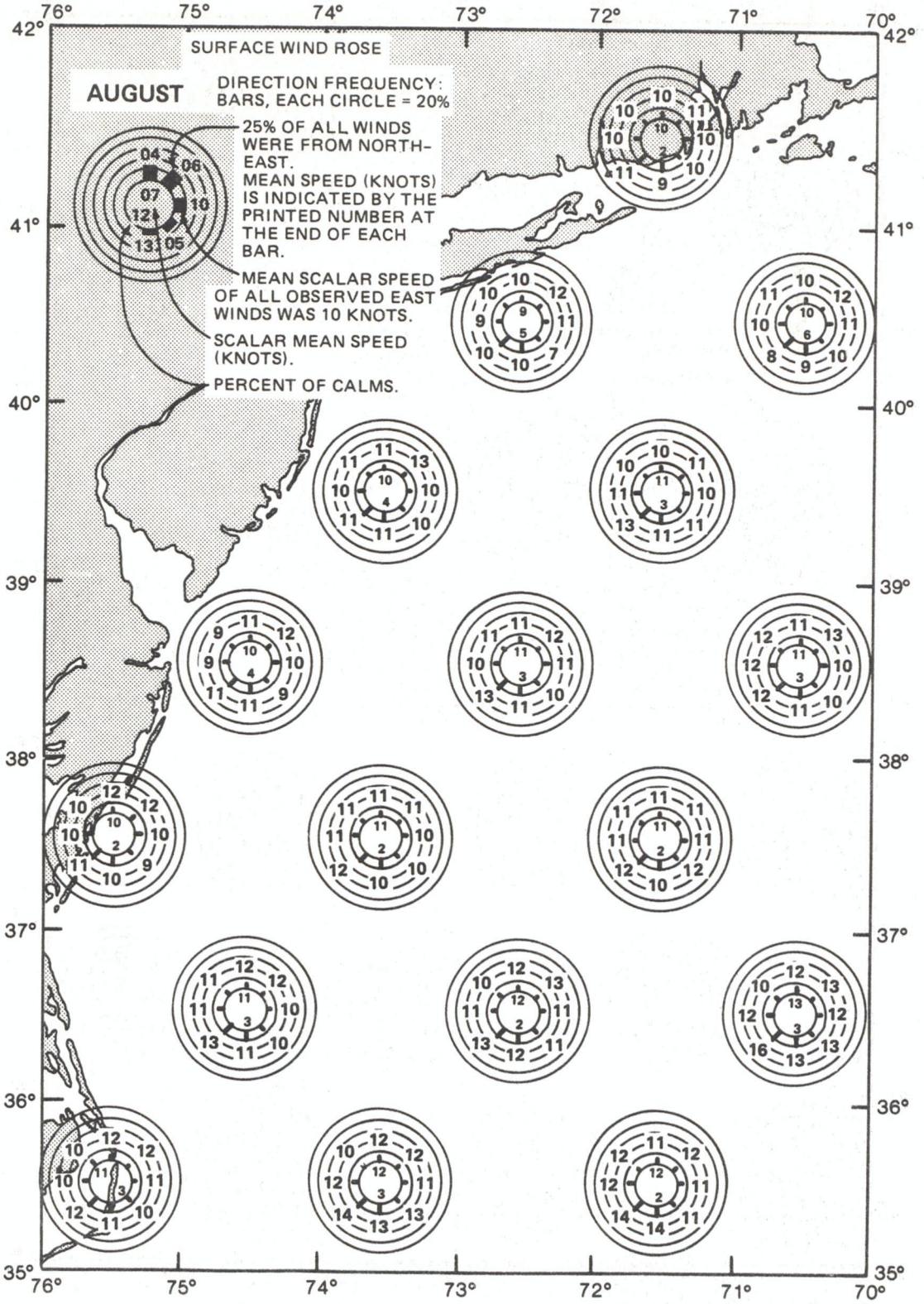

Figure 18.--Monthly surface wind roses for the New York Bight (after the Naval Weather Service Detachment, 1976)

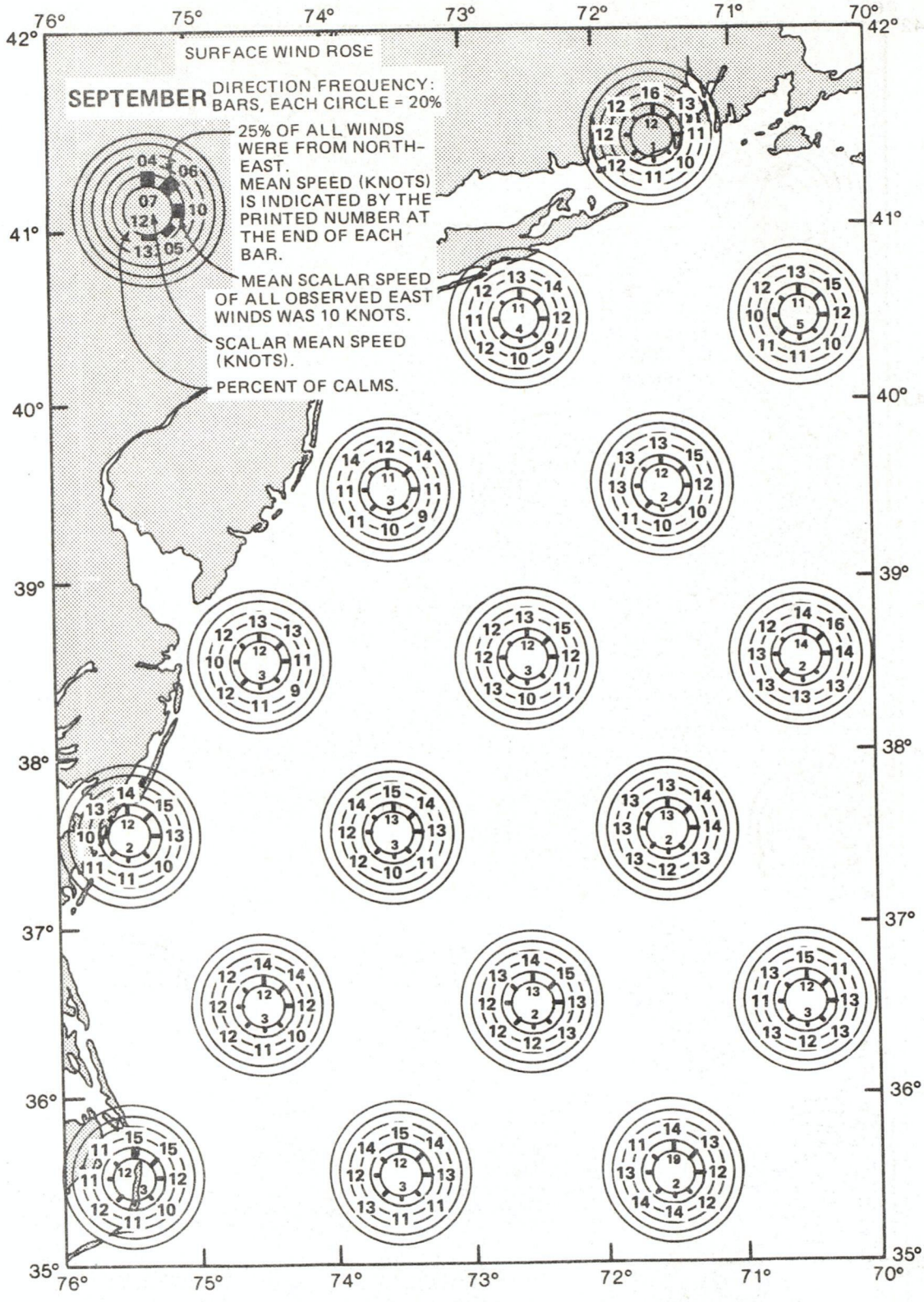

Figure 19.--Monthly surface wind roses for the New York Bight (after the Naval Weather Service Detachment, 1976)

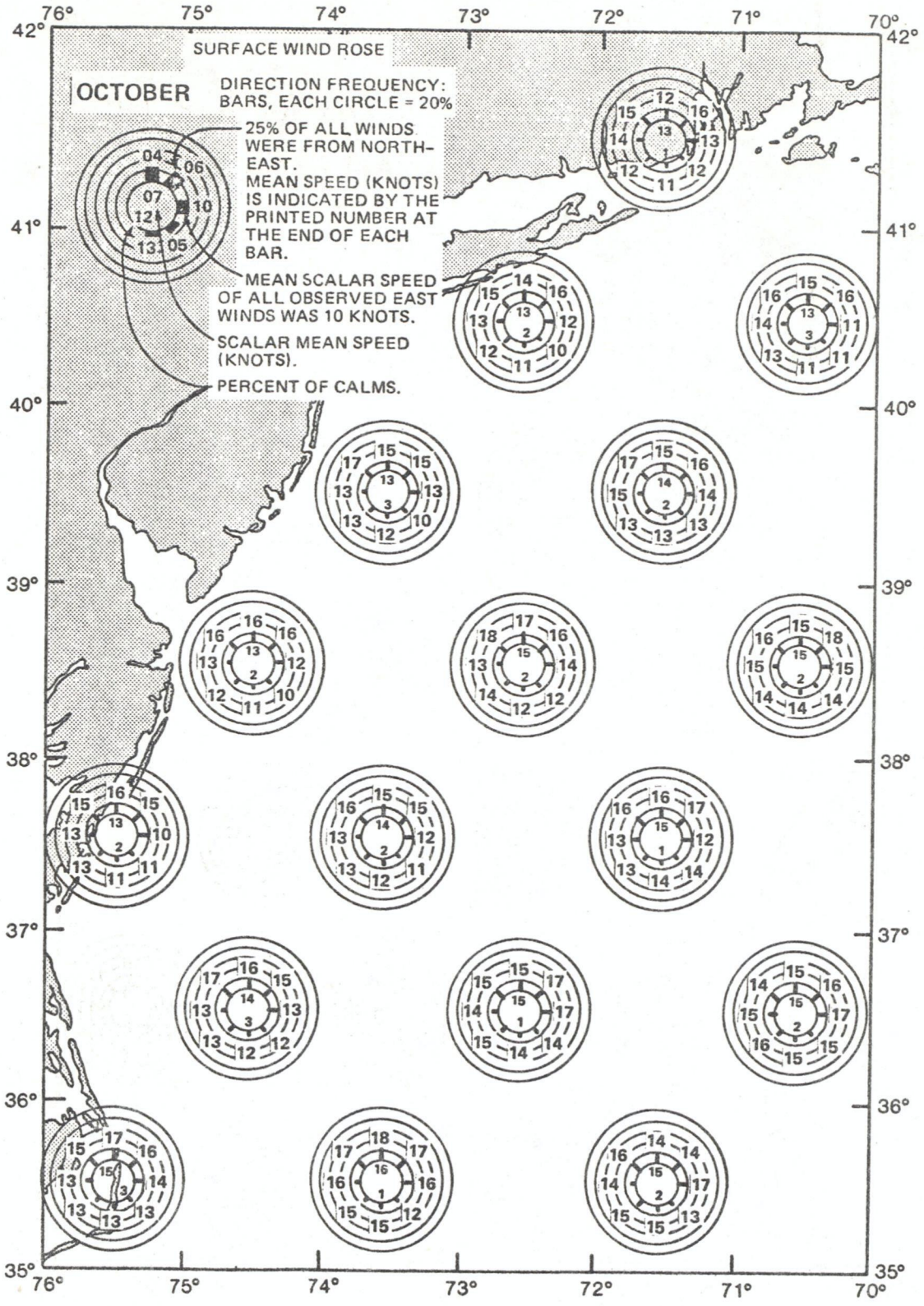

Figure 20.--Monthly surface wind roses for the New York Bight (after the Naval Weather Service Detachment, 1976)

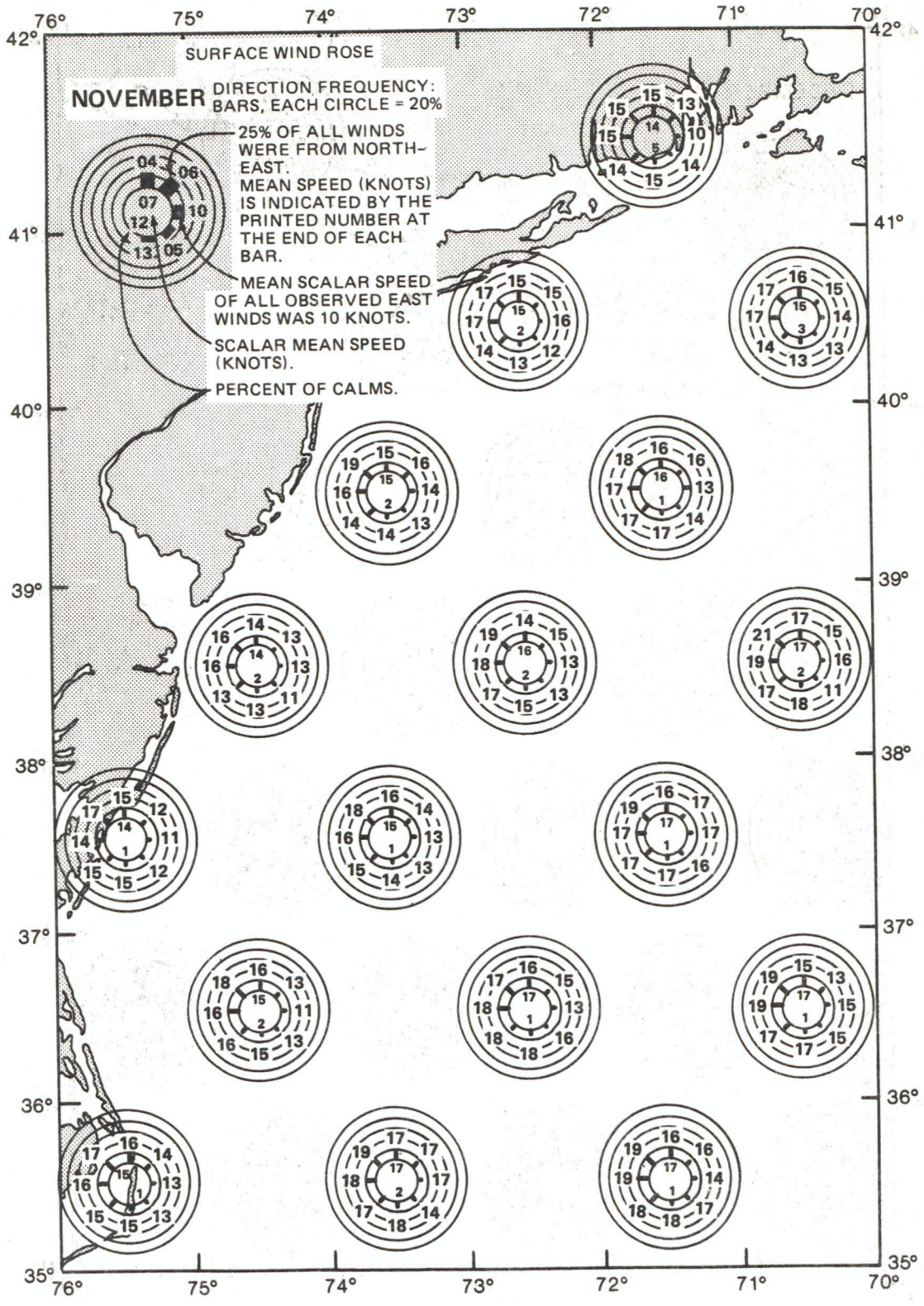

Figure 21.--Monthly surface wind roses for the New York Bight (after the Naval Weather Service Detachment, 1976)

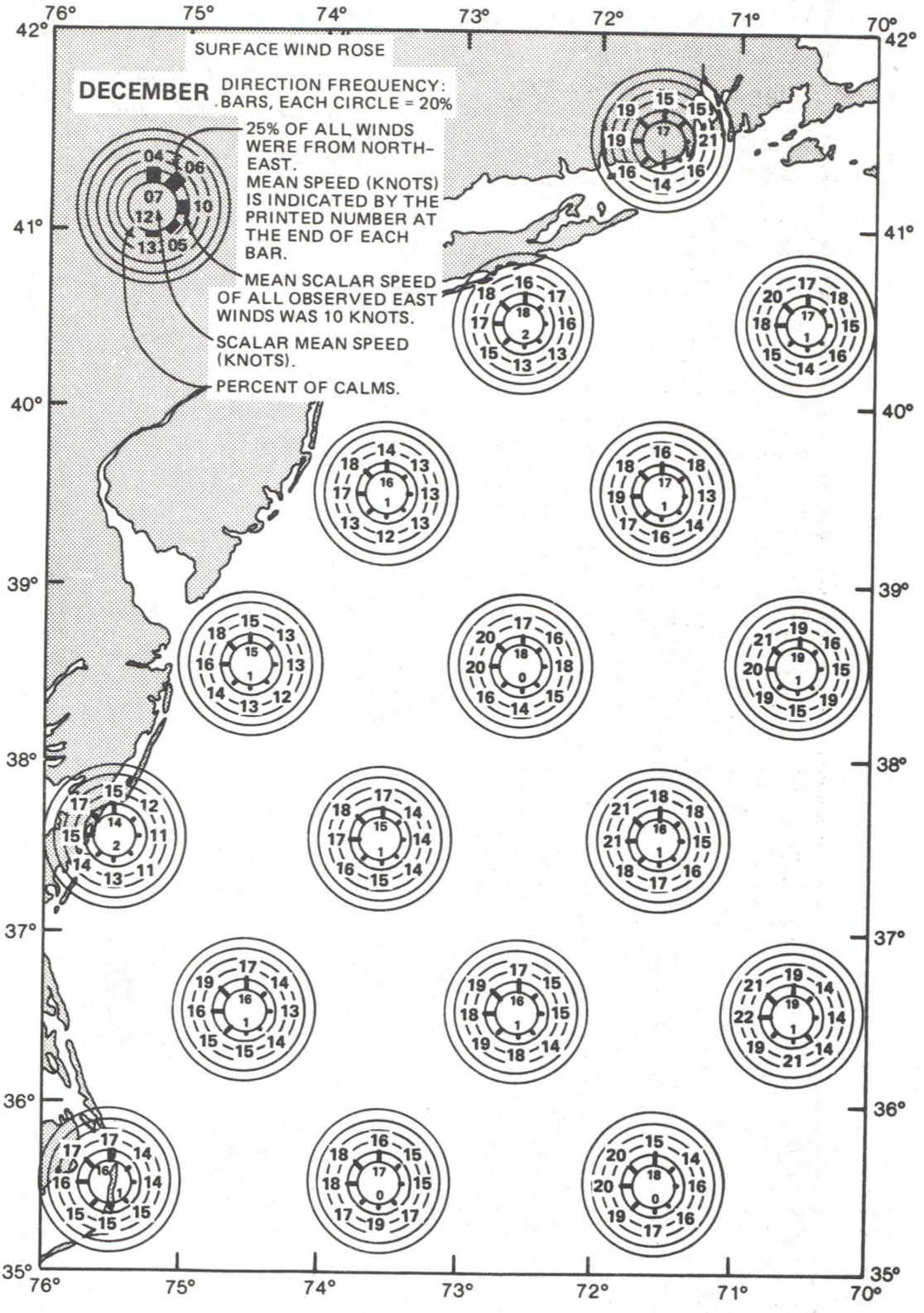

Figure 22.--Monthly surface wind roses for the New York Bight (after the Naval Weather Service Detachment, 1976)

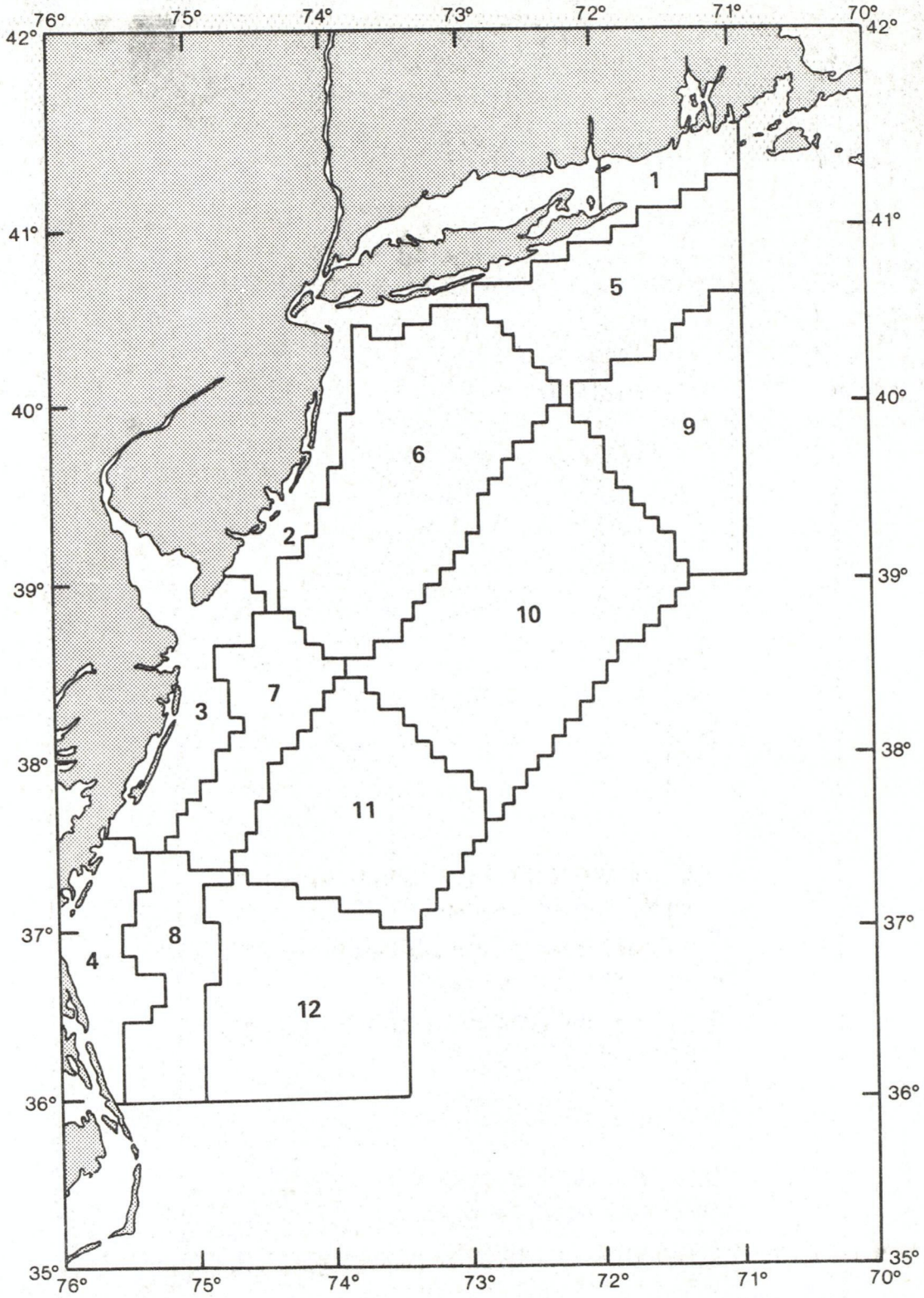

Figure 23.--Areas used for summaries of oceanographic data (after Williams and Godshall, 1977)

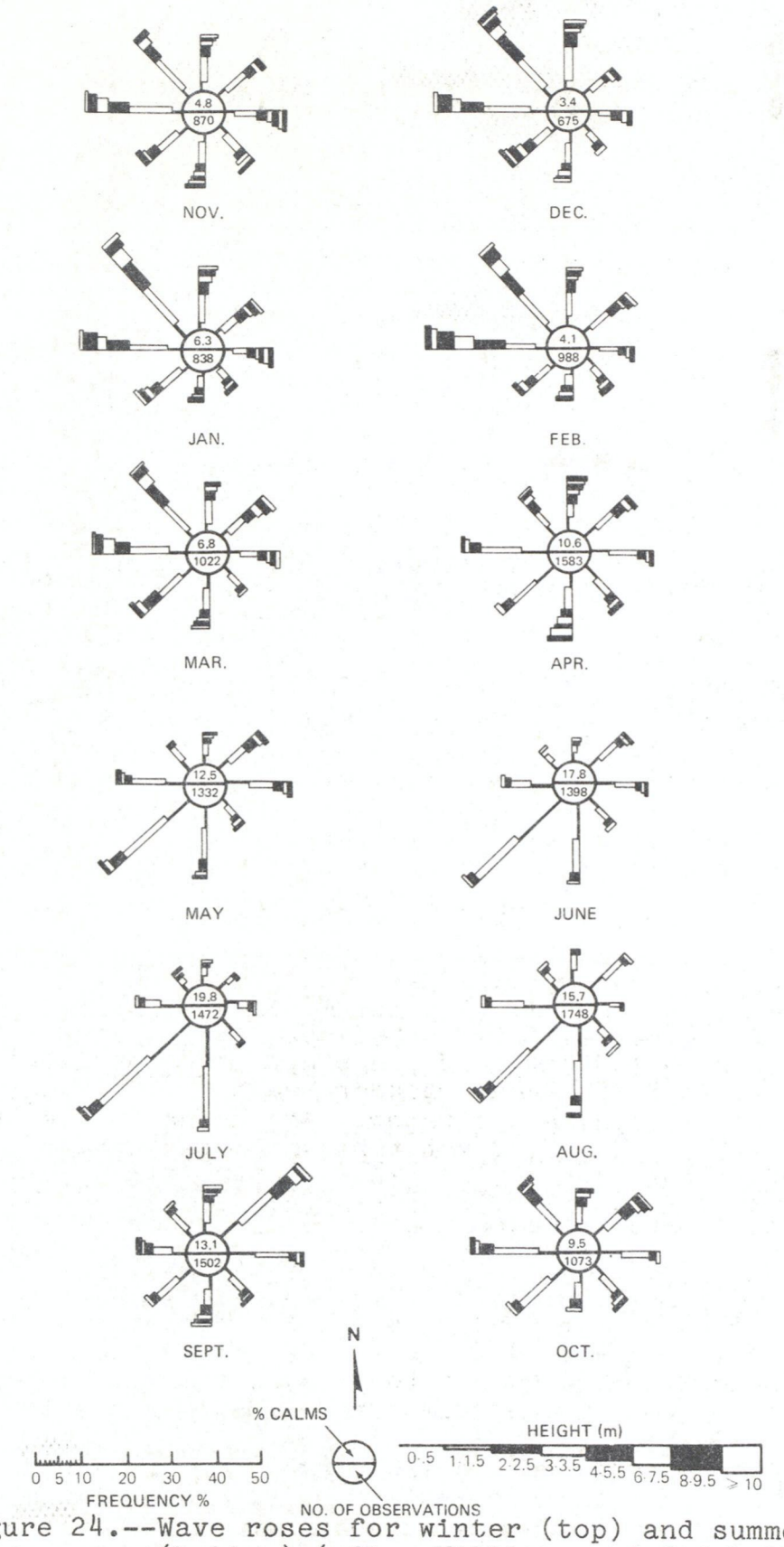

Figure 24.--Wave roses for winter (top) and summer (bottom) (after Williams and Godshall, 1977)

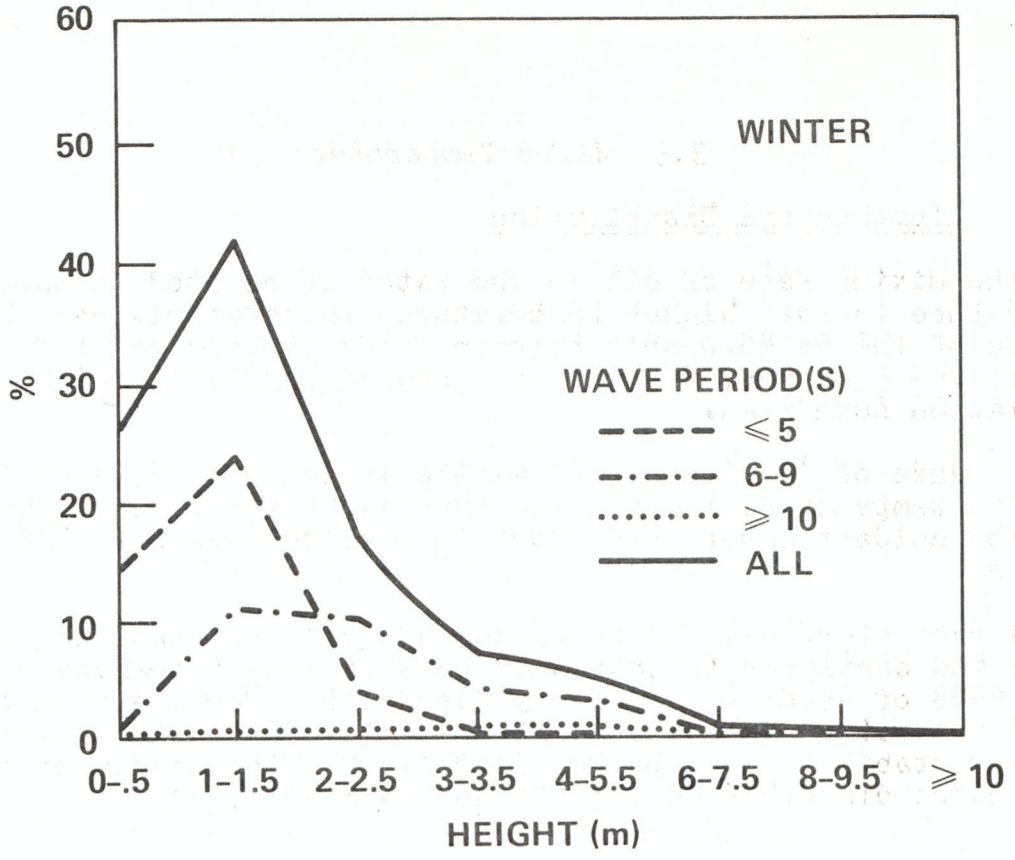

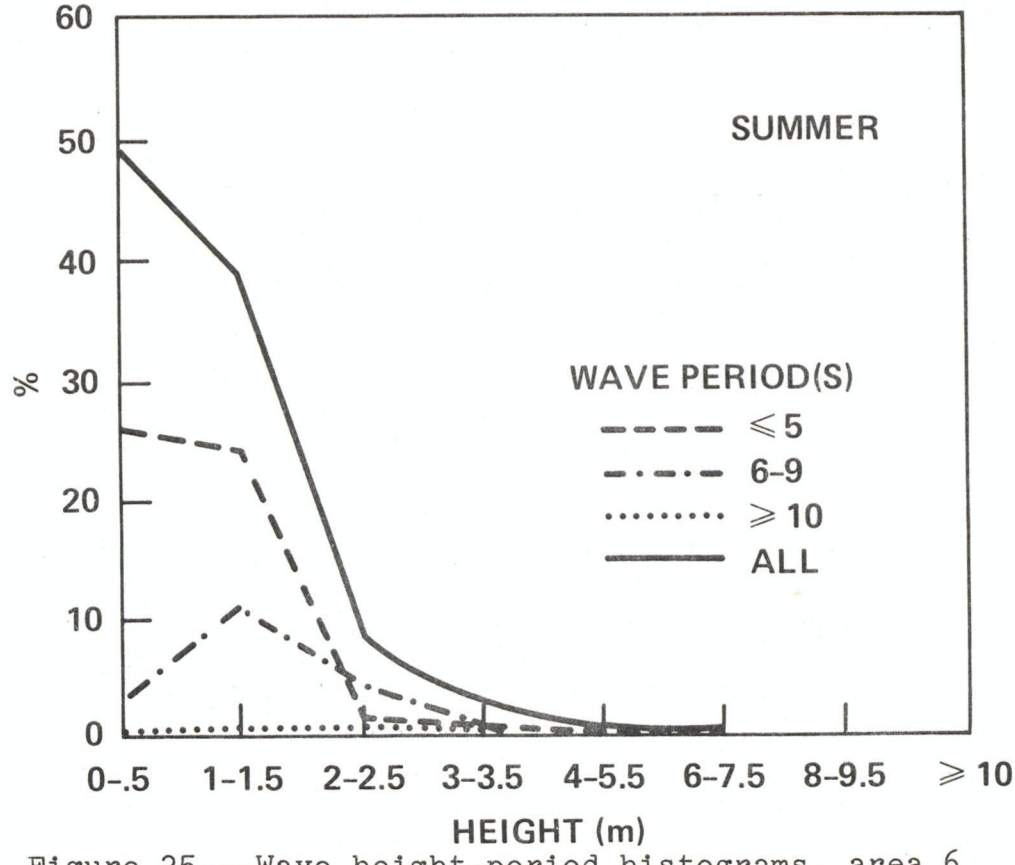

Figure 25.--Wave height-period histograms, area 6 (after Williams and Godshall, 1977)

3.3 Water Temperature

3.3.1 Temperature Distribution

The mixing rate of oil in the water is related to water temperature in that higher temperatures increase mixing. Also, because of the relationship between water temperature and circulation features, temperature gradients usually coincide with circulation boundries.

Because of increased wind mixing in the winter, a vertically constant temperature is observed throughout the water column, with the coldest water near shore increasing toward the 200 m isobath.

A rapid vertical change of temperature (thermocline) appears in May and continues to intensify to a maximum temperature difference of about 17^{o} in early September. Thus, during the summer the water column is a point of minimum mixing ability (maximum stability). Figures 26 to 37 show the mean monthly temperature distribution for the New York Bight.

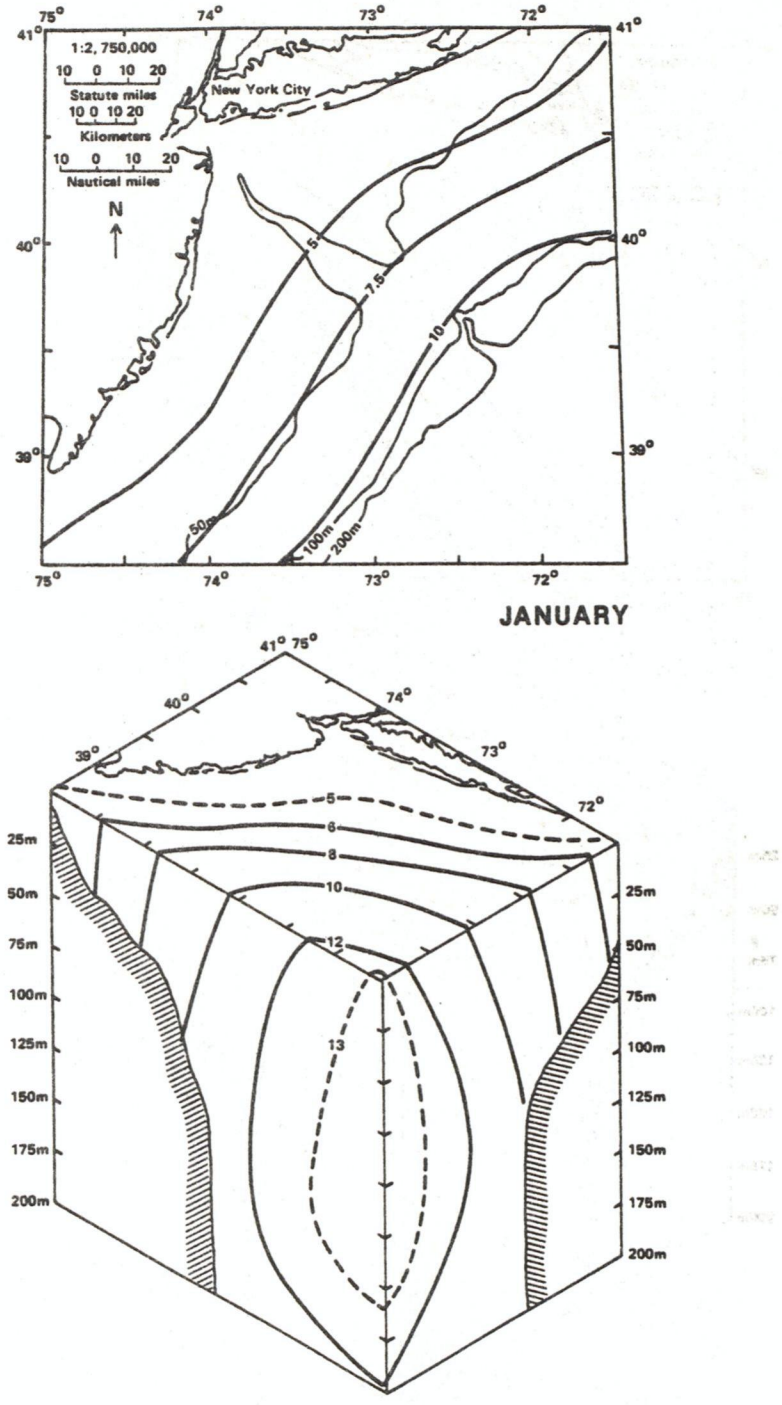

Figure 26.--Mean monthly temperature distribution in the New York Bight. Map pairs show bottom contours (top), surface and vertical contours (bottom). Units are ^{o}C. (after Bowman and Lewis, 1977)

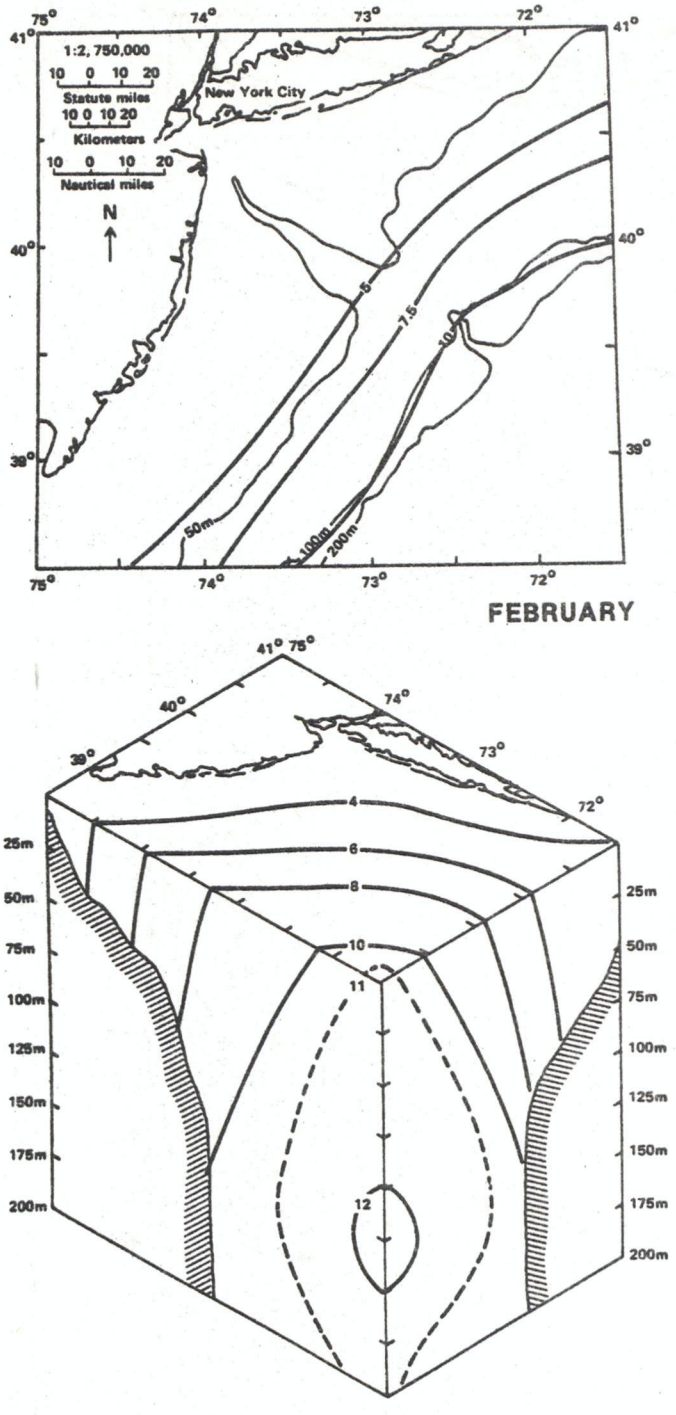

Figure 27.--Mean monthly temperature distribution in the New York Bight. Map pairs show bottom contours (top), surface and vertical contours (bottom). Units are ^{o}C. (after Bowman and Lewis, 1977)

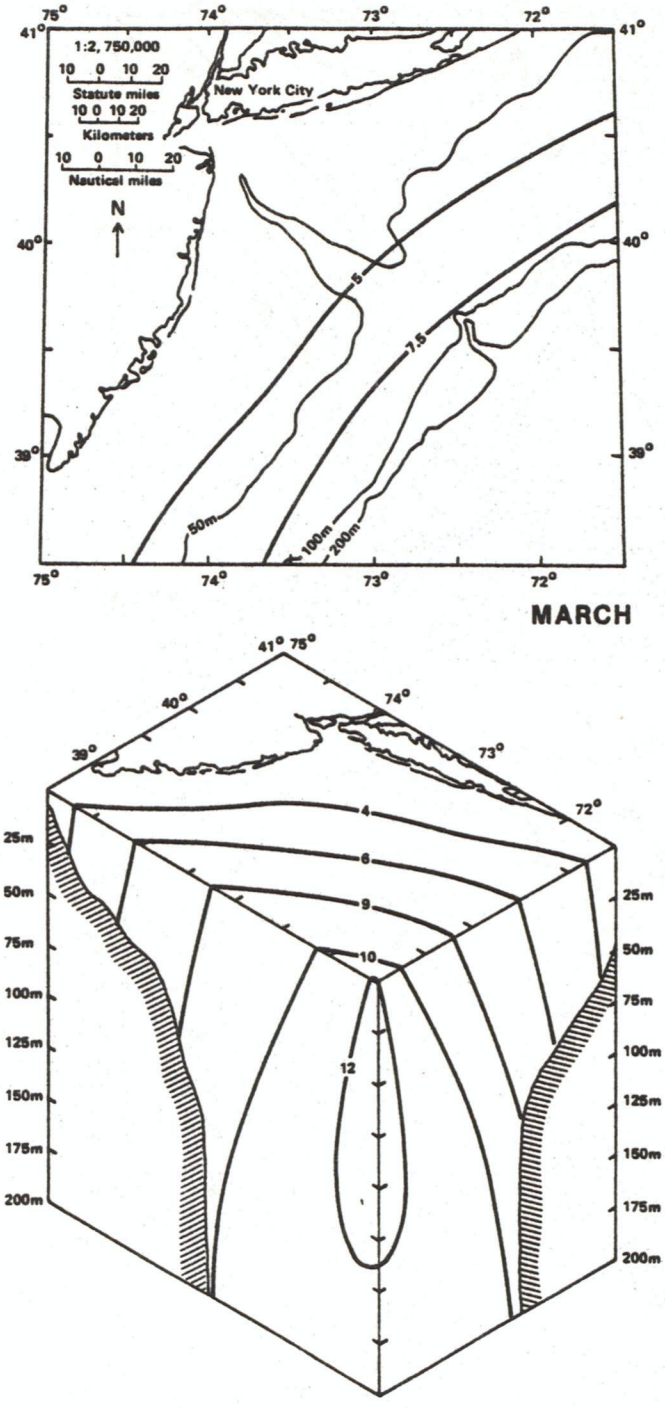

Figure 28.--Mean monthly temperature distribution in the New York Bight. Map pairs show bottom contours (top), surface and vertical contours (bottom). Units are ^{o}C. (after Bowman and Lewis, 1977)

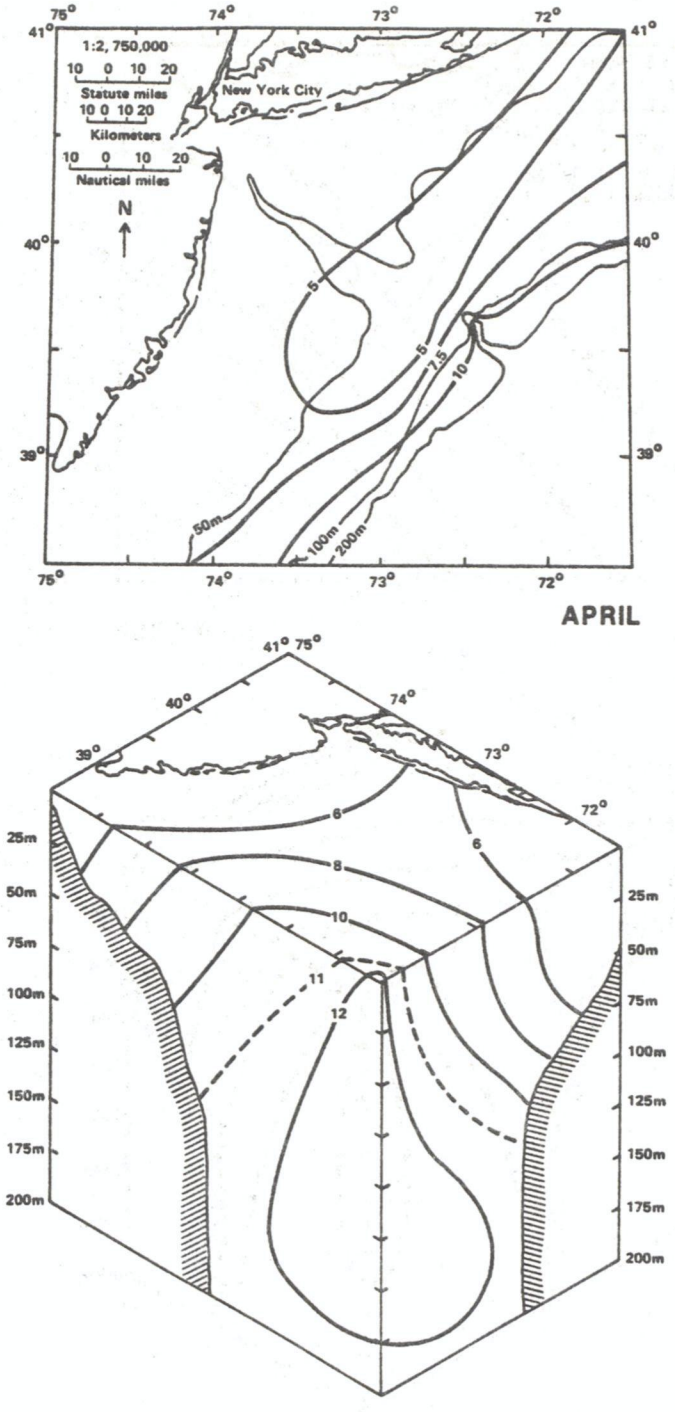

Figure 29.--Mean monthly temperature distribution in the New York Bight. Map pairs show bottom contours (top), surface and vertical contours (bottom). Units are ^{o}C. (after Bowman and Lewis, 1977)

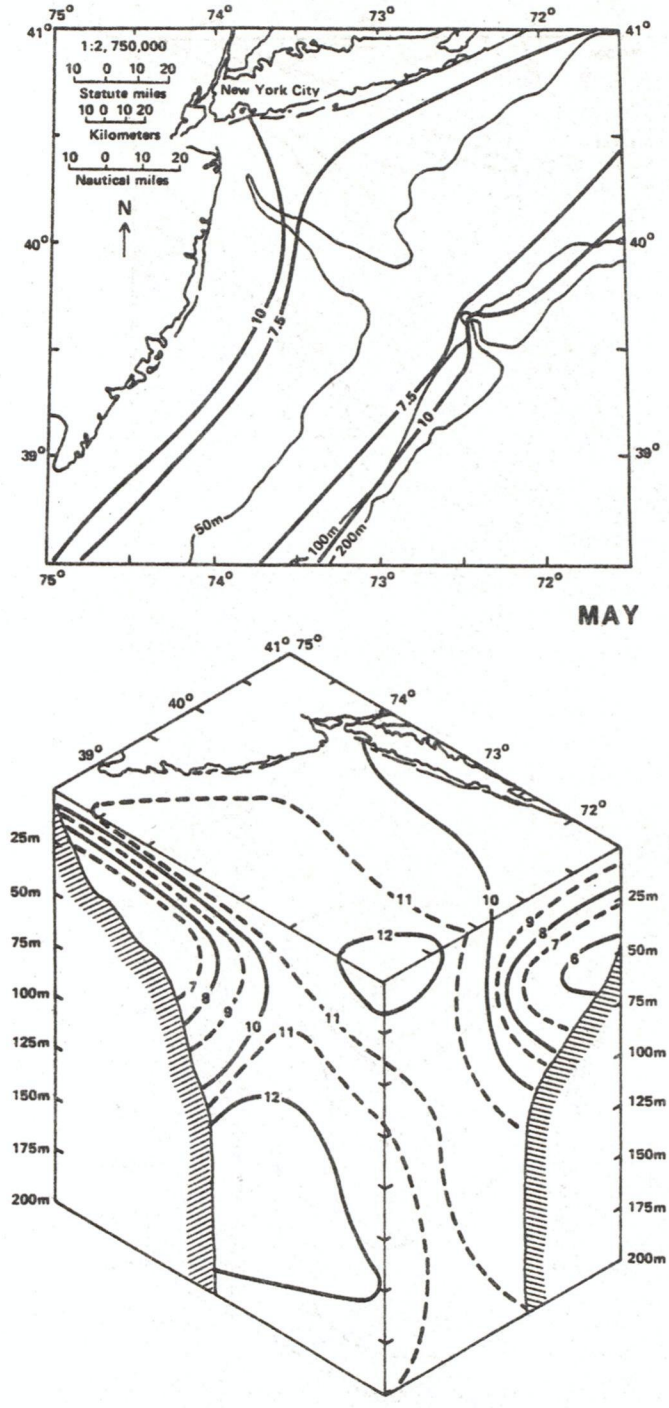

Figure 30.--Mean monthly temperature distribution in the New York Bight. Map pairs show bottom contours (top), surface and vertical contours (bottom). Units are ^{o}C. (after Bowman and Lewis, 1977)

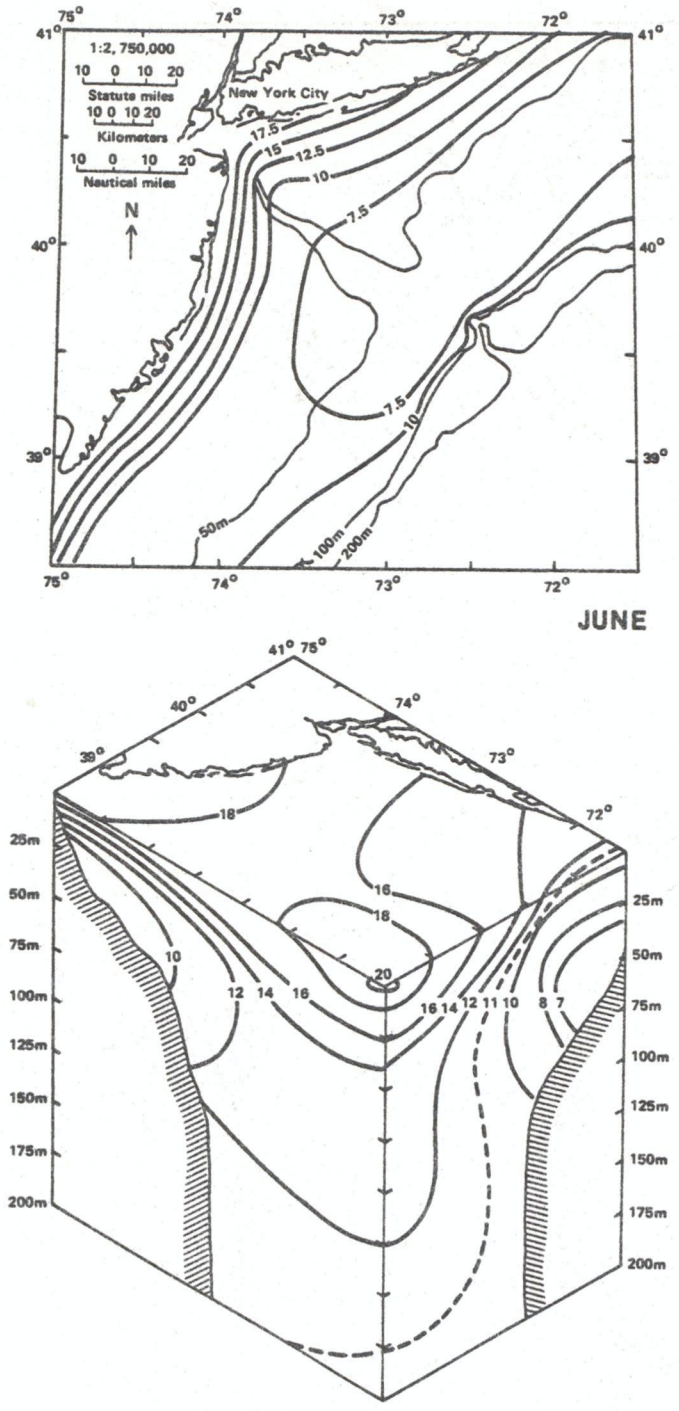

Figure 31.--Mean monthly temperature distribution in the New York Bight. Map pairs show bottom contours (top), surface and vertical contours (bottom). Units are °C. (after Bowman and Lewis, 1977)

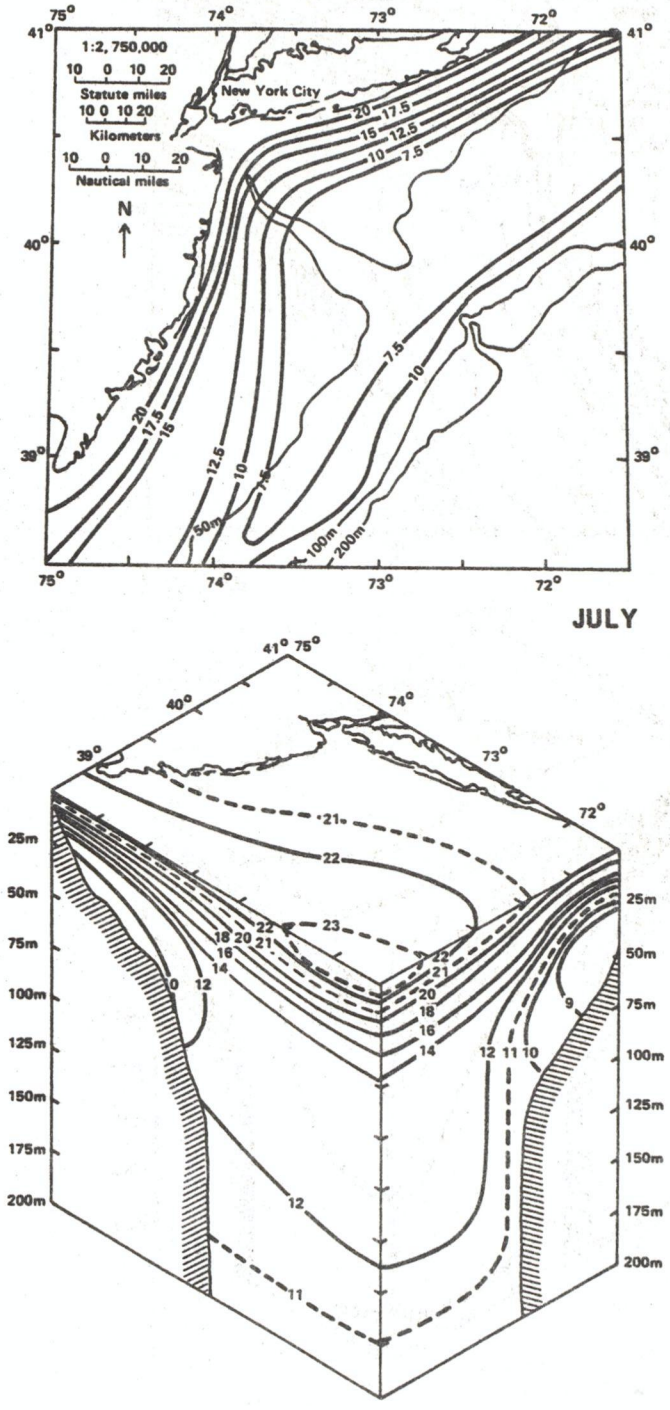

Figure 32.--Mean monthly temperature distribution in the New York Bight. Map pairs show bottom contours (top), surface and vertical contours (bottom). Units are ^{o}C. (after Bowman and Lewis, 1977)

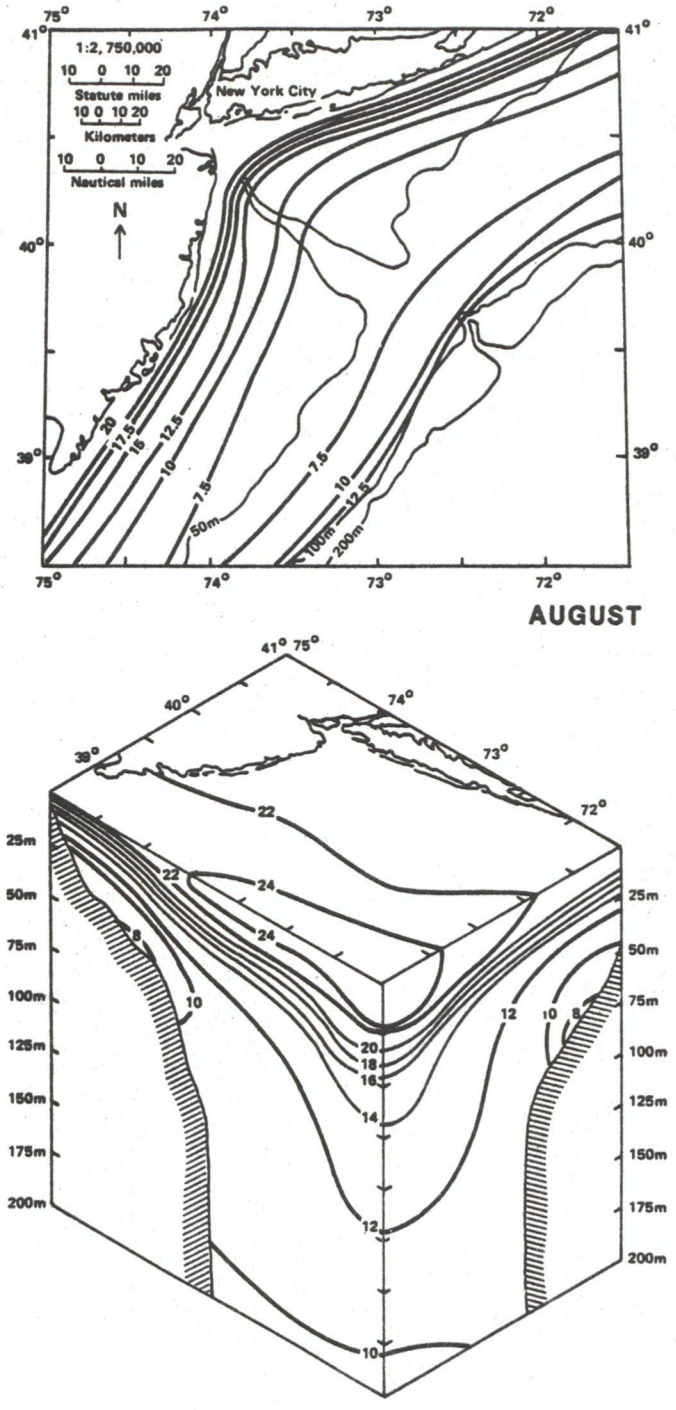

Figure 33.--Mean monthly temperature distribution in the New York Bight. Map pairs show bottom contours (top), surface and vertical contours (bottom). Units are ^{o}C. (after Bowman and Lewis, 1977)

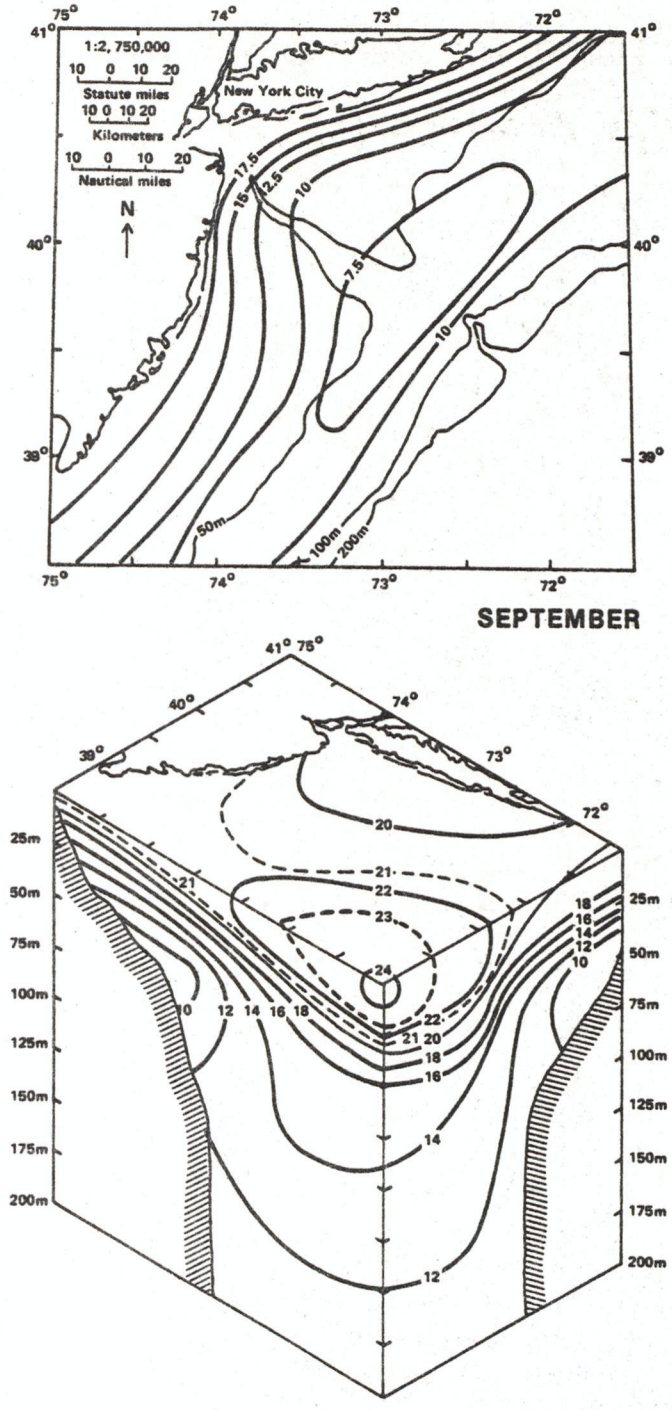

Figure 34.--Mean monthly temperature distribution in the New York Bight. Map pairs show bottom contours (top), surface and vertical contours (bottom). Units are °C. (after Bowman and Lewis, 1977)

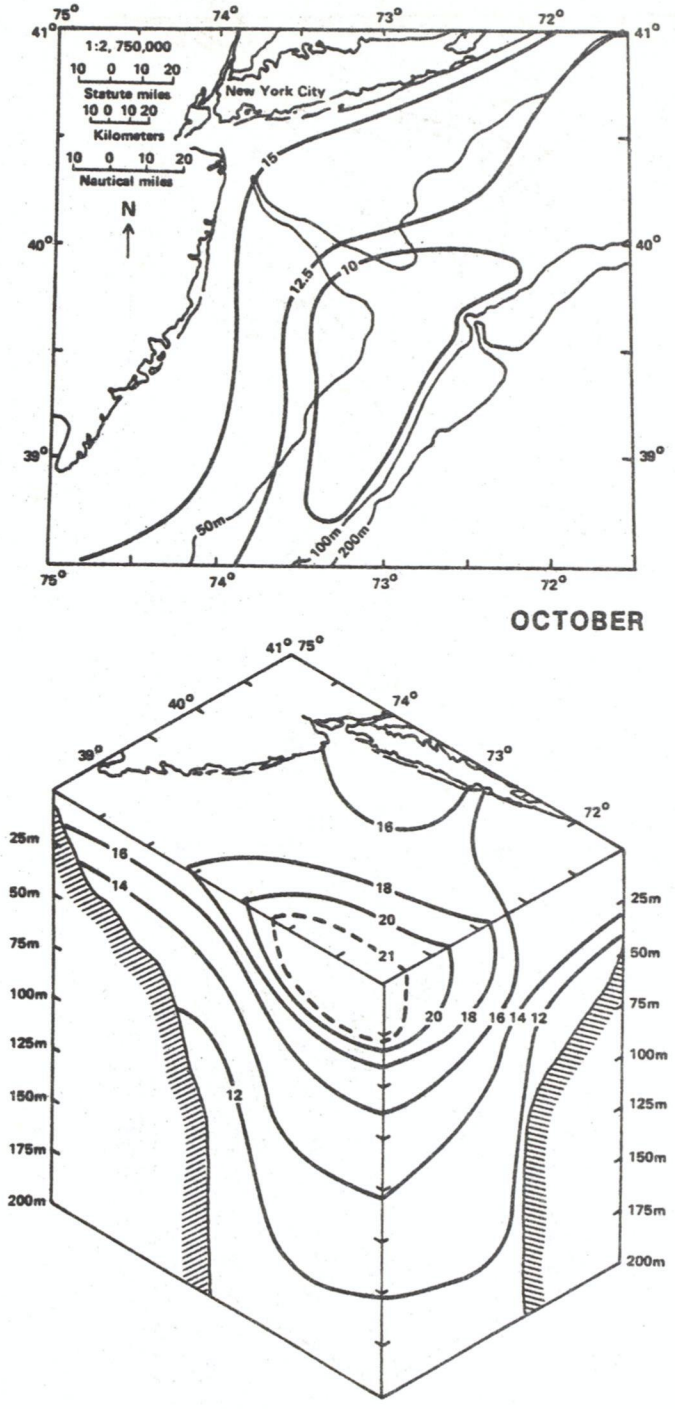

Figure 35.--Mean monthly temperature distribution in the New York Bight. Map pairs show bottom contours (top), surface and vertical contours (bottom). Units are ^{o}C. (after Bowman and Lewis, 1977)

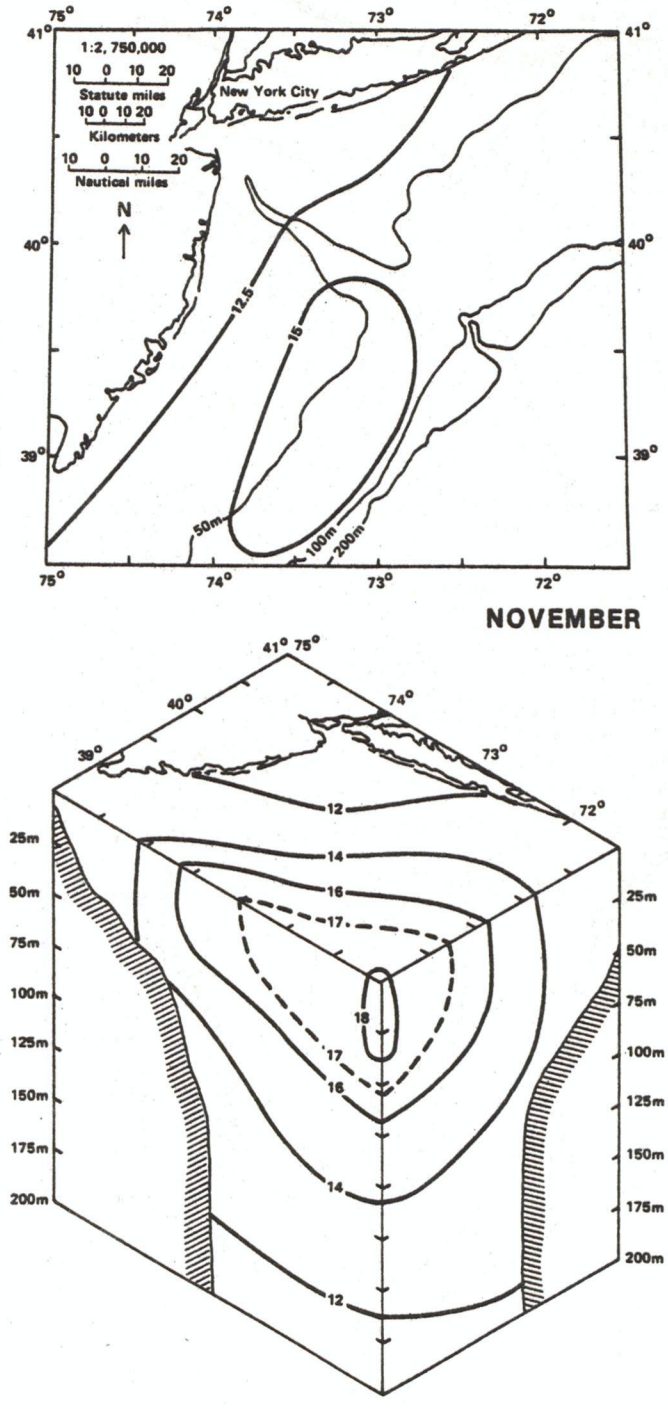

Figure 36.--Mean monthly temperature distribution in the New York Bight. Map pairs show bottom contours (top), surface and vertical contours (bottom). Units are °C. (after Bowman and Lewis, 1977)

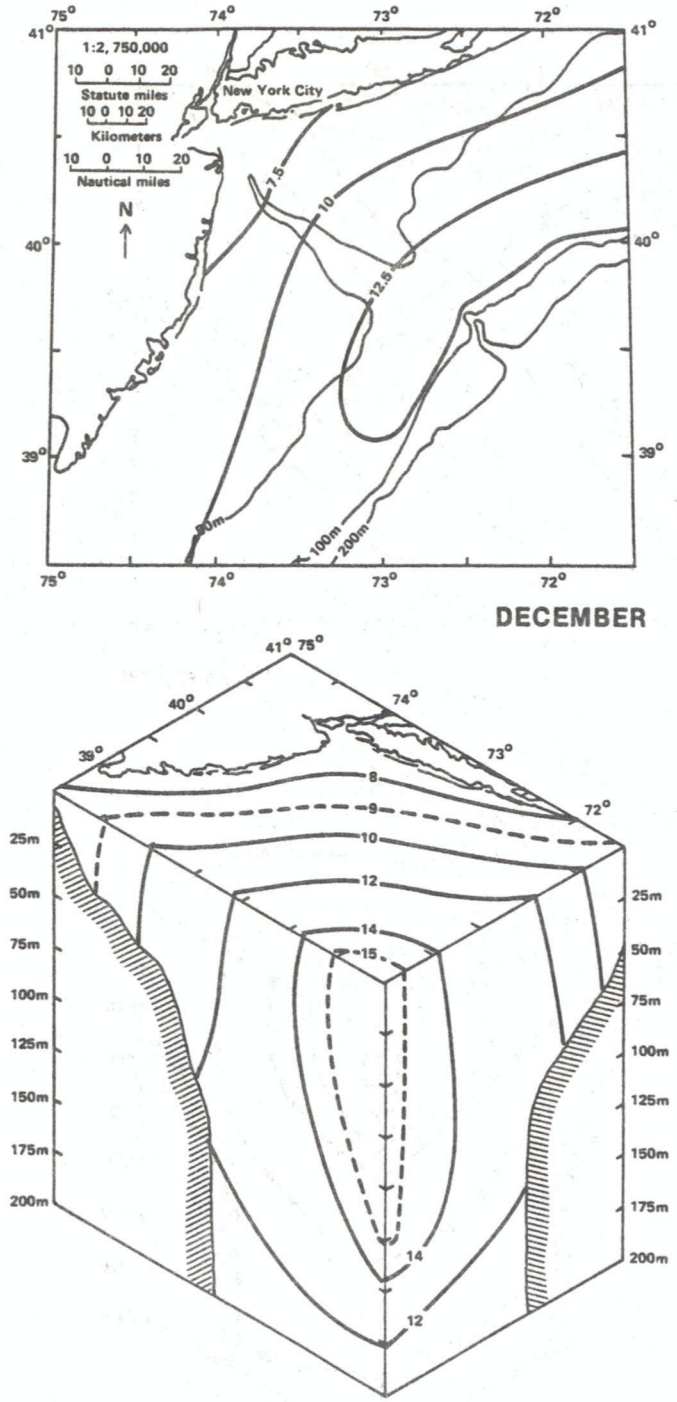

Figure 37.--Mean monthly temperature distribution in the New York Bight. Map pairs show bottom contours (top), surface and vertical contours (bottom). Units are ^{o}C. (after Bowman and Lewis, 1977)

3.3.2 Sea-Surface Temperature (remote sensing techniques)

The "average" picture of water temperatures presented in the previous section is clearly an oversimplification that tends to smooth out the convoluted fronts and sharp gradients which may exist. The complexity of the sea surface temperature structure in this region has been confirmed by high resolution satellite imagery.

One operational product based on these satellite images is the analysis which has been produced weekly by the USCG Oceanographic Unit, the U.S. Navy, and NOAA. Each analysis, based on several days of observation, shows the positions of the major thermal fronts in schematic form and the locations of cold and warm eddies, and identifies the different water masses. Two of these analyses (figs. 38 and 39) show, for example, that conditions can range from the relatively simple to the complicated; both are for the same month (April) but two different years. These analyses may be obtained by writing to:

NOAA/NESS S132
Director, Environmental Products Br.
World Weather Bldg., Room 510
Washington, DC 20233

Satellites are extremely valuable tools to map large scale circulation features such as permanent currents, water mass boundaries, and large eddies, but they do have limitations.

1. At best, they record only the skin temperature of the ocean, as opposed to the bulk temperature measured by ordinary, immersed thermometers. Except during periods of unusual calm, the normal stirring by waves eliminates this as a serious problem. However, even bulk surface temperatures are not reliable indicators of deeper temperature patterns.

2. More serious is the effect of water vapor in the intervening atmosphere on satellite measurements. These errors can be corrected to some extent by using an assumed water vapor profile from a model atmosphere. A better solution will be possible with the forthcoming advances which will have two infrared bands that respond quite differently to water vapor. The differences in measured radiance can be used to determine the atmospheric correction. It is expected that absolute temperatures should be accurate to about 1°C. (Research Institute of the Gulf of Maine, 1974).

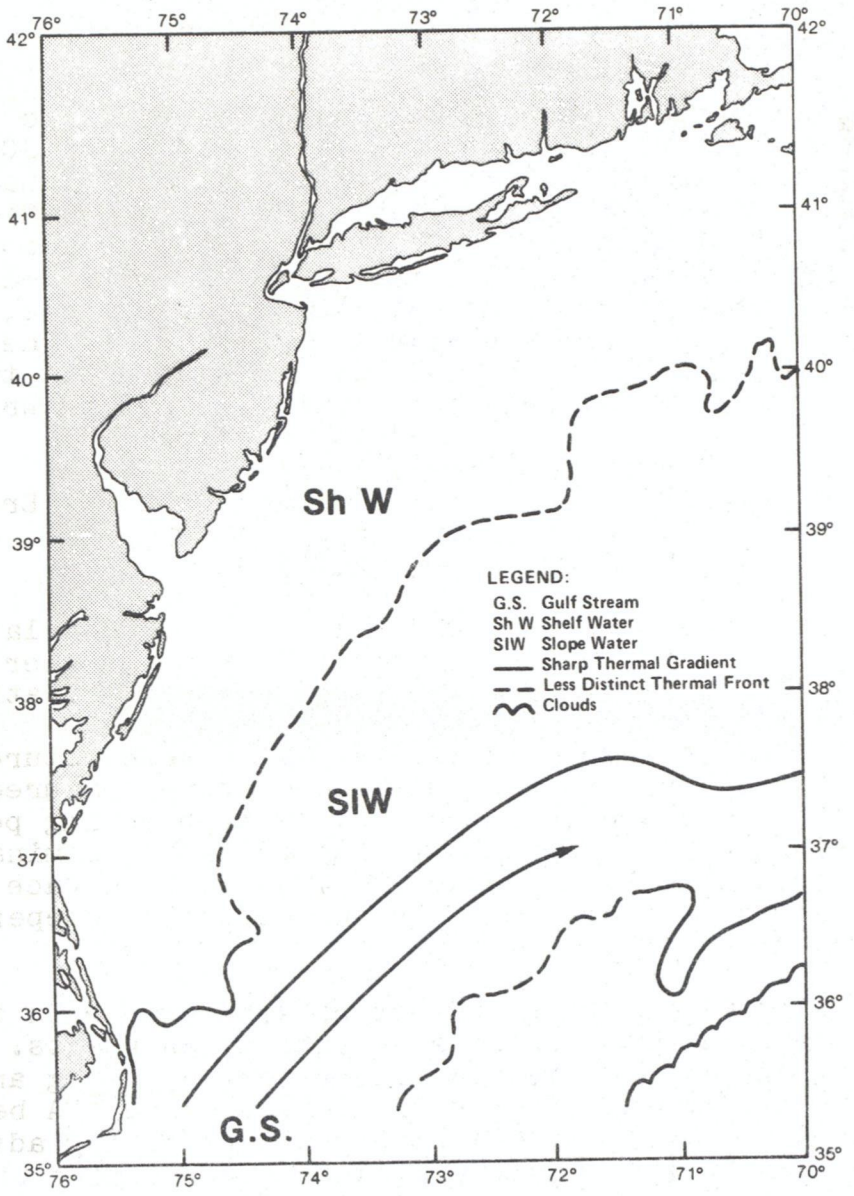

Figure 38.--Experimental Gulf Stream analysis produced by NOAA satellite monitoring (after the Research Institute of the Gulf of Maine, 1974)

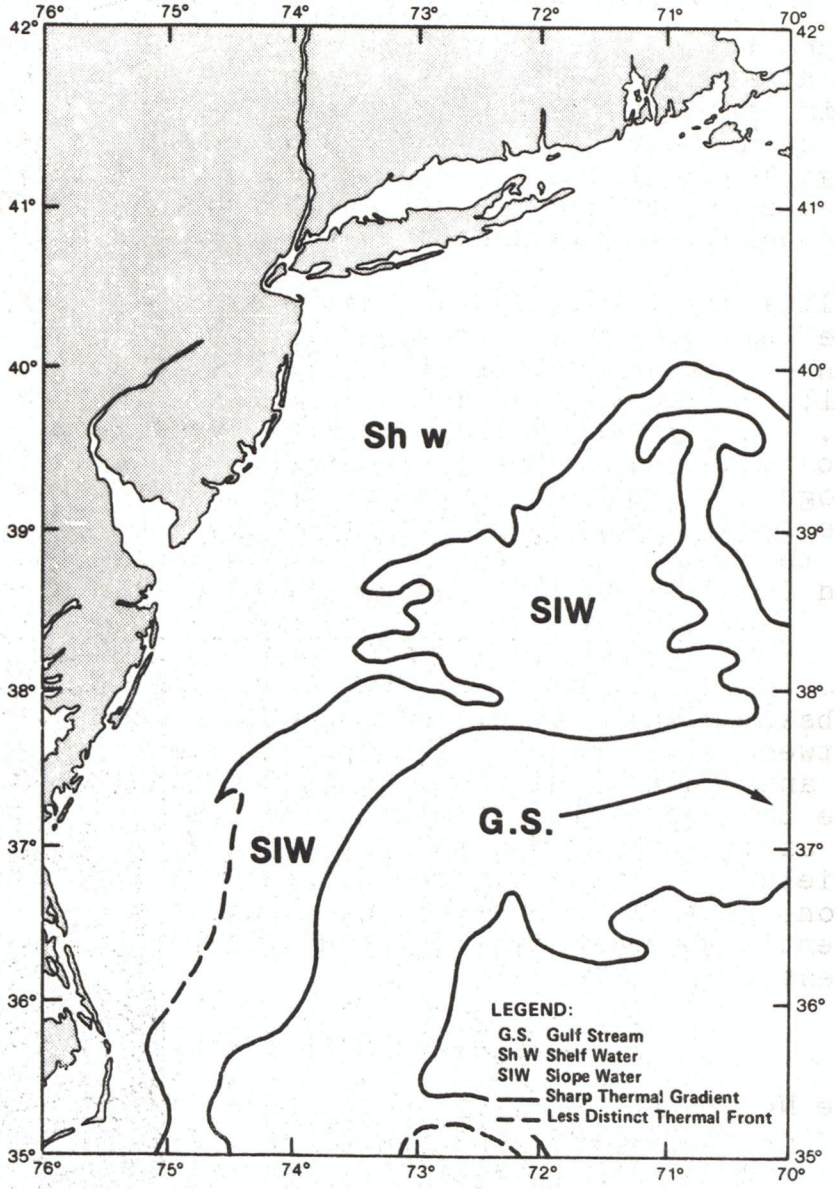

Figure 39.--Experimental Gulf Stream analysis produced by NOAA satellite monitoring (after the Research Institute of the Gulf of Maine, 1974)

3. Cloud cover is a serious limitation to satellite mapping, since sea-surface temperatures can be observed only when the satellite pass happens to coincide with a cloud-free period. Oceanic phenomena change more slowly than those in the atmosphere, so that the continually improving coverage in time will eliminate much of this problem, except for periods of extended cloud cover.

A second technique for mapping sea-surface temperatures is the use of air-borne radiation thermometry (ART). This technique is useful in locating the region of sharp gradients, such as those that occur near major current boundaries and large scale eddies (fig. 40). Except for special studies, ART data should be supplemented by satellite imagery which provides broader coverage and is more nearly instantaneous over a large area.

For climatological purposes, the best regular reports on sea-surface temperature are provided by "Gulfstream", a monthly publication of the National Weather Service. The reports are based on all available information from ships, aircraft, and satellites. Each issue includes a schematic drawing of the locations of the oceanic fronts and eddies, a selection of bathythermograms (BTs) and charts giving the mean surface temperature for the month, anomaly from the 100-year mean for the month, and the change from the previous month, all on a one-degree grid from 25° to 45°N and 55° to 85°W.

3.4 Salinity Distribution

The observed salinity distribution is a result of the balance between river runoff, evaporation minus precipitation, advection, and mixing. Salinity is at a maximum at the end of winter (due to subfreezing conditions on the continent) and at a minimum in early summer (due to spring runoff). Although the salinity field is critical in the determination of the density distribution, salinity charts are not presented here, since there is no presently accepted link between this parameter and oil spill processes.

3.5 Density Distribution

In the New York Bight region the water reaches its maximum density during the winter months because of the annual minimum in temperature and maximum in salinity. In the spring, vernal warming of the suface water coupled with a large increase in runoff produce a marked vertical and horizontal stratification of the water column. The resulting cross-shelf horizontal stratification drives a southward directed coastal flow that increases in magnitude (i.e., 10-15 cm/sec) into late summer. This mean baroclinic (density driven) current may be important in

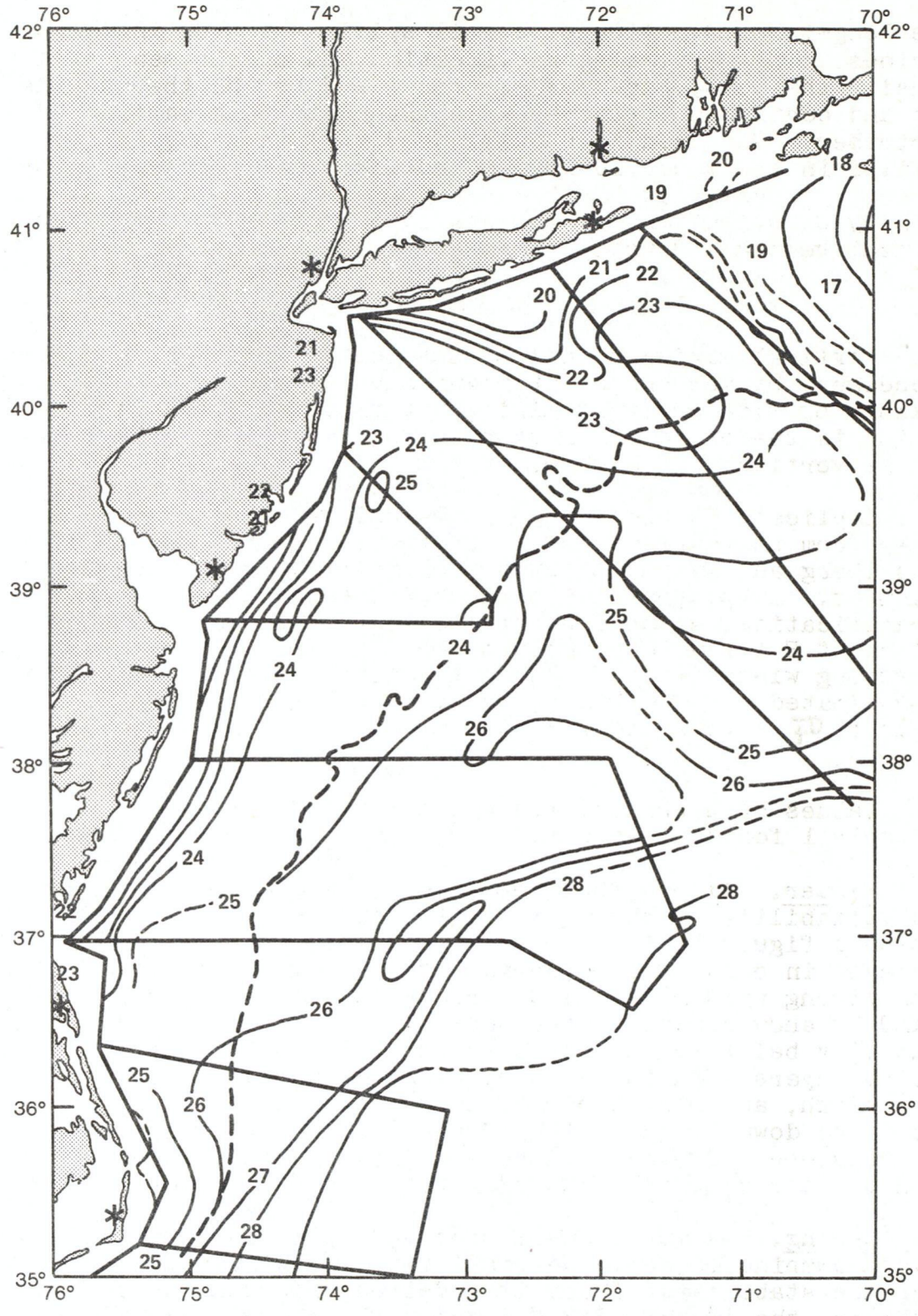

Figure 40.--Sea-surface temperature through U.S. Coast Guard Airborne Radiation Thermometer (after the Research Institute of the Gulf of Maine, 1974)

the long-term advection of an oil spill at sea during calm periods. The vertical stratification and development of a sharp density change (pycnocline) starts (as does the thermocline) in May and continues to increase in intensity to a maximum in September. This condition will lead to a tendency for oil spilled in the upper 10-15 m mixed layer to be trapped above the strong pycnocline at 15-30 m. Figures 41 to 45 show the mean density distribution for the New York Bight. Figure 46 shows typical vertical density profiles.

3.6 Vertical Mixing

Vertical mixing of oil in the ocean can occur by convective processes, by mechanical stirring such as surface wind-wave mixing, by tidal current mixing, or by diffusion. Vertical mixing is therefore a function of the density stratification and of the vertical turbulence.

Implications regarding the extent of vertical mixing are drawn from the analysis of water "stability," E, defined by Hesselberg and Sverdrup (1914) to be the vertical density gradient. Large positive values of E imply strong vertical stratification, which inhibits vertical mixing; small positive values of E imply deep vertical mixing, as caused, for example, by strong winter winds. Here, E will be closely approximated by $\Delta\sigma_t / \Delta z$, the vertical gradient of sigma-t[σ_t = (density-1)1000], to provide a convenient numerical range.

Values of stability for areas 5, 6, 8, 9, and 12 are given in table 1 for all seasons.

Winter. In mid-shelf areas 5, 6, and 8, stability is low and variability is high. The water column for area 6 in winter, shown in figure 46 is nearly homogeneous with only a slight increase in density from surface to bottom. This is associated with strong wind mixing and surface cooling. The offshore areas 9 and 12 show similar characteristics in the first 100 m, but stability below 100 m decreases smoothly to near zero in the bottom layers. During winter, density increases very gradually with depth, and mixing occurs throughout the water column on the shelf and down to the depth of penetration of seasonal influence on the slope (>200 m). These conditions lead to enhanced mixing of a surface oil spill throughout the water column.

Spring. Warmer temperatures and river runoff in the surface layers combine to decrease density in the surface layers and thus increase stability. There is a decrease in density on both the shelf and the slope. Table 1 shows the slight increase in stability. Under these conditions, vertical mixing will not be

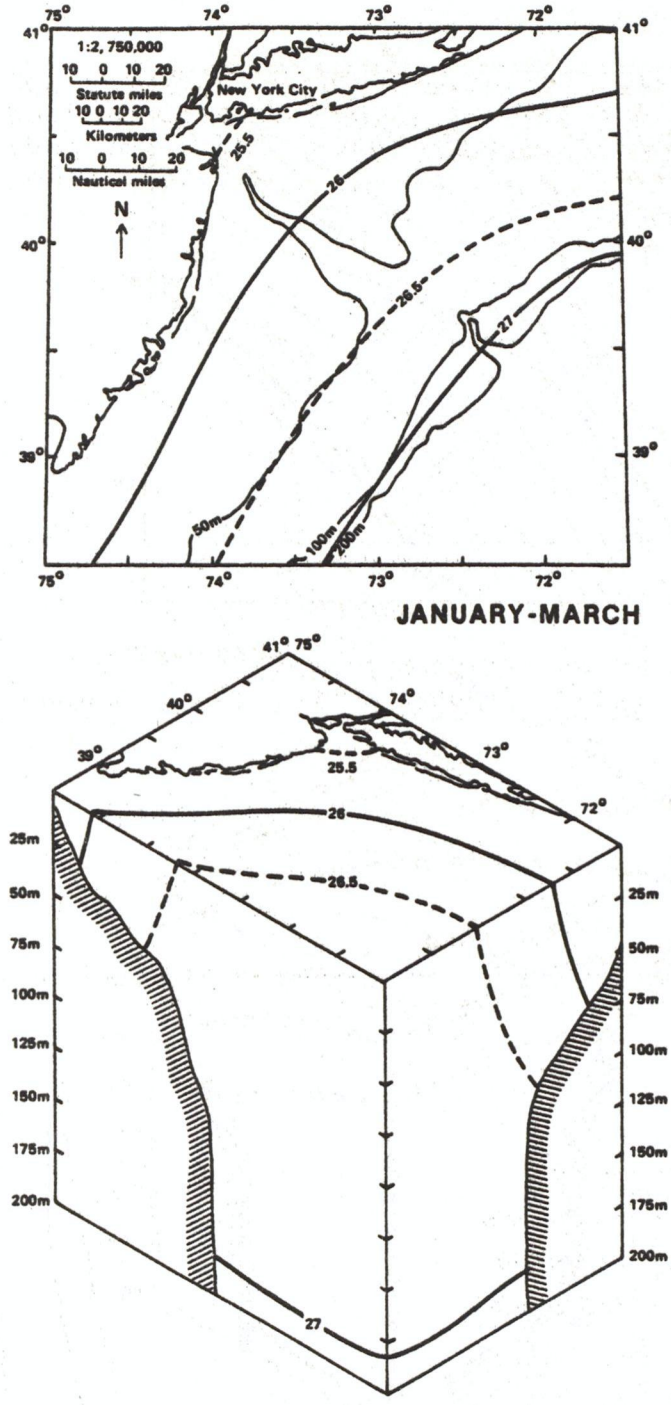

Figure 41.--Seasonal mean density distribution. Map pairs show bottom contours (top), surface and vertical contours (bottom). Units are sigma-t. (after Bowman and Lewis, 1977)

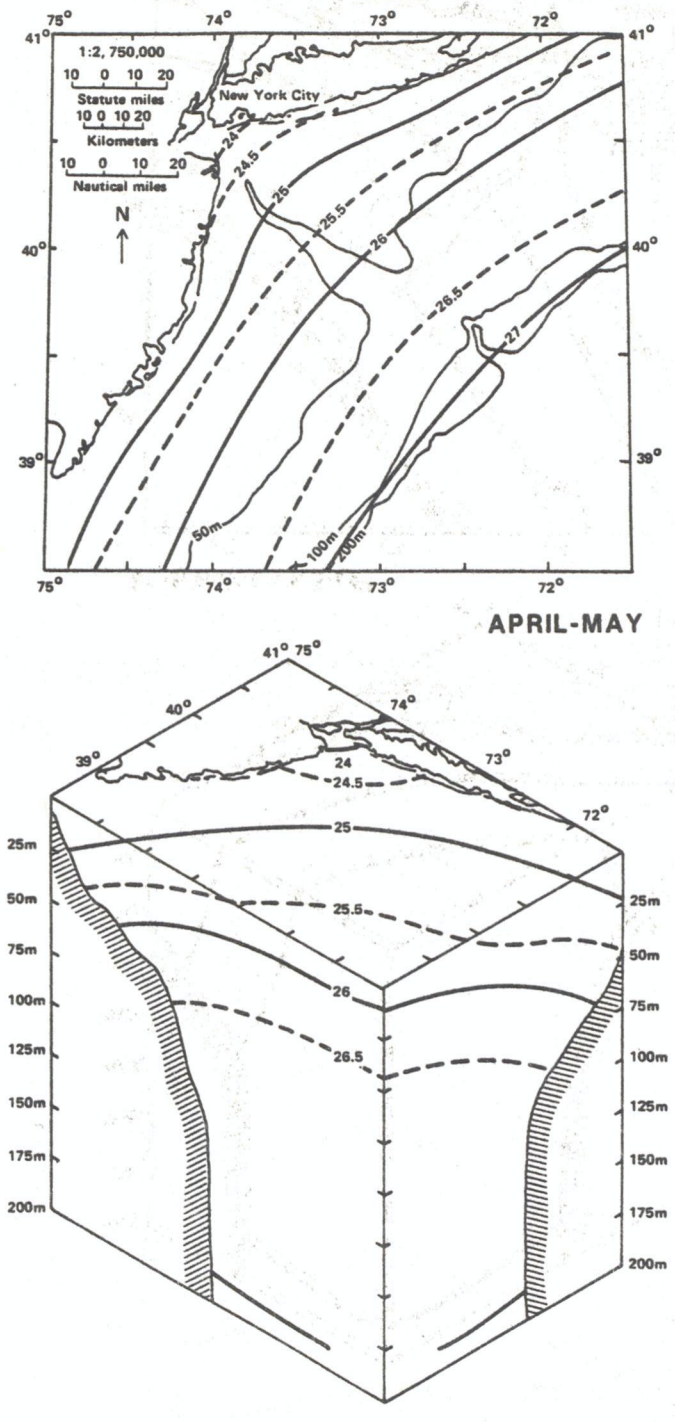

Figure 42.--Seasonal mean density distribution. Map pairs show bottom contours (top), surface and vertical contours (bottom). Units are sigma-t. (after Bowman and Lewis, 1977)

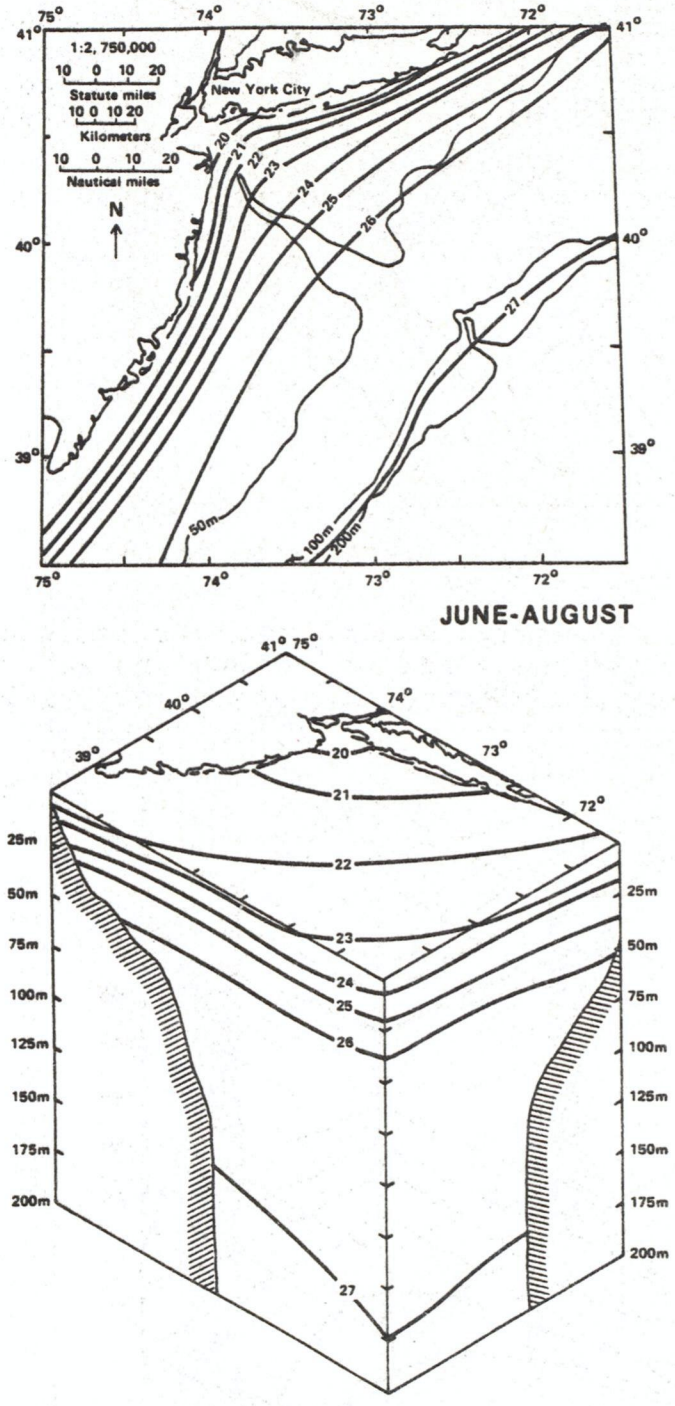

Figure 43.--Seasonal mean density distribution. Map pairs show bottom contours (top), surface and vertical contours (bottom). Units are sigma-t. (after Bowman and Lewis, 1977)

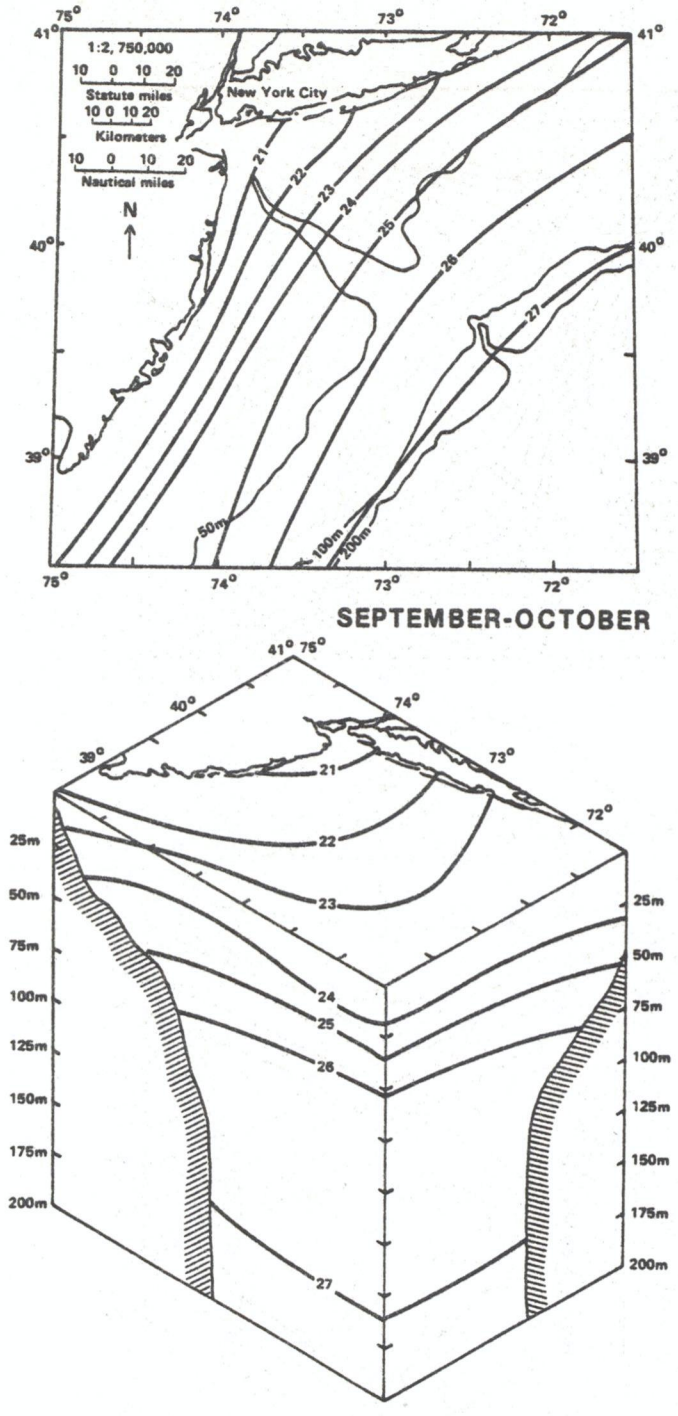

Figure 44.--Seasonal mean density distribution. Map pairs show bottom contours (top), surface and vertical contours (bottom). Units are sigma-t. (after Bowman and Lewis, 1977)

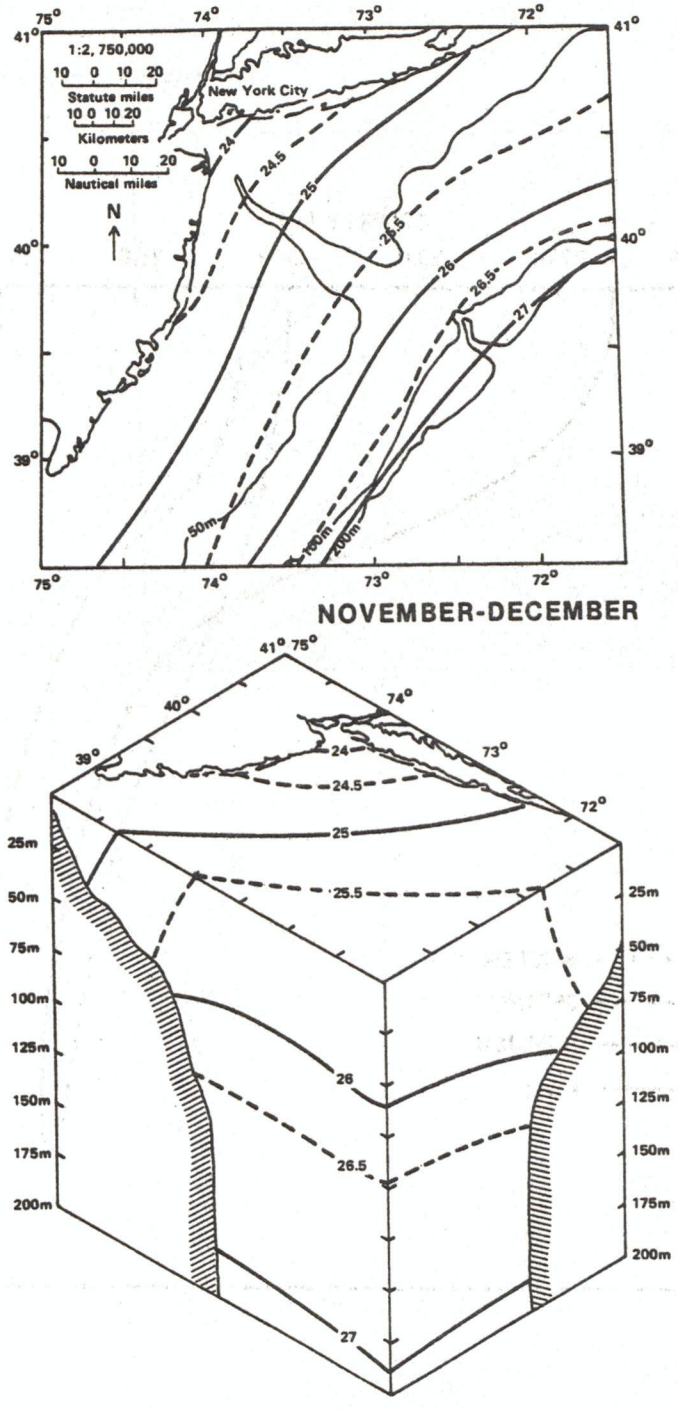

Figure 45.--Seasonal mean density distribution. Map pairs show bottom contours (top), surface and vertical contours (bottom). Units are sigma-t. (after Bowman and Lewis, 1977)

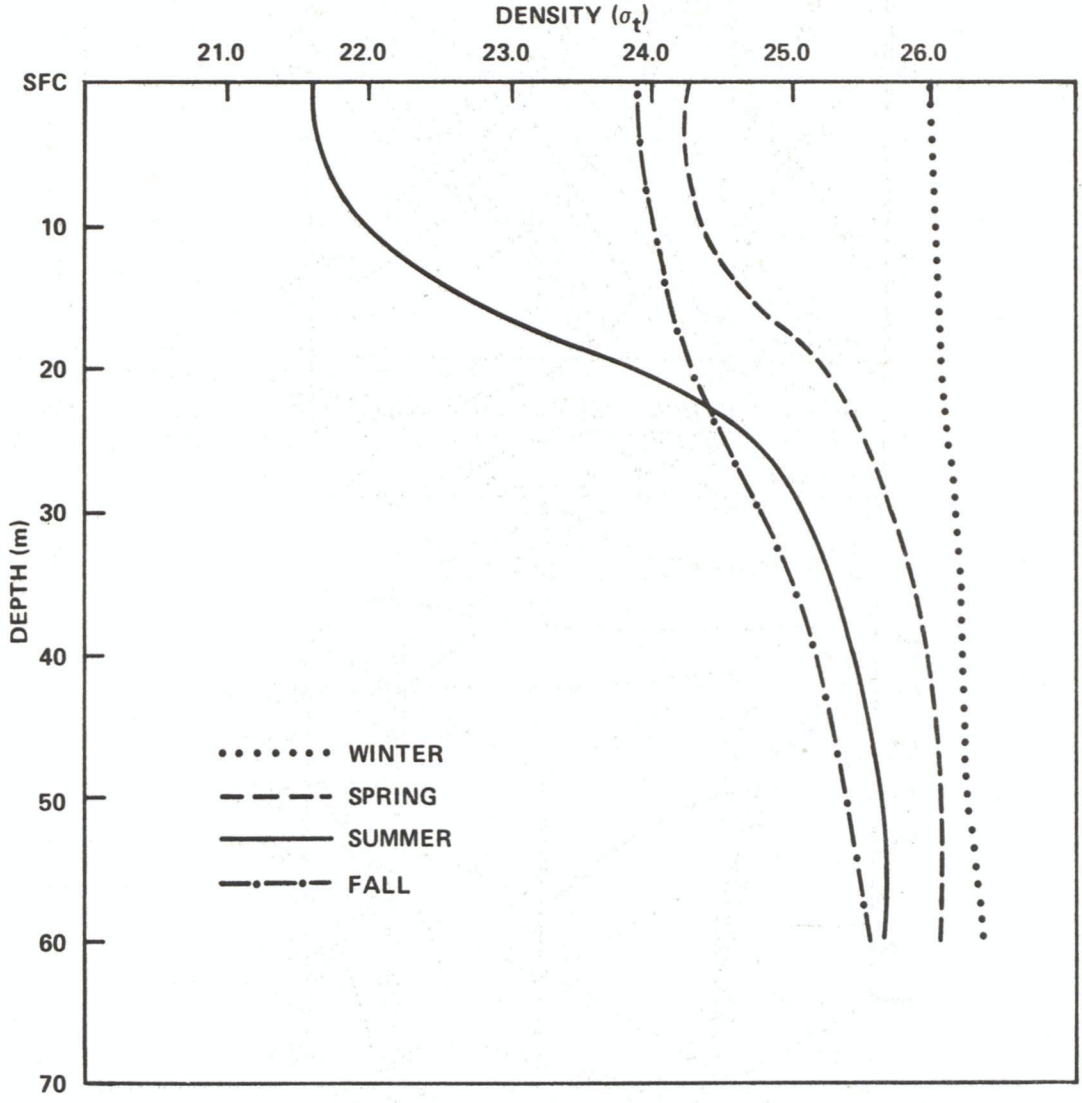

Figure 46.--Mean vertical density profiles for area 6 (after Williams and Godshall, 1977)

Table 1.--Vertical stability E = $(\Delta\sigma_t / \Delta z) \times 10^3$ (after Williams and Godshall, 1977)

Depth (m)	Winter Mean	Winter Stand. dev.	Spring Mean	Spring Stand. dev.	Summer Mean	Summer Stand. dev.	Fall Mean	Fall Stand. dev.
				Area 5				
10	9.1	20.6	54.1	51.5	100.0	43.4	8.0	13.0
20	15.2	3.2	49.3	36.7	92.8	41.6	6.2	13.8
30	2.2	6.7	23.5	14.6	61.5	22.9	6.3	8.3
40	1.7	2.8	14.4	8.4	33.2	16.7	13.0	12.1
50					30.0	7.1		
				Area 6				
10	5.3	20.5	74.5	108.8	167.0	123.2	16.1	28.6
20	17.4	36.2	74.5	85.6	125.4	81.1	44.1	68.8
30	6.2	14.2	29.0	42.1	65.3	45.3	26.6	32.1
40	2.0	6.0	9.6	10.1	31.6	19.5	38.4	13.1
				Area 8				
10	24.7	74.5	147.9	164.7	226.4	225.5	50.2	104.7
20	2.6	5.8	38.4	45.9	119.8	102.0	14.8	27.2
				Area 9				
10	2.5	4.8	5.0	28.9	50.2	49.2	9.5	29.3
20	3.1	5.0	30.0	19.6	64.4	36.4	10.9	19.5
30	4.3	6.3	22.3	23.4	63.8	19.8	15.2	19.7
40	4.3	5.3	19.8	9.6	48.6	17.3	16.8	18.0
50	4.0	4.3	14.3	7.2	32.8	11.2	16.7	13.8
60	3.5	4.0	8.3	13.7	23.0	8.3	16.8	12.6
70	3.6	3.6	8.9	12.1	16.5	6.5	14.5	9.4
80	3.6	4.5	6.7	8.5	12.8	5.3	12.9	10.0
90	3.7	4.1	7.3	6.6	9.6	4.3	11.5	7.8
100	3.2	3.2	7.1	8.2	7.6	3.6	10.1	5.1
				Area 12				
10	0.1	13.8	53.3	84.2	123.6	148.7	26.3	52.5
20	2.5	5.7	36.6	35.4	130.3	95.0	26.6	31.0
30	2.8	7.2	19.3	22.0	58.2	50.4	34.9	28.0
40	2.5	4.4	18.4	15.3	36.1	24.8	29.6	22.4
50	1.9	2.8	15.0	11.5	25.8	17.8	22.9	17.8
60	2.6	4.2	13.0	9.6	18.2	16.3	18.4	17.4
70	2.9	2.9	10.3	8.3	15.8	14.6	18.5	12.2
80	3.4	2.7	9.0	6.8	16.0	11.4	20.7	17.5
90	3.5	3.9	8.2	5.5	11.9	7.3	14.9	8.5
100	3.8	4.8	6.6	4.5	8.1	5.4	11.4	8.1

as strong as during winter, but there is no "barrier" to vertical mixing, as occurs in the summer when a strong pycnocline develops.

Summer. Surface heating and inflow of river water are associated with a further increase in the near-surface stability on the shelf (fig. 46). Stability is also high in the top 30 m on the slope, as seen in table 1, with increasing values toward the south. Area 9 shows evidence of a definable mean mixed layer 15 m deep. During this season, a surface oil spill will most probably be trapped in the upper mixed layer due to the development of the strong pycnocline.

Fall. Surface cooling and evaporation increase density both on the shelf and on the slope, resulting in lowered stability of both shelf and slope water (table 1). Autumn convective overturn on the shelf in the fall, with subsequent return to winter conditions, can be quite rapid (within a week) and dramatic, as has been shown by Shonting et al. (1966).

3.7 Ocean Fronts, Meanders, and Eddies

The boundary between coastal (shelf) water and slope water is delineated by a sharp front at about the 200 m isobath (fig. 47). Surface temperature differences across the winter front are about 2° to 4°C to a maximum of 8°C. Salinity differences are on the order 1 to 2 ppt over 10-15 km horizontally and 20 to 40 m vertically. Meanders of the frontal surface of $\pm$ 75 Km (toward land or sea) have been observed to propagate southwest (the opposite of Gulf Stream meanders). The strong horizontal stratification and velocity shears in the frontal region would tend to trap an oil spill in this region.

Anticyclonic eddies that break off from the Gulf Stream are an important mechanism for transferring properties (heat, momentum, salt) from the Gulf Stream to the slope water. They form when a large, inshore Gulf Stream meander detaches to form a clockwise vortex (fig. 48). The strong currents and stratification also make eddy location important in the predictions of oil spill advection.

The meanders of the Gulf Stream occasionally become elongated and pinched off to form separate rings of current that retain their identity for long periods of time. The rings, which break off in the Sargasso Sea, rotate in the counterclockwise, or cyclonic, sense and enclose slope water, which at any depth is colder than the surrounding Sargasso Sea water (fig. 49). Therefore, they are called cyclonic or cold-core rings or eddies. Conversely, those which break off in the slope water

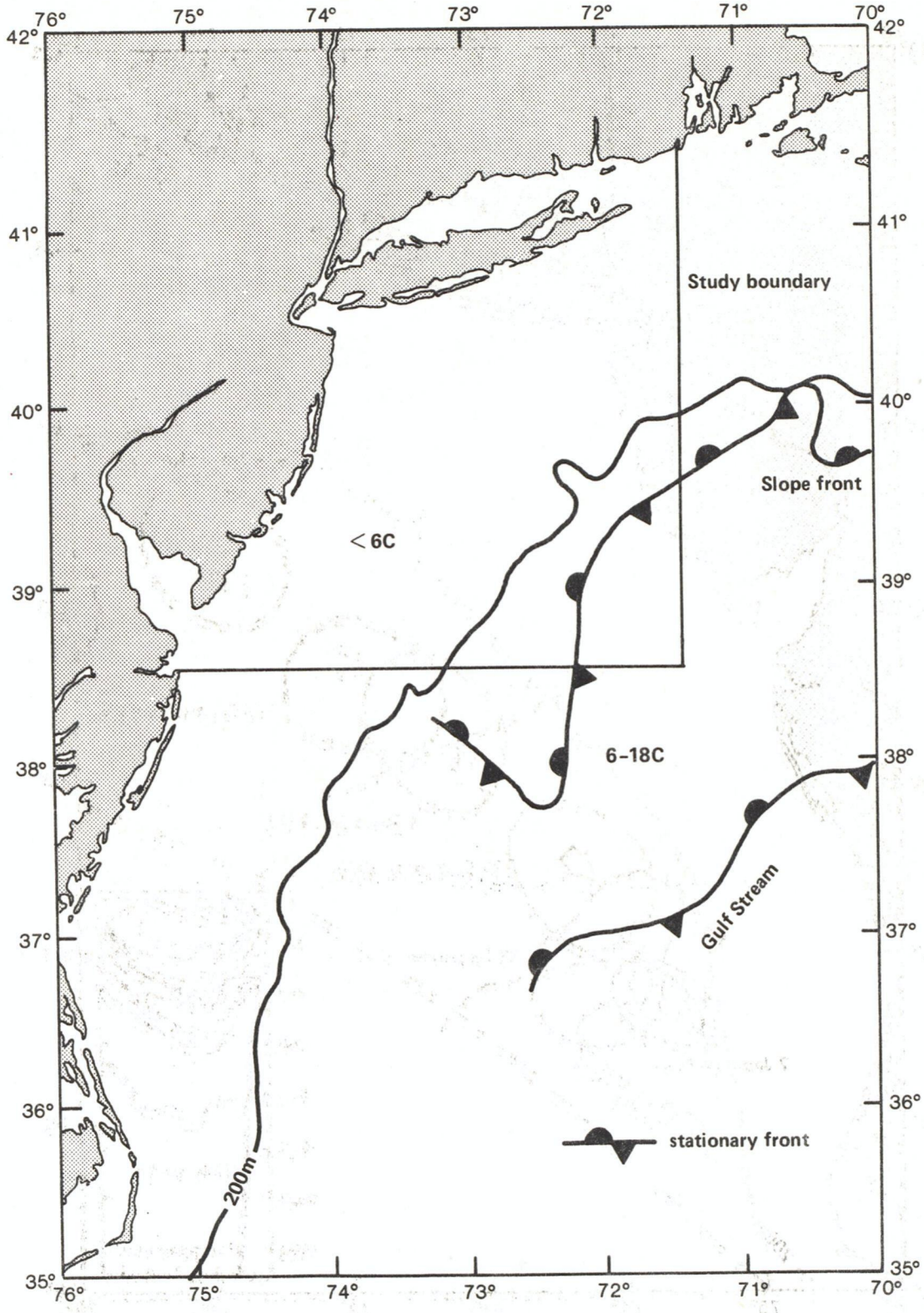

Figure 47.--Slope front and Gulf Stream, March 31, 1970 (after Bowman, 1977)

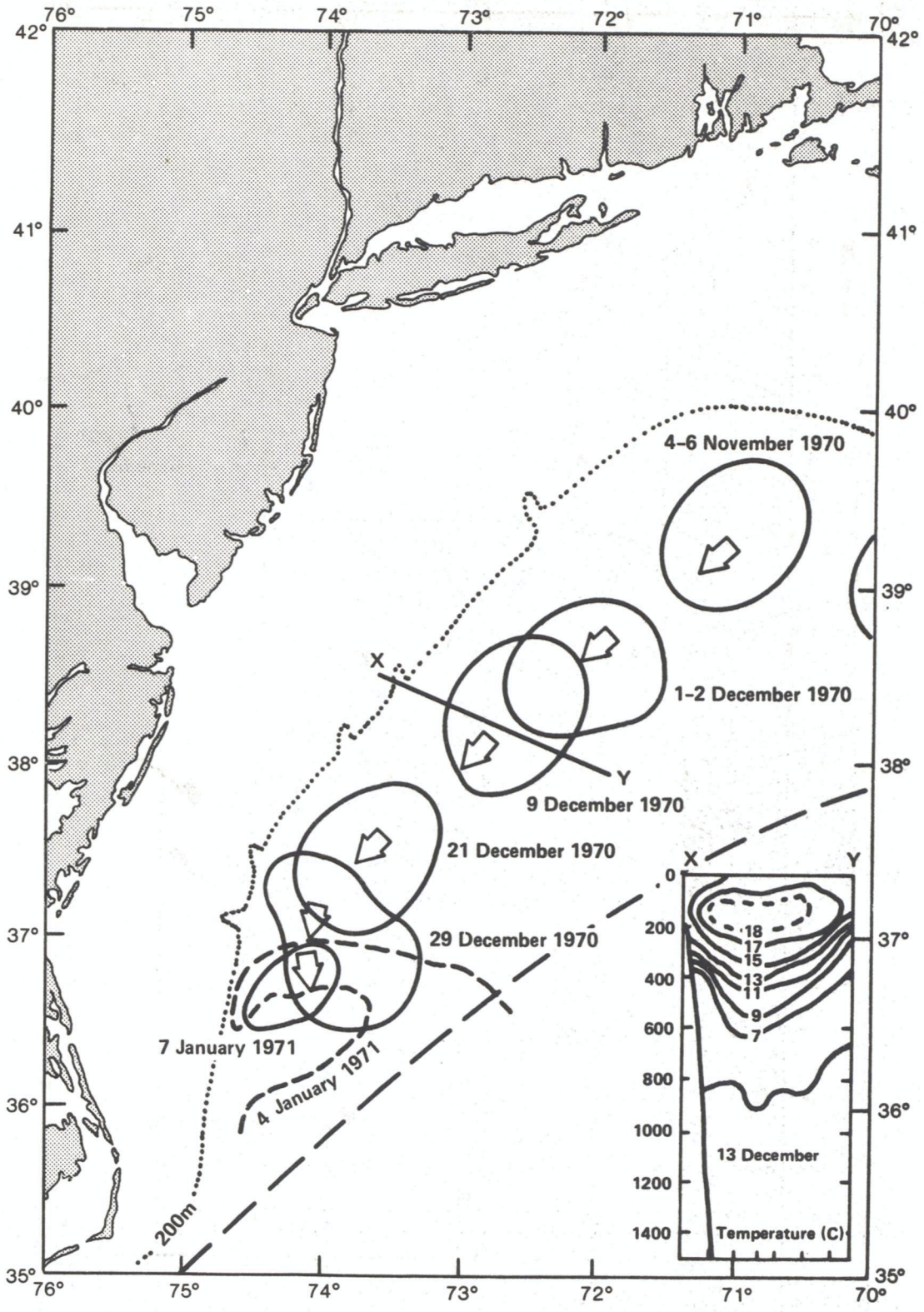

Figure 48.--Drift of anticyclonic eddy (after Bowman, 1977)

rotate clockwise and contain water that is anomalously warmer; they are known as anti-cyclonic or warm core rings or eddies (fig. 50).

The cyclonic rings, five to eight yearly, move off through the Sargasso Sea and either dissipate after about a year or are reassimilated within the Gulf Stream. They are associated with the slope water only as a mechanism for transferring slope water across the Gulf Stream. In contrast, the warmer core rings which bring Sargasso and Gulf Stream water into the slope water are much more important because of the limited area of the slope water and because of the significant role they are believed to play in determining its character and circulation.

The occurrence and movement of warm core rings are being documented by both satellite imagery and ART aircraft flights and the monthly "Gulfstream" summaries now regularly show their shape and position. Most warm-core rings appear to develop in the region of large Gulf Stream meanders east of 66°W, but some are formed in the western slope water. At the same time that the ring is moving, it is also rotating with speeds near the outer edge ranging up to about 1 kt (50 cm/sec). From satellite observations, it appears that the rotating rings entrain surface shelf water along the shelf slope boundary and draw it out into the slope water in long, narrow filaments. Warm-core rings begin to decay shortly after formation; first the surface cools to the temperature of the surrounding slope water, then the warm water begins to mix away around the circumference. The lifetime of a ring is estimated at 6 months to a year, but many appear to be re-absorbed by the Gulf Stream before they lose their identity.

An eddy normally has an elongated shape and, when newly formed, its long axis is oriented east-west. This axis rotates with time, and has a general north-south orientation when the eddy reaches 70° to 71°W. At this point, the eddy shape becomes more rounded and the elongation is not as pronounced.

The diameter of an eddy varies from about 100 to 200 km at the surface, as determined by airborne radiation thermometer observations and temperature gradients. At the 200 m depth (an eddy normally being located by the 15°C isotherm at this depth), the diameter is 70 to 120 km. There is a tendency for an eddy to decrease somewhat in size once it crosses 70°W.

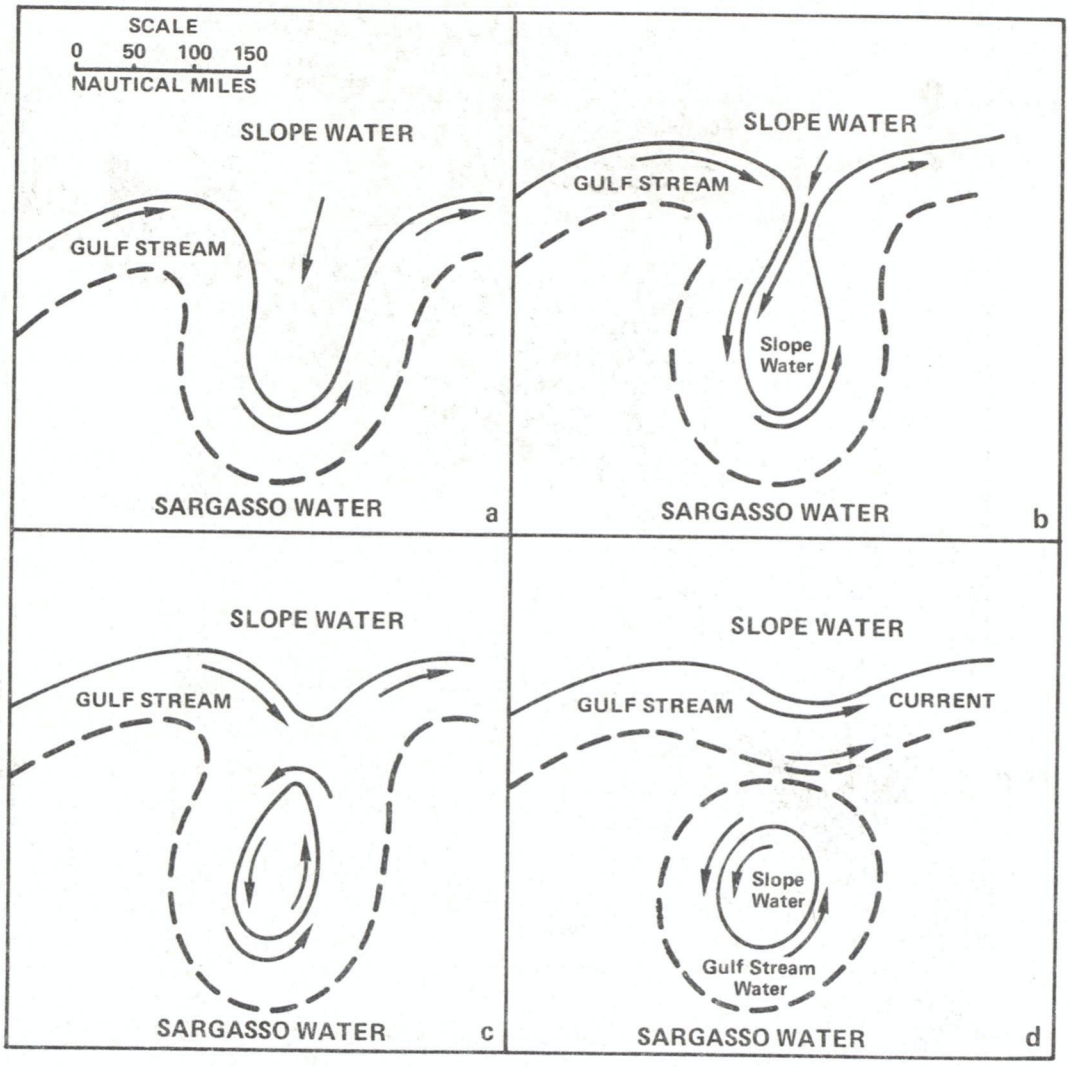

Figure 49.--Diagram of ring formation from meander development to separation of the Stream. Solid lines represent the position of the 15°C isotherm at 200 m. Dashed lines represent the approximate limit of the Sargasso sea and the Gulf Stream. (after the Research Institute of the Gulf of Maine, 1974)

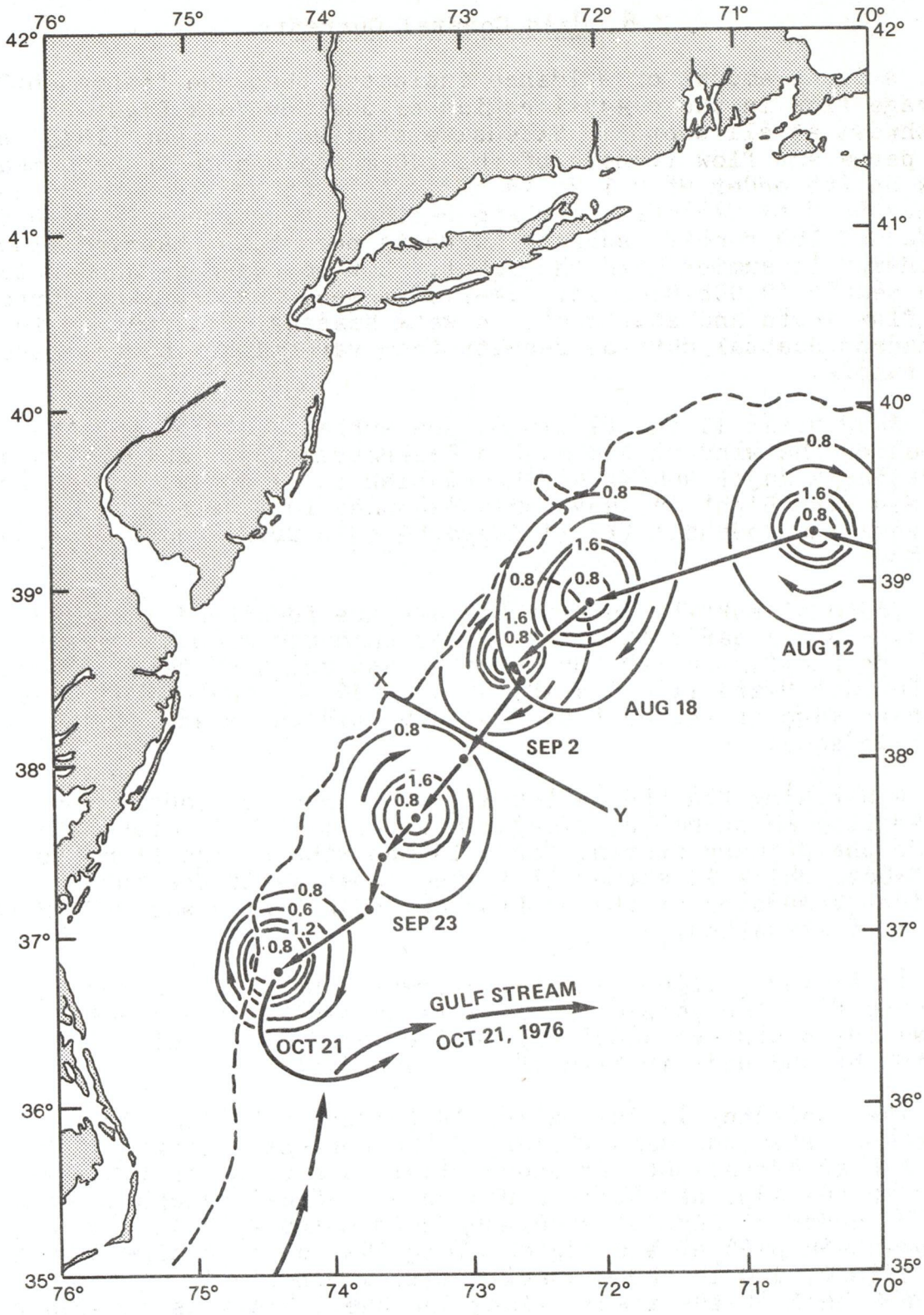

Figure 50.--Surface current speed (Kt) and direction of circulation (after Williams and Godshall, 1977)

3.8 Mean Coastal Currents

A large amount of evidence indicates that the "permanent" average flow in the coastal region of the New York Bight is southwest at all depths. Extensive studies by Bumpus (1973) of the permanent flow inshore of the 100 m isobath indicate a mean flow on the order of 0.1 kt (5 cm/sec) southwest from Nantucket Shoals to Cape Hatteras. During periods of prolonged southwest winds and low runoff, surface currents have been observed flowing northward in summer near the coast. Bottom currents appear to be much weaker (0.008-0.02 kt; 0.4-1.0 cm/sec) than surface currents and flow south and southwest. A weak seasonal fluctuation in the permanent coastal current results from variations in wind stress and runoff.

Ship drift is the result of the surface current and the action of the wind on the ship's superstructure. Ship-drift data represent a major source of information on large-scale flow in the New York Bight and have been examined in some detail. Williams and Godshall (1977) prepared ship drift charts for this region.

Seasonal surface current vectors are presented in figures 51 to 54. They clearly show the well-documented mean southwest flow over the shelf, the turn to seaward just north of Cape Hatteras, and the northward flow seaward of the 200 m isobath along the northern edge of the Gulf Stream. The typical mean speed is 0.1 kt (5 cm/sec).

A striking feature is the lack of strong seasonal variability in currents, except near the mouths of estuaries. In winter the primary driving force is the wind stress from the northwest, while in summer it is the cross-shelf pressure gradient generated by the outflow of low-salinity water from the mouths of estuaries.

In summer, slight seasonal decrease in current strength inferred from the ship-drift data is probably because the prevailing southwest winds oppose the "coastal circulation" created by the distribution of the mass field.

The constancy is the ratio, in percent, of the speed associated with the mean vector of the current velocities to the mean scalar average of the speed; i.e., a current that always flows in the same direction would have a constancy approaching 1. The areas of highest constancy were calculated in the southeastern part of the region along the northern edge of the Gulf Stream, and in the midshelf region, especially in the southern half of the area. Along the shelf break is an area of low constancy, i.e., high variability in current direction. There is little apparent seasonal variation in constancy.

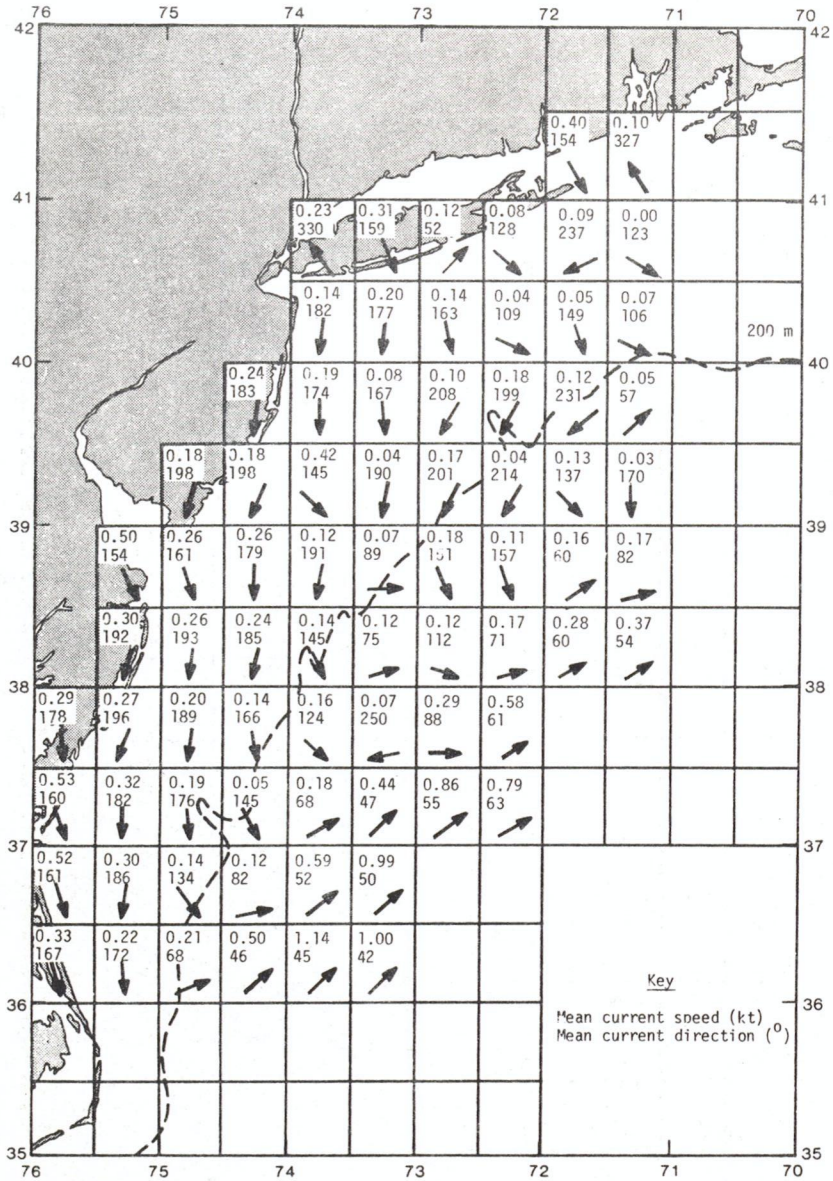

Figure 51.--Winter current vectors (after Williams and Godshall, 1977)

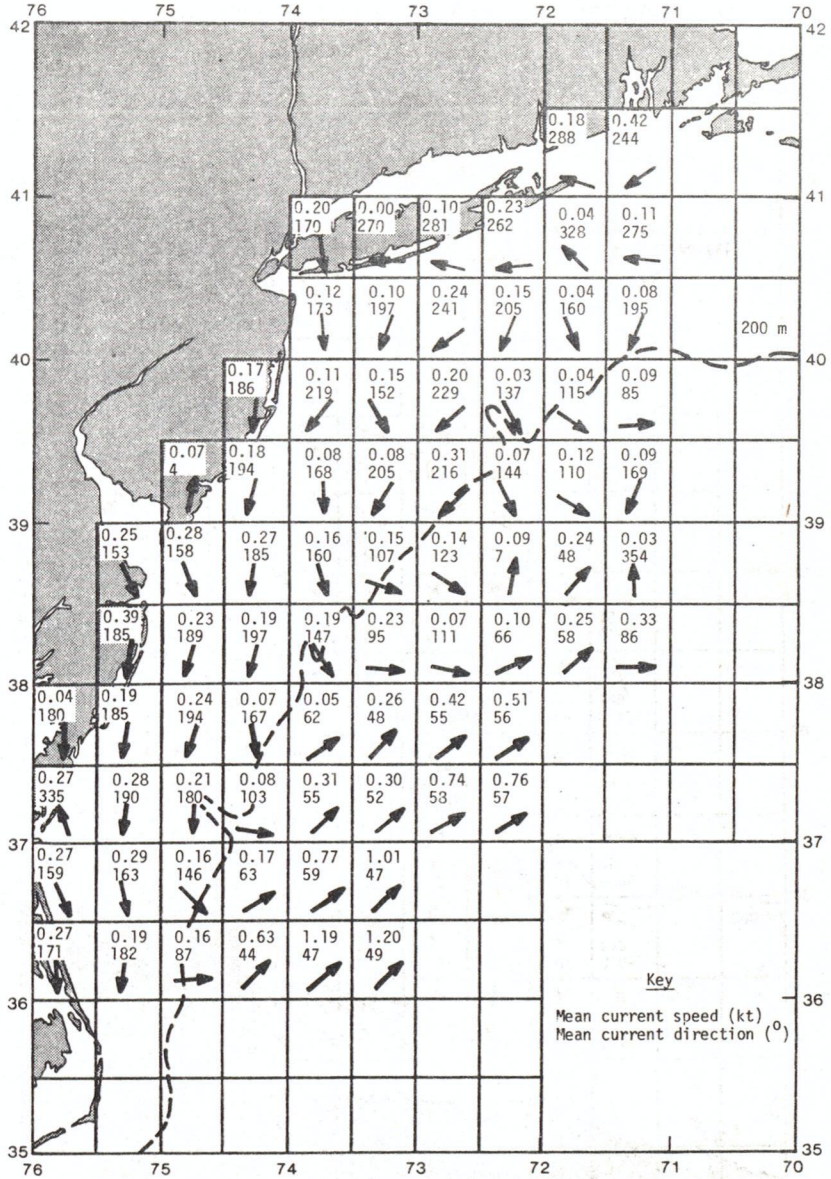

Figure 52.--Spring current vectors (after Williams and Godshall, 1977)

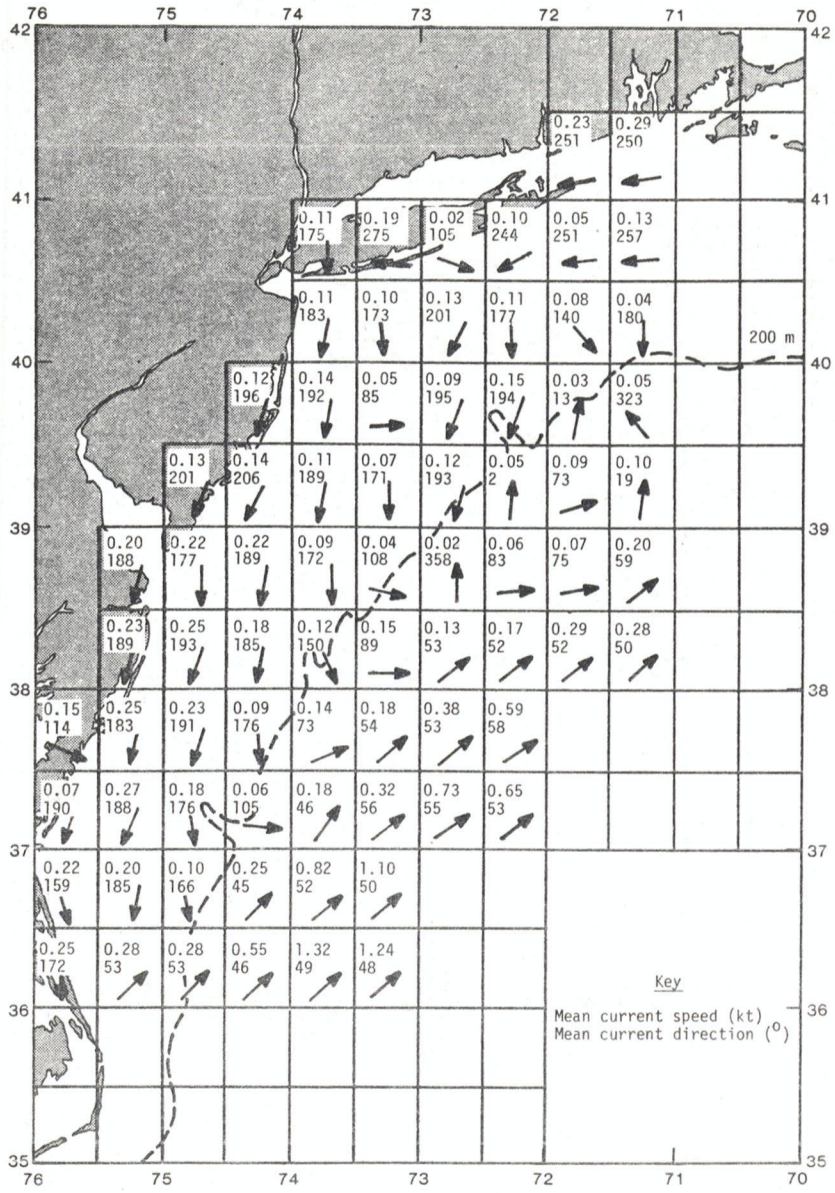

Figure 53.--Summer current vectors (after Williams and Godshall, 1977)

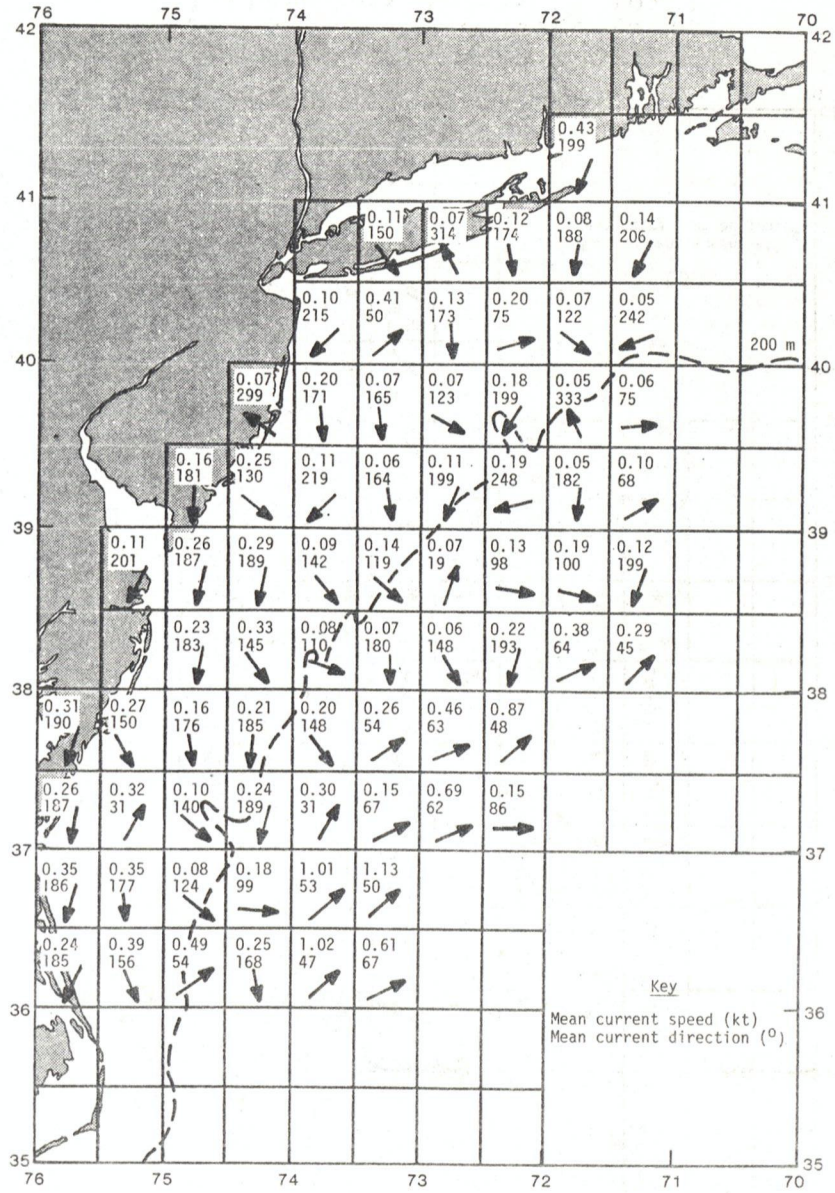

Figure 54.--Fall current vectors (after Williams and Godshall, 1977)

3.9 Simulated Oil Drift Experiment

A field experiment designed to simulate the movement of oil spills in the New York Bight was conducted by the Marine Sciences Center, State University of New York at Stony Brook (Hardy, Baylor, and Moskowitz 1976). More than 21,000 plastic driftcards were released at 24 release points (figs. 55 and 56) between January 23 and September 16, 1974. The results were summarized in terms of summer and winter periods as follows:

> The prevailing wind for the five-month period November to March was west to northwest which imparted a general seaward drift away from Long Island's south shore. In the open outer continental shelf the sea surface motion was generally deflected to the right of the wind by 0° to 10° so that prevailing winds from the west and northwest set up a drift which was seaward from Long Island. The prevailing onshore winds of summer (112° to 147° T) blow toward Long Island. However, the boundary conditions imposed by the land mass of Long Island interfer with the simple downwind transport. This deflects advection more parallel to the shoreline. In these cases, the release-recovery paths of drift cards may appear to be deflected from the wind direction by large angles. The southwest wind appeared to cause the surface layer to move easterly or parallel to the shoreline without converging on Long Island.

3.10 Location of Biological and Recreational Resources

In making an analysis of oil spill impact one must not only consider the trajectory of the oil and the important environmental parameters, but also the resources of the potential impact regions. The following diagrams give the location of selected biological and recreational resources. (figs. 58-105). Relative impact charts (fig. 57) based on the climatological oil trajectory model, as explained in section 3.11, can be combined with such data to estimate relative risk of impact from spills at various locations. These climatological relative risk charts can be used as an overlay on the resource charts (fig. 58-105) to estimate locations of high risk areas.

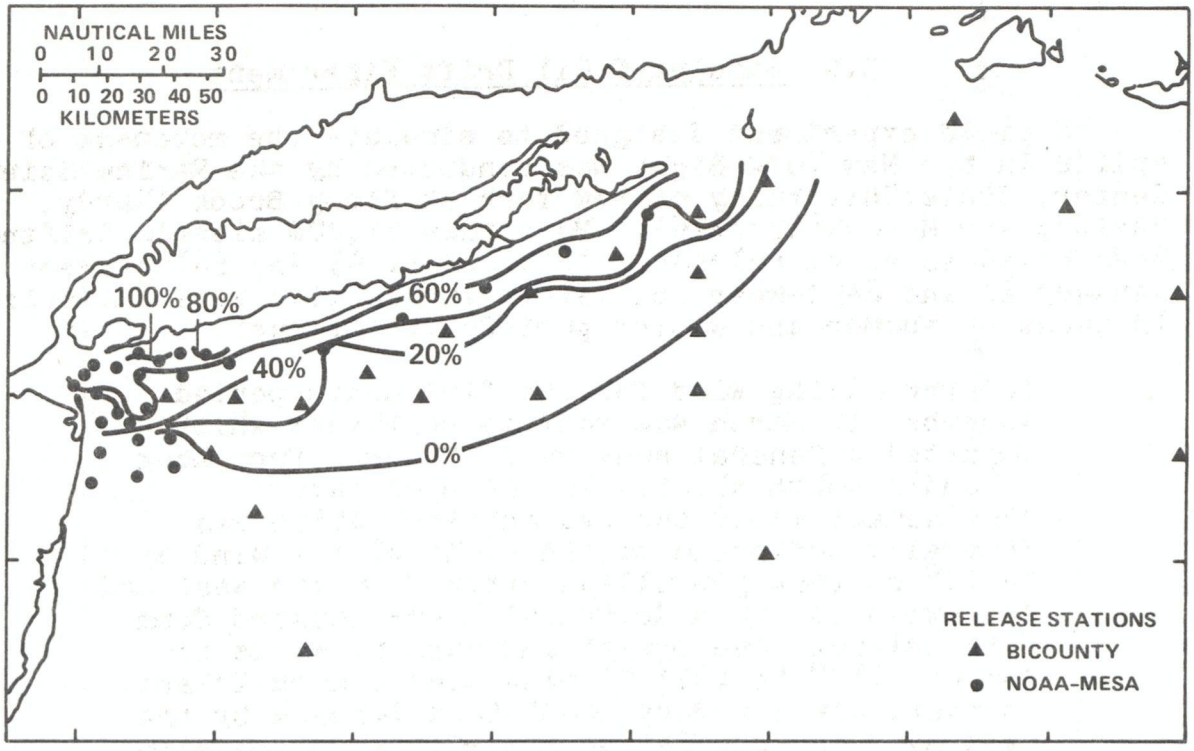

Figure 55.--Percent probability contours that some fraction of oil spills will strand within 10 days on Long Island in winter (January-March) 1974. Based on drift card return frequencies per station (Hardy et al., 1975)

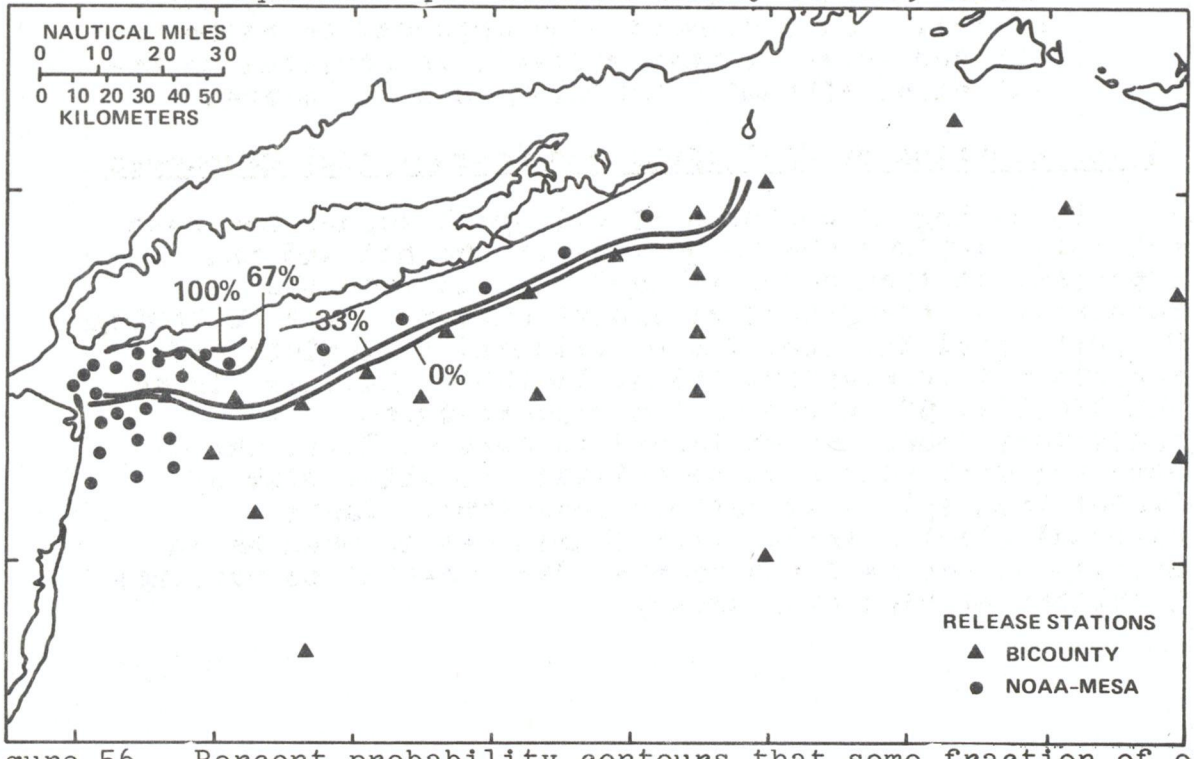

Figure 56.--Percent probability contours that some fraction of oil spills will strand within 10 days on Long Island in summer (April-September) 1974. Based on drift card return frequencies per station (Hardy el al., 1975)

3.11 Calculated Climatological Relative Risk Ellipses of the New York Bight

To obtain a first-order estimate of the most probable path an oil spill will take, a climatological approach was used. This technique is based on the assumption that advection of the oil slick by wind-driven currents is the most important factor. With this approach, wind drift was given as 3 percent of the hourly wind speed directed 15° to the right of the wind. Trajectories were started from a hypothetical spill site and tracked on an area geographic chart by computer for 10 nautical miles by 10 nautical mile areas. The climatological wind record for Kennedy Airport was obtained from the National Climatic Center at Asheville, N.C., and thousands of trajectories were tracted for the summer and winter seasons. The resulting area impacts were divided by the total trajectories, and relative risk ellipses were formed.

These ellipses (fig. 57), will be assumed appropriate for the whole New York Bight region. The ellipses mirror the statistics of the wind field since the winter mean wind is toward the southeast and wind variability is relatively low. Thus the risk calculations show a northwest/southeast elliptical distribution. In the summer, when the mean wind is toward the northeast and variability is high, a more circular distribution is calculated. The use of these ellipses as an overlay on the resource charts is a novel and important technique to estimate spill impact from selected spill sites. Such a use would be essential in pre-spill contingency planning.

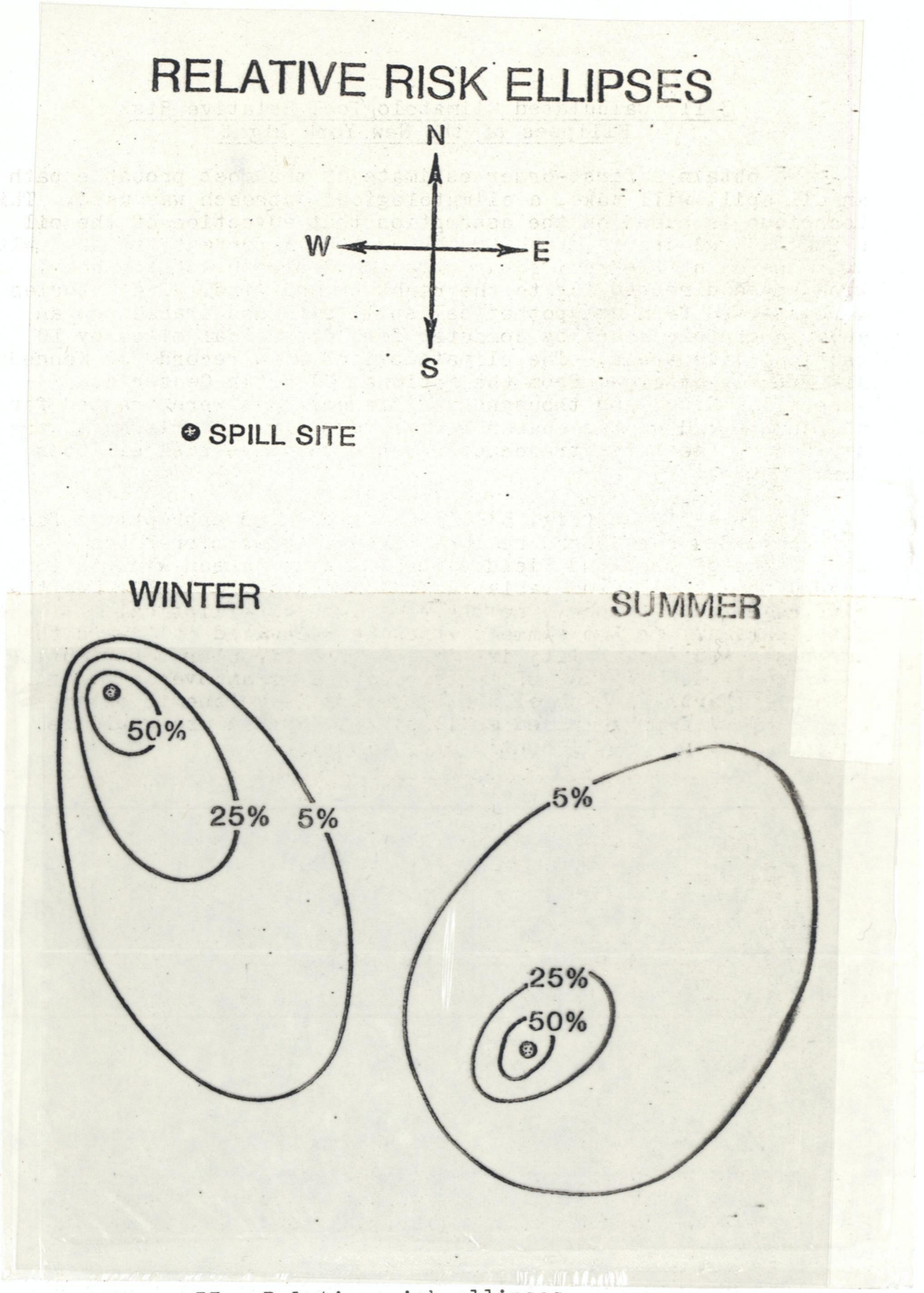

Figure 57.--Relative risk ellipses.

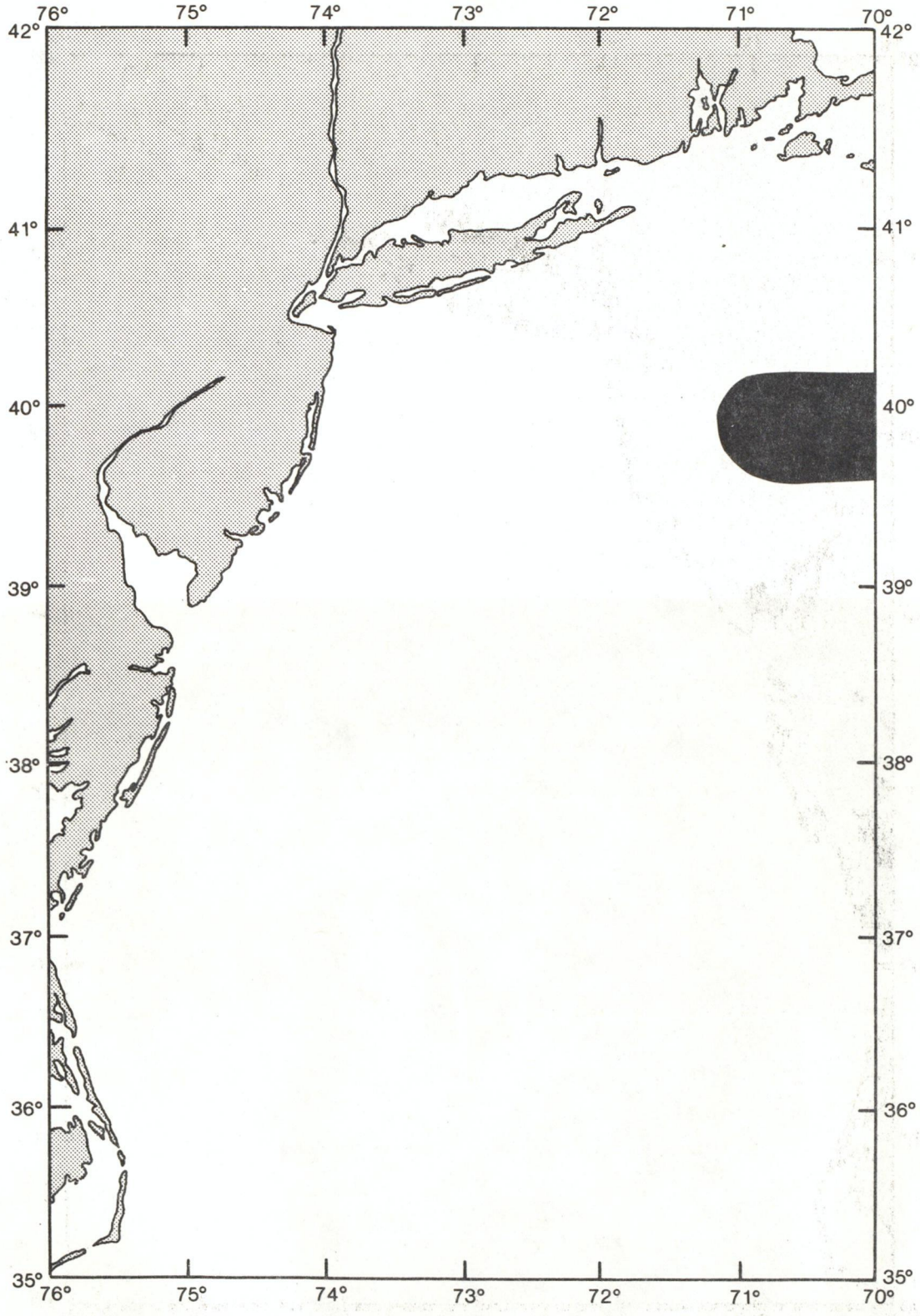

Figure 58.--Natural resource chart for silver and red hake spawning areas (after Smith, Slack, and Davis, 1976)

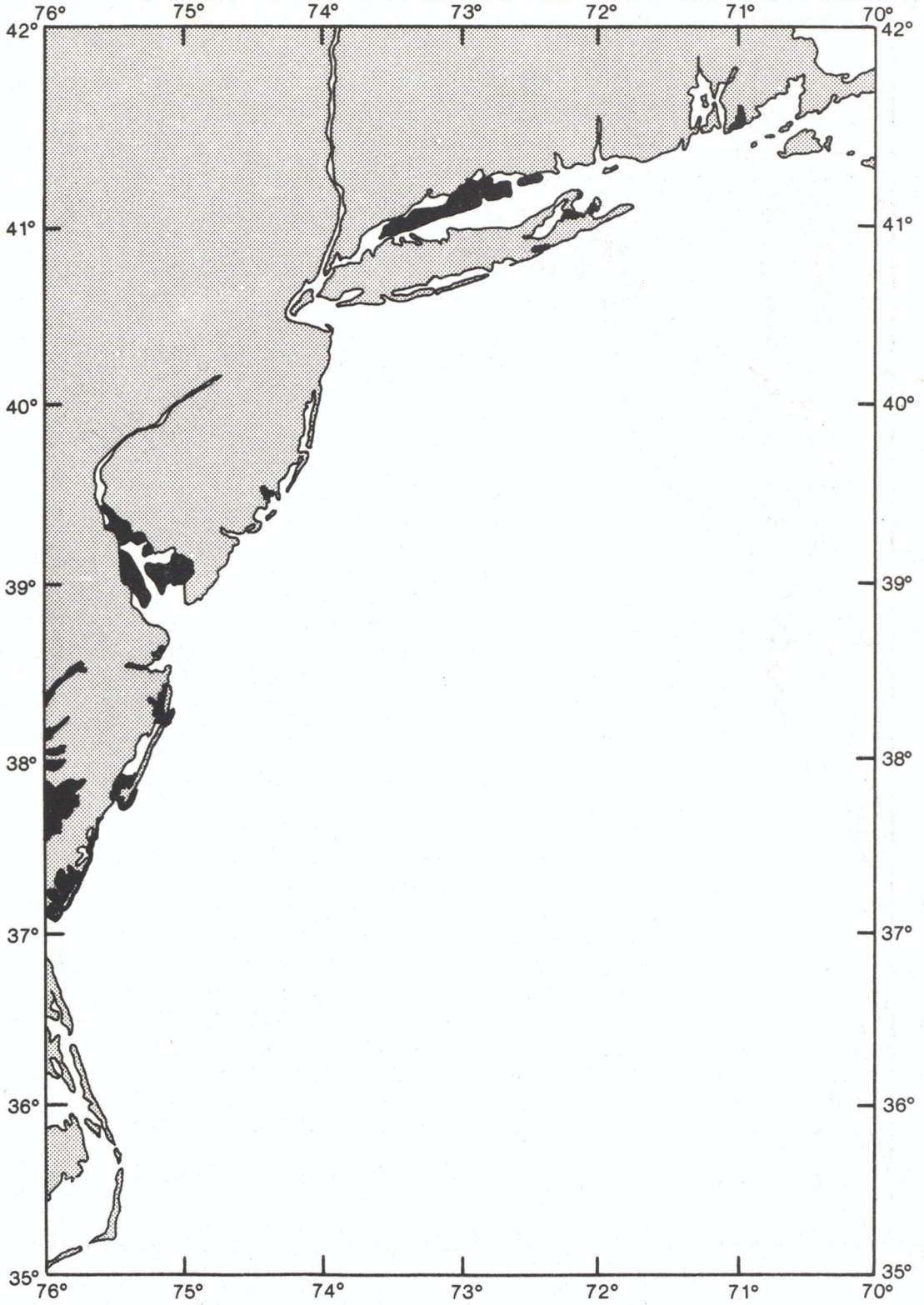

Figure 59.--Natural resource chart for harbor seal whelping areas (after Smith, Slack, and Davis, 1976)

Figure 60.--Natural resource chart for hard clam grounds (after Slack and Wyant, 1978)

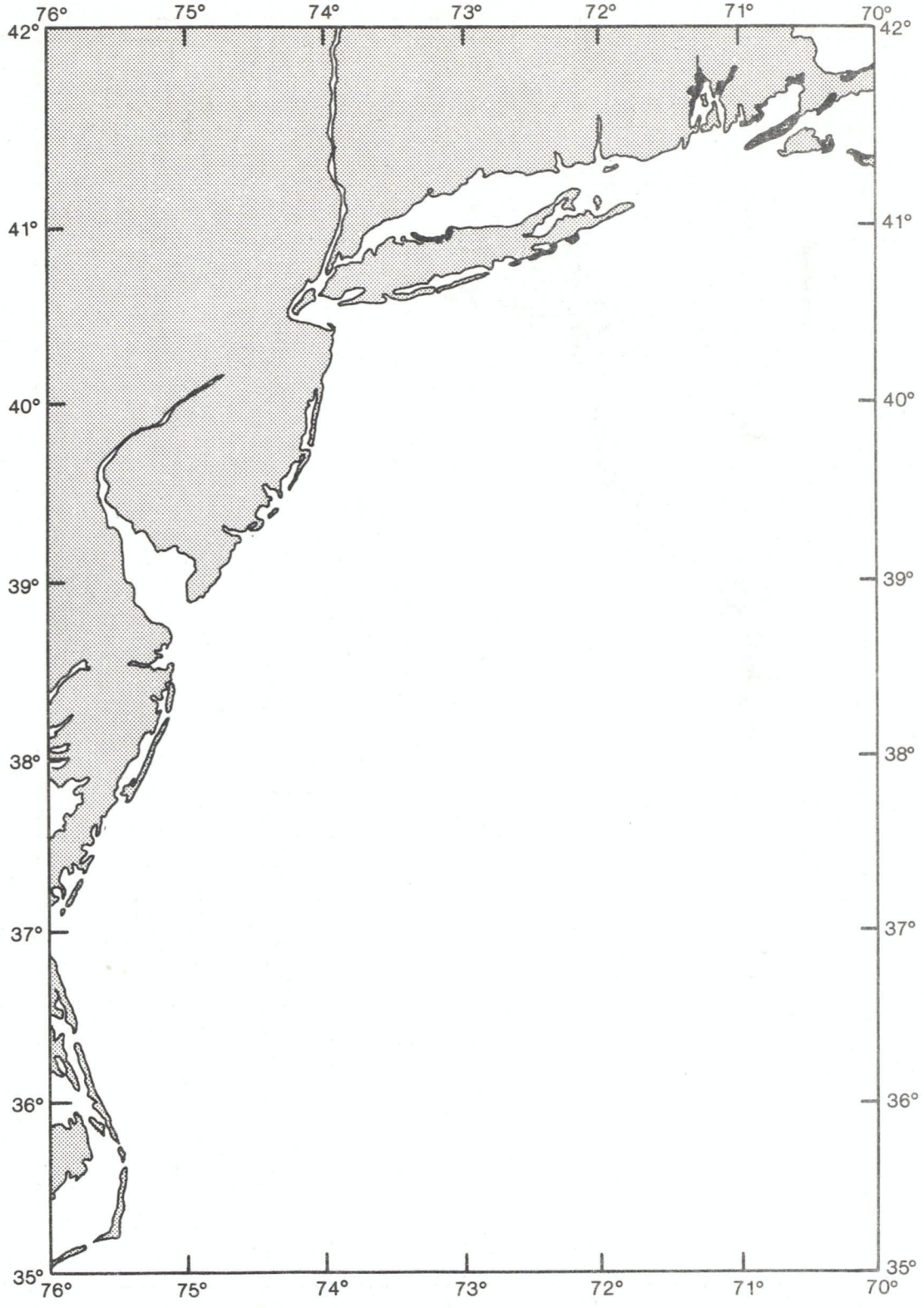

Figure 61.--Natural resource chart for soft clam grounds (after Slack and Wyant, 1978)

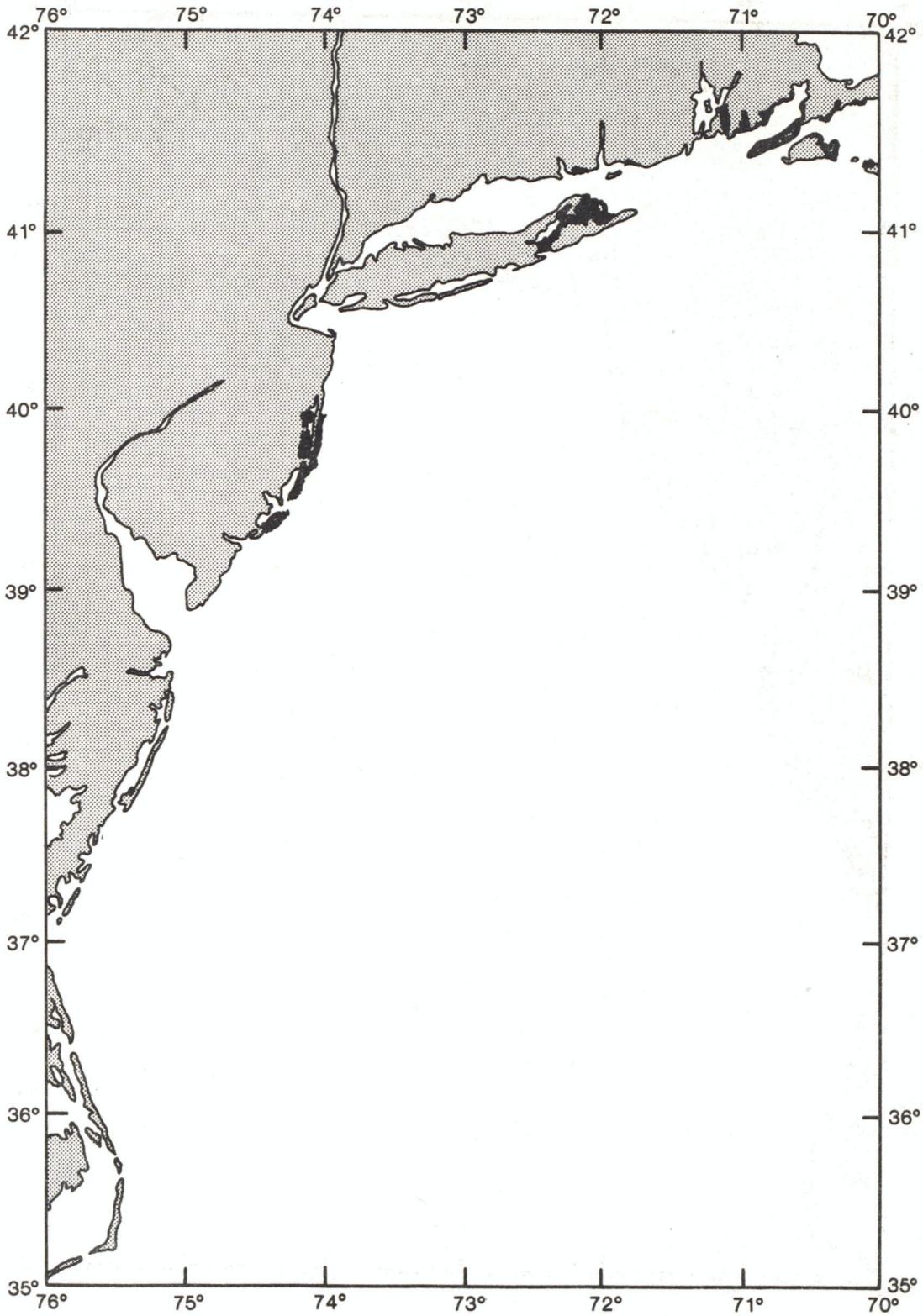

Figure 62.--Natural resource chart for bay scallop areas (after Slack and Wyant)

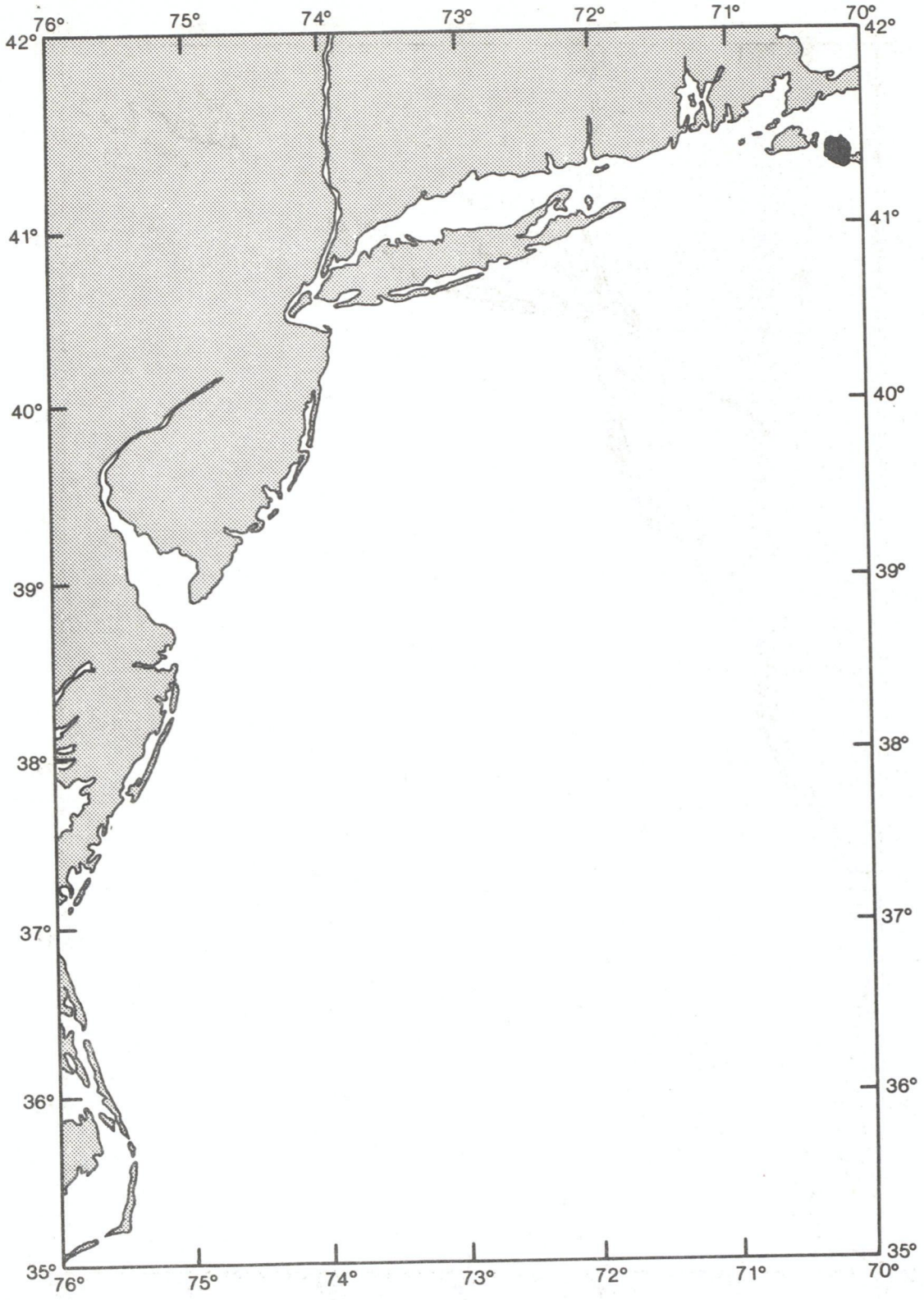

Figure 63.--Natural resource chart for grey seal areas (after Slack and Wyant, 1978)

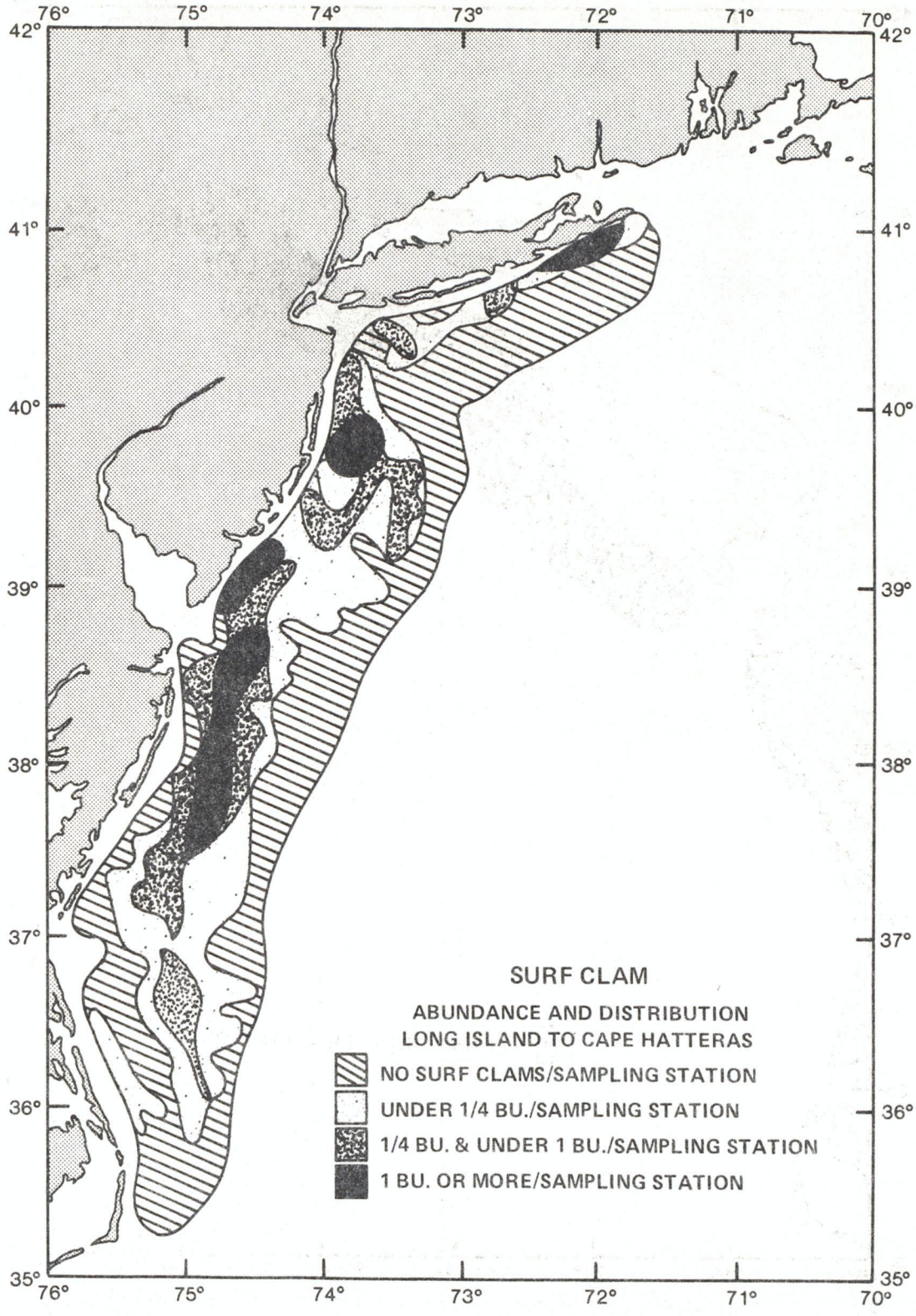

Figure 64.--Natural resource chart for surf clams (after Gusey, 1976)

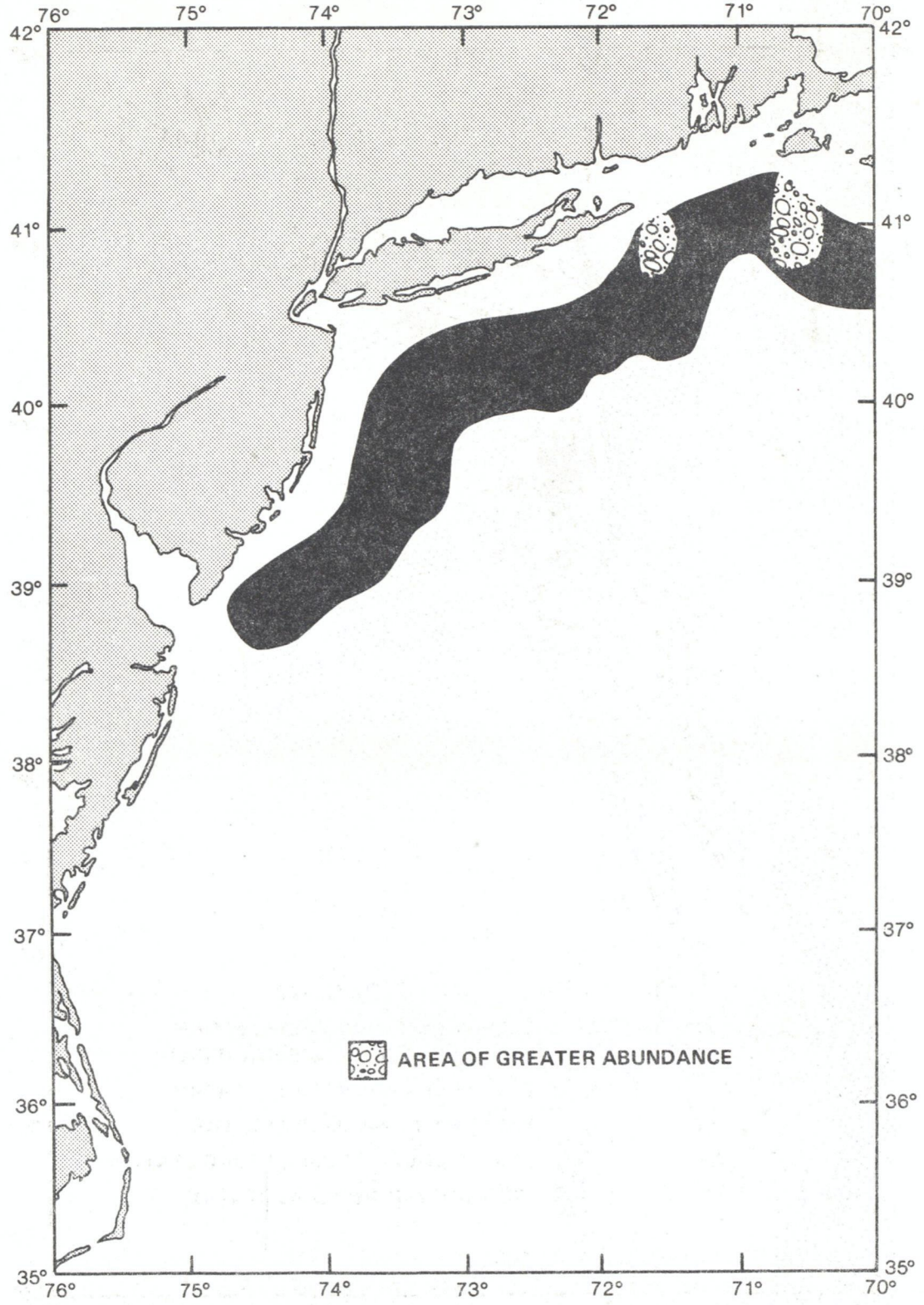

Figure 65.--Natural resource chart for Atlantic cod (after Gusey, 1976)

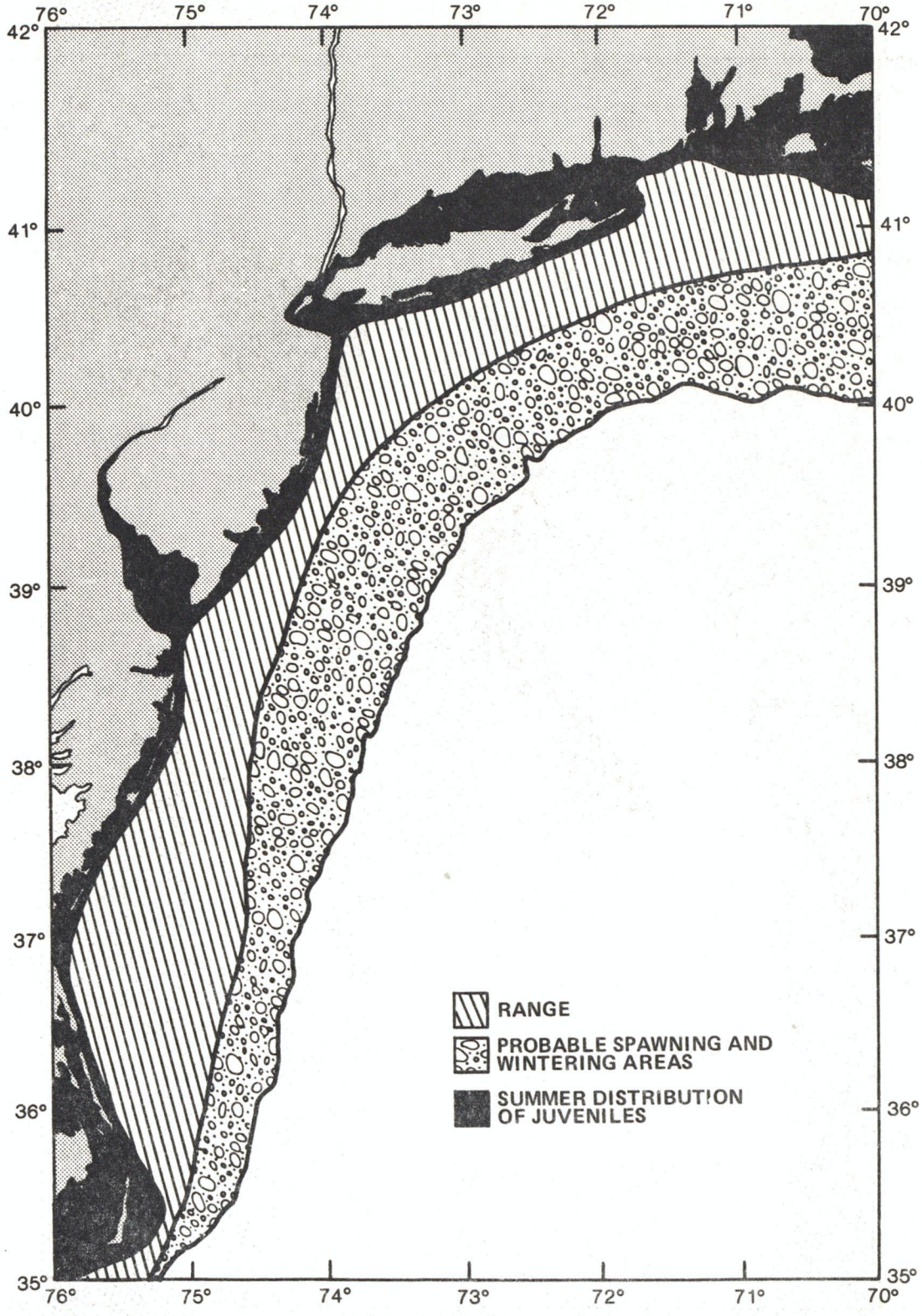

Figure 66.--Natural resource chart for bluefish (after Gusey, 1976)

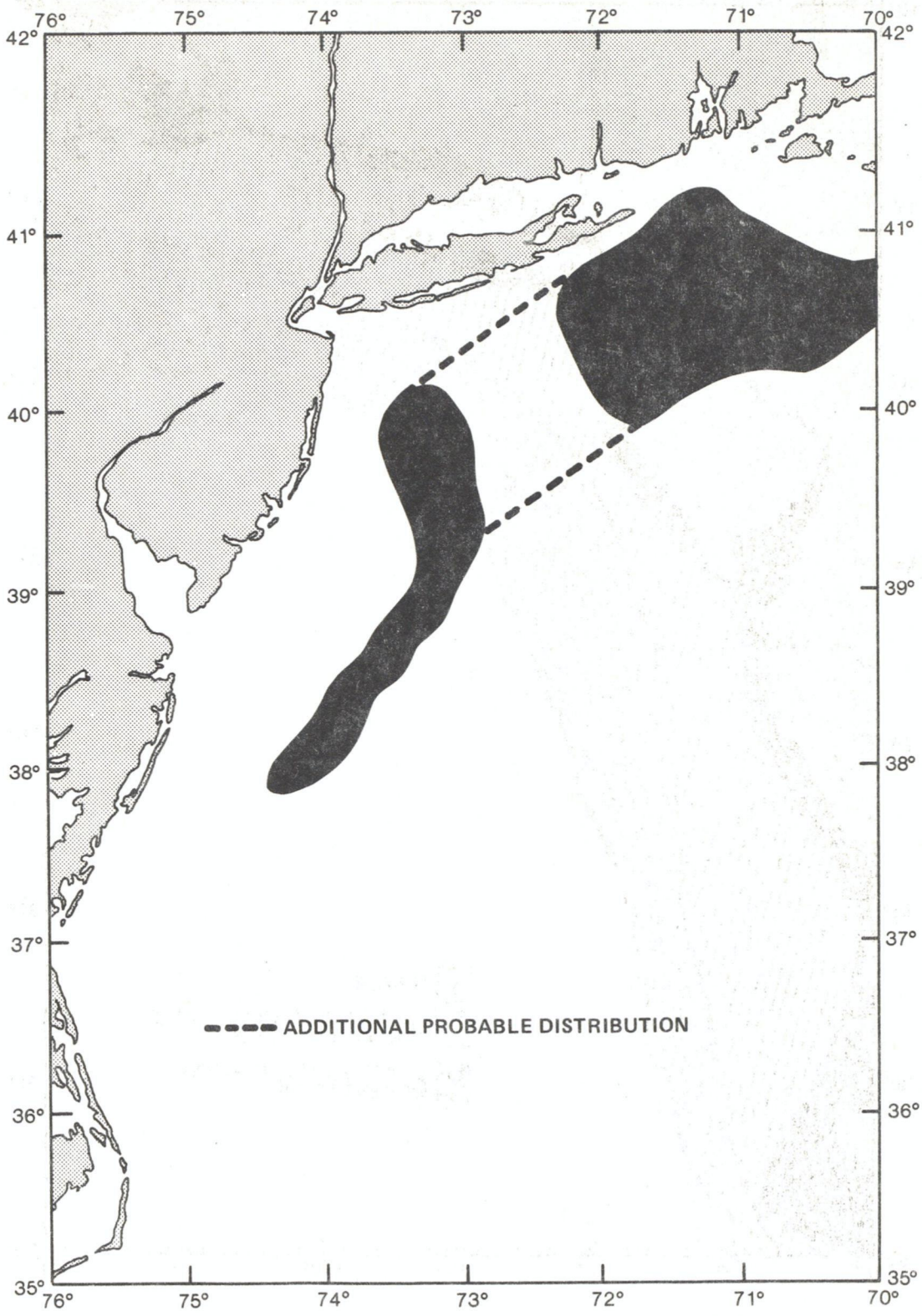

Figure 67.--Natural resource chart for Atlantic mackerel (fall) (after Gusey, 1976)

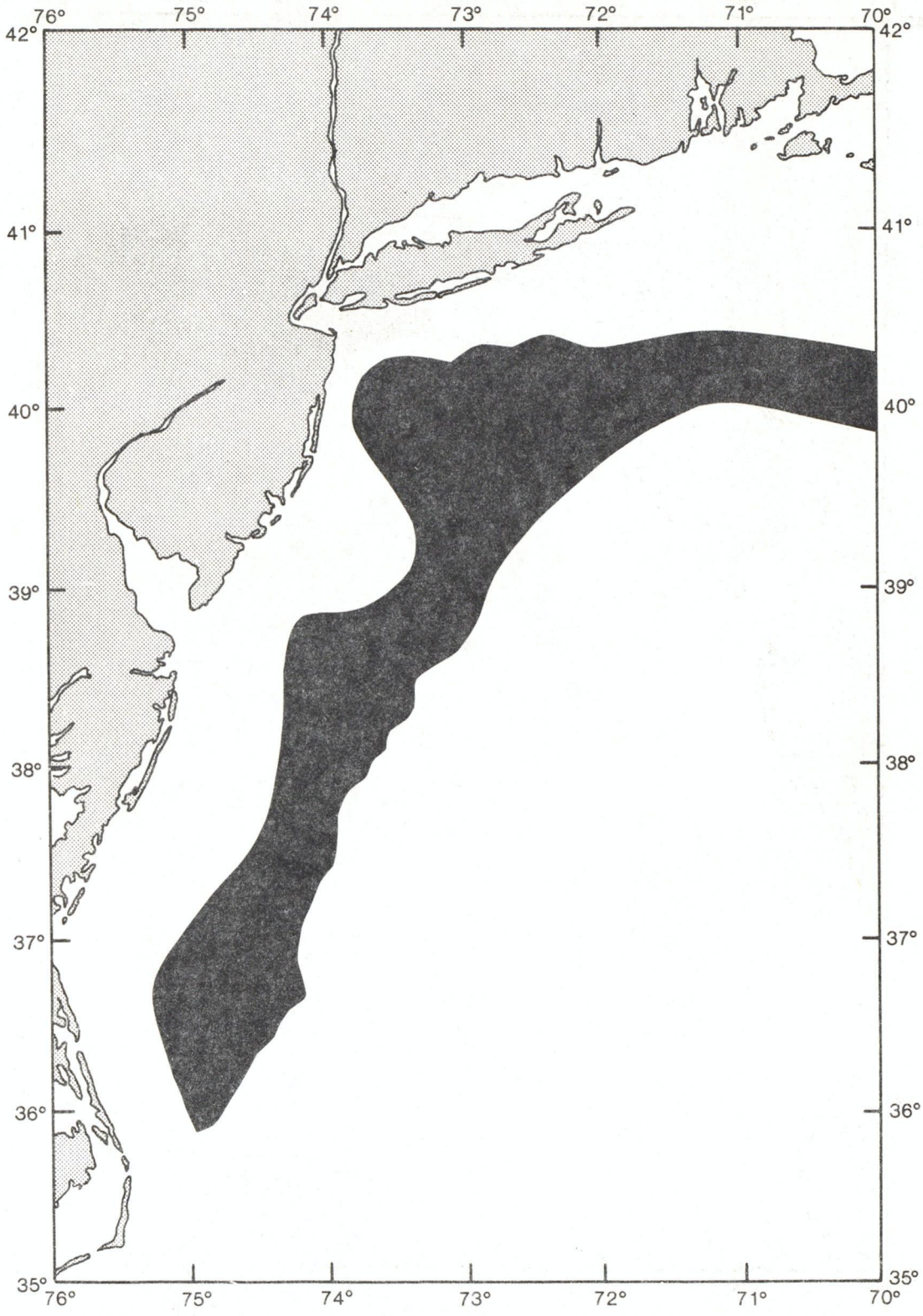

Figure 68.--Natural resource chart for Atlantic mackerel (spring) (after Gusey, 1976)

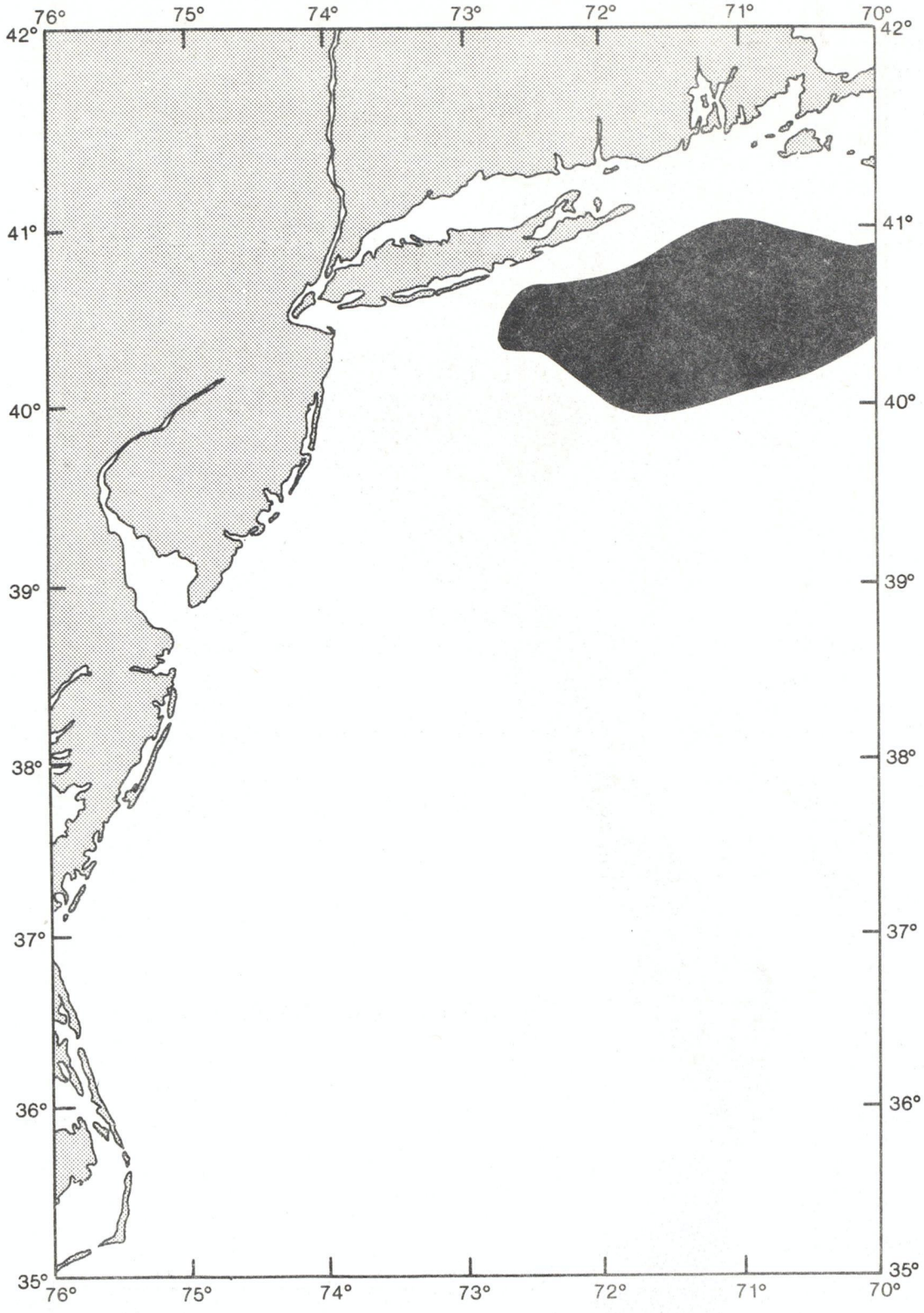

Figure 69.--Natural resource chart for Atlantic herring (fall) (after Gusey, 1976)

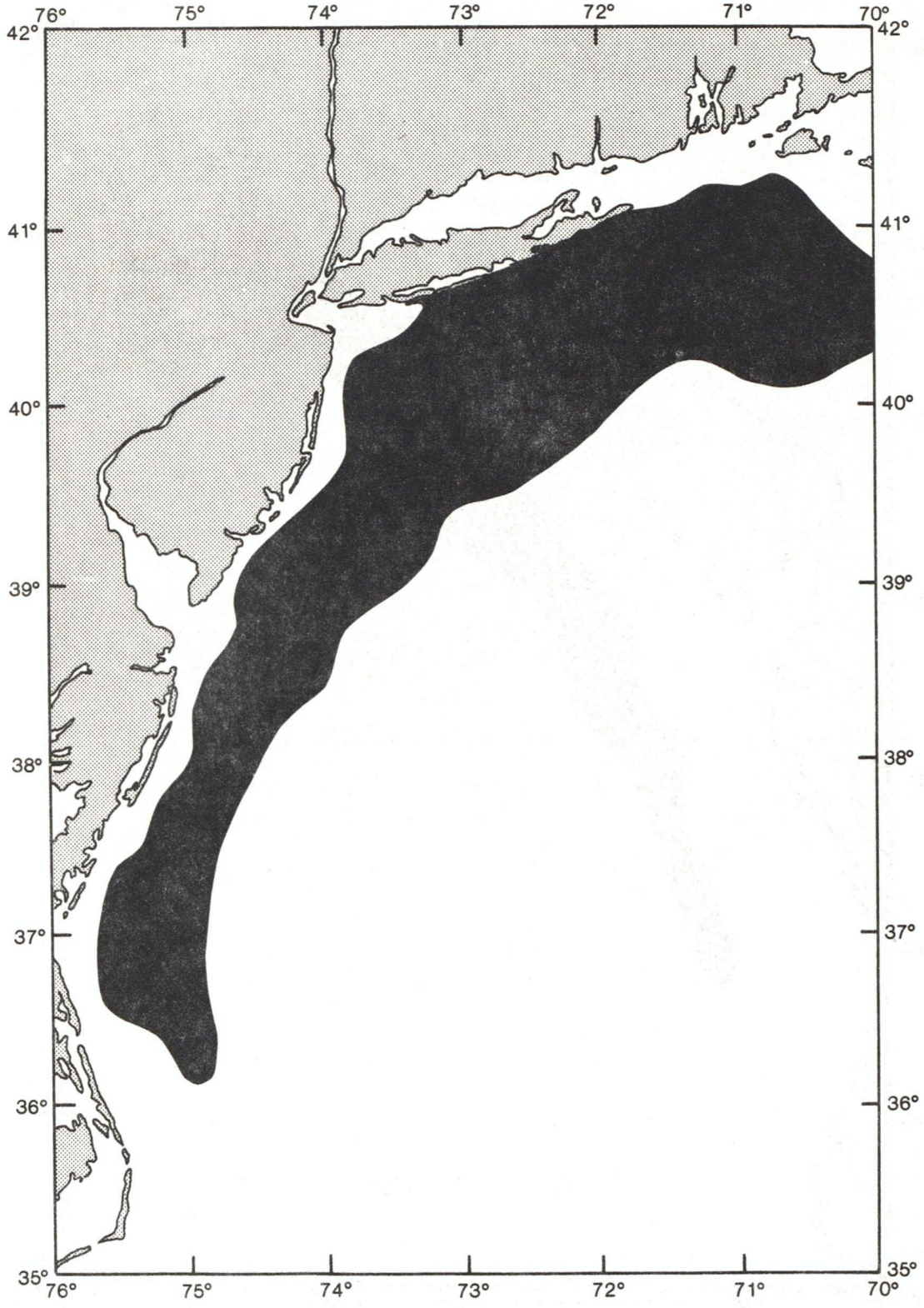

Figure 70.--Natural resource chart for Atlantic herring (spring) (after Gusey, 1976)

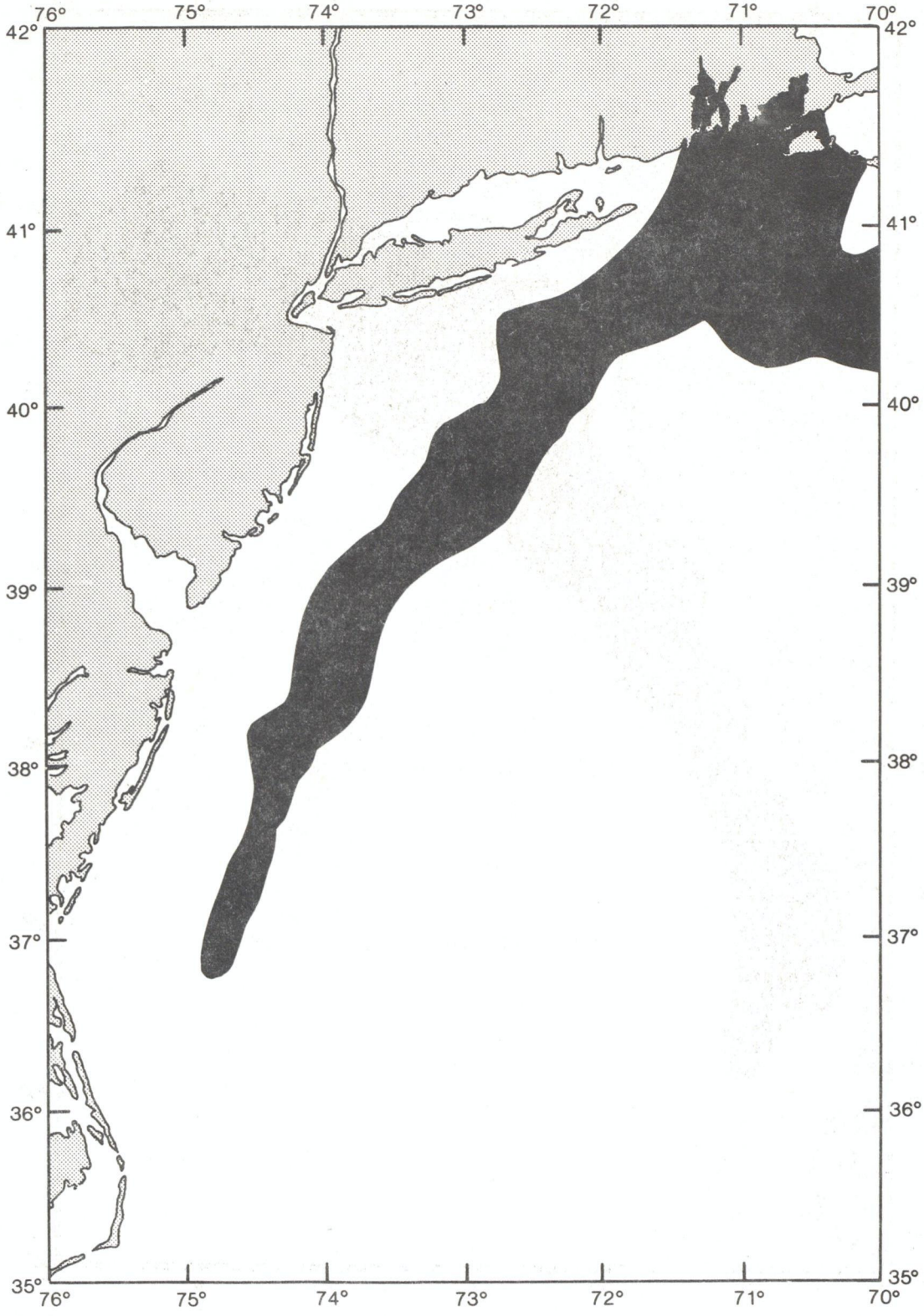

Figure 71.--Natural resource chart for red hake (fall) (after Gusey, 1976)

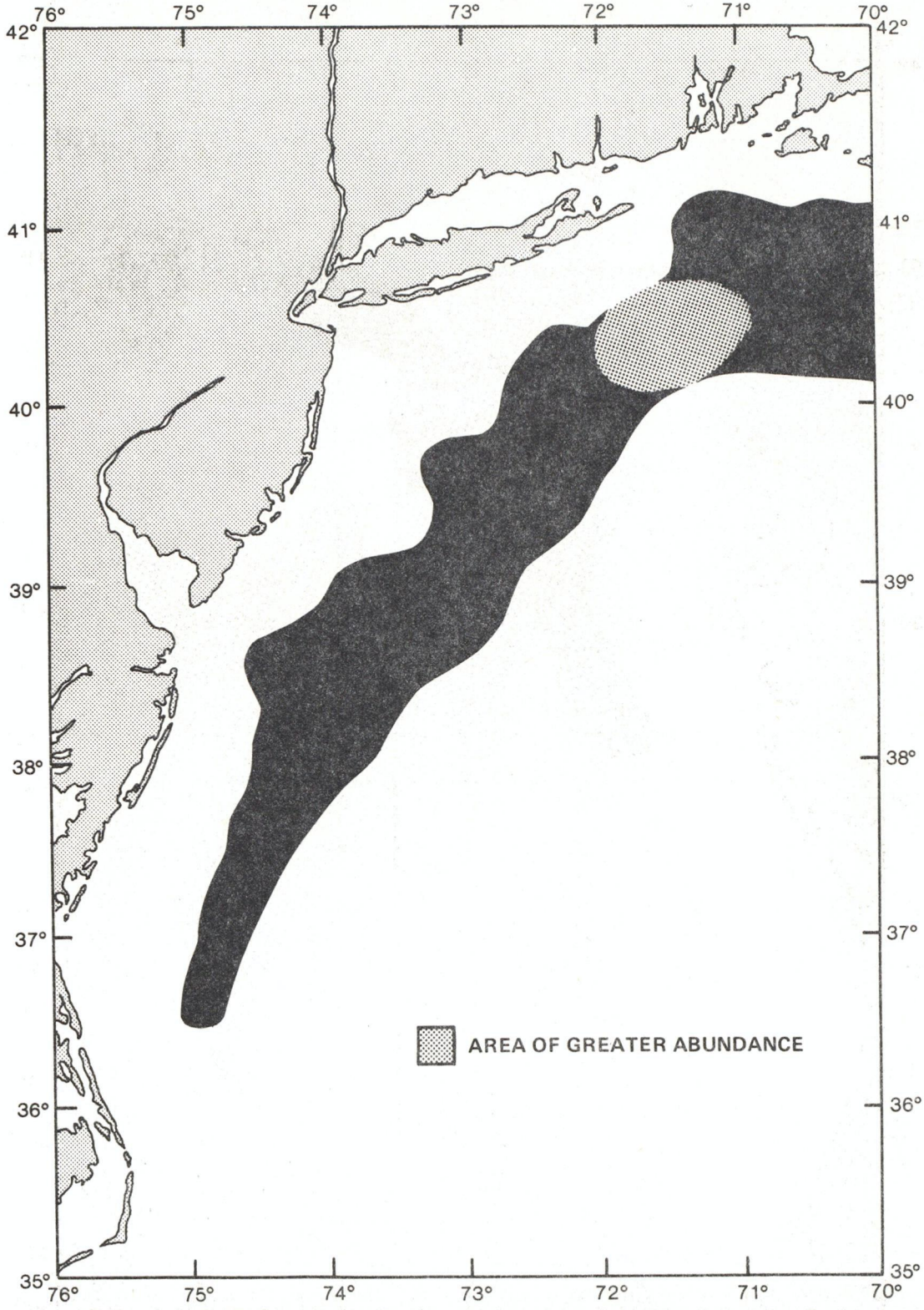

Figure 72.--Natural resource chart for red hake (spring) (after Gusey, 1976)

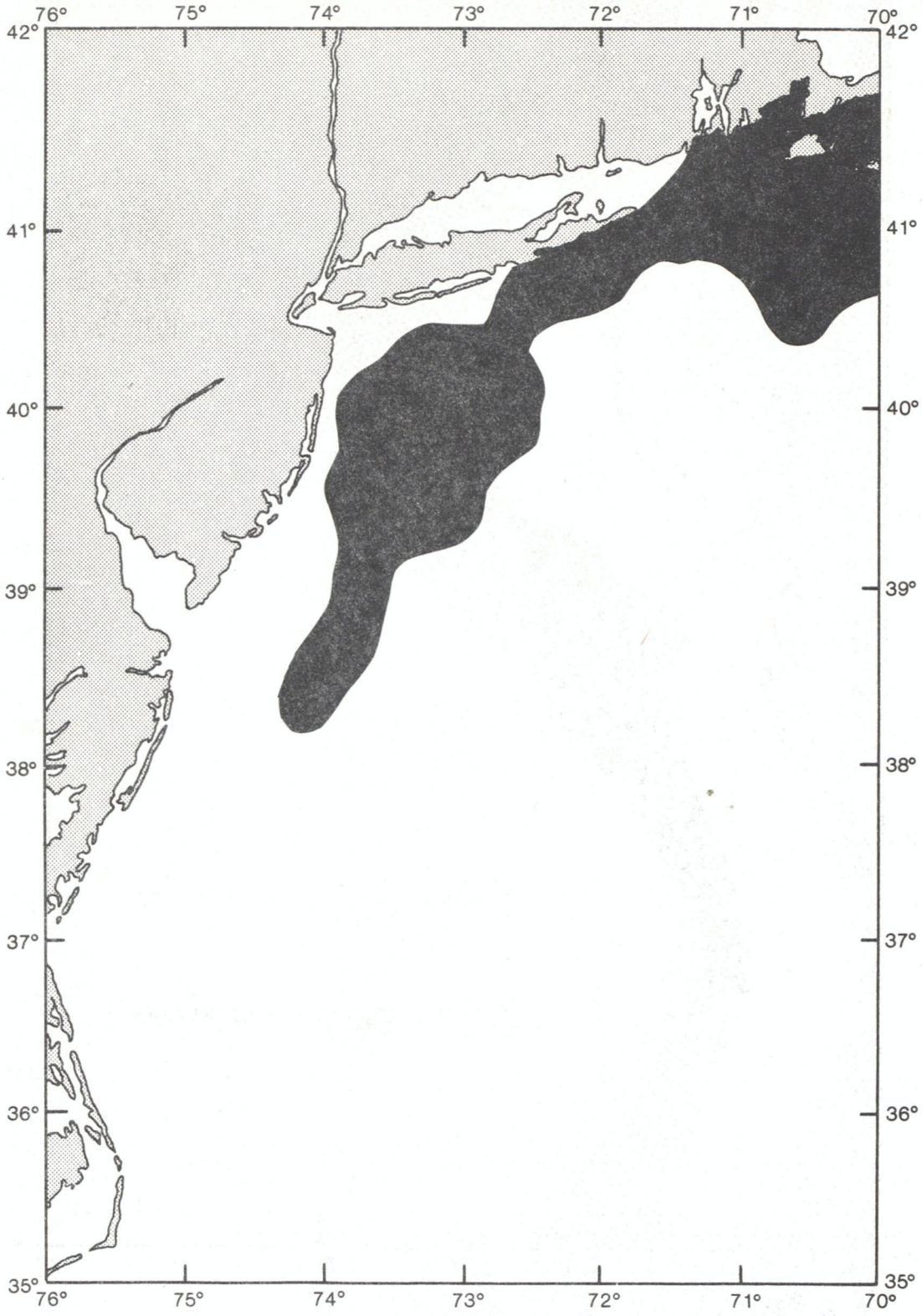

Figure 73.--Natural resource chart for winter flounder (fall) (after Gusey, 1976)

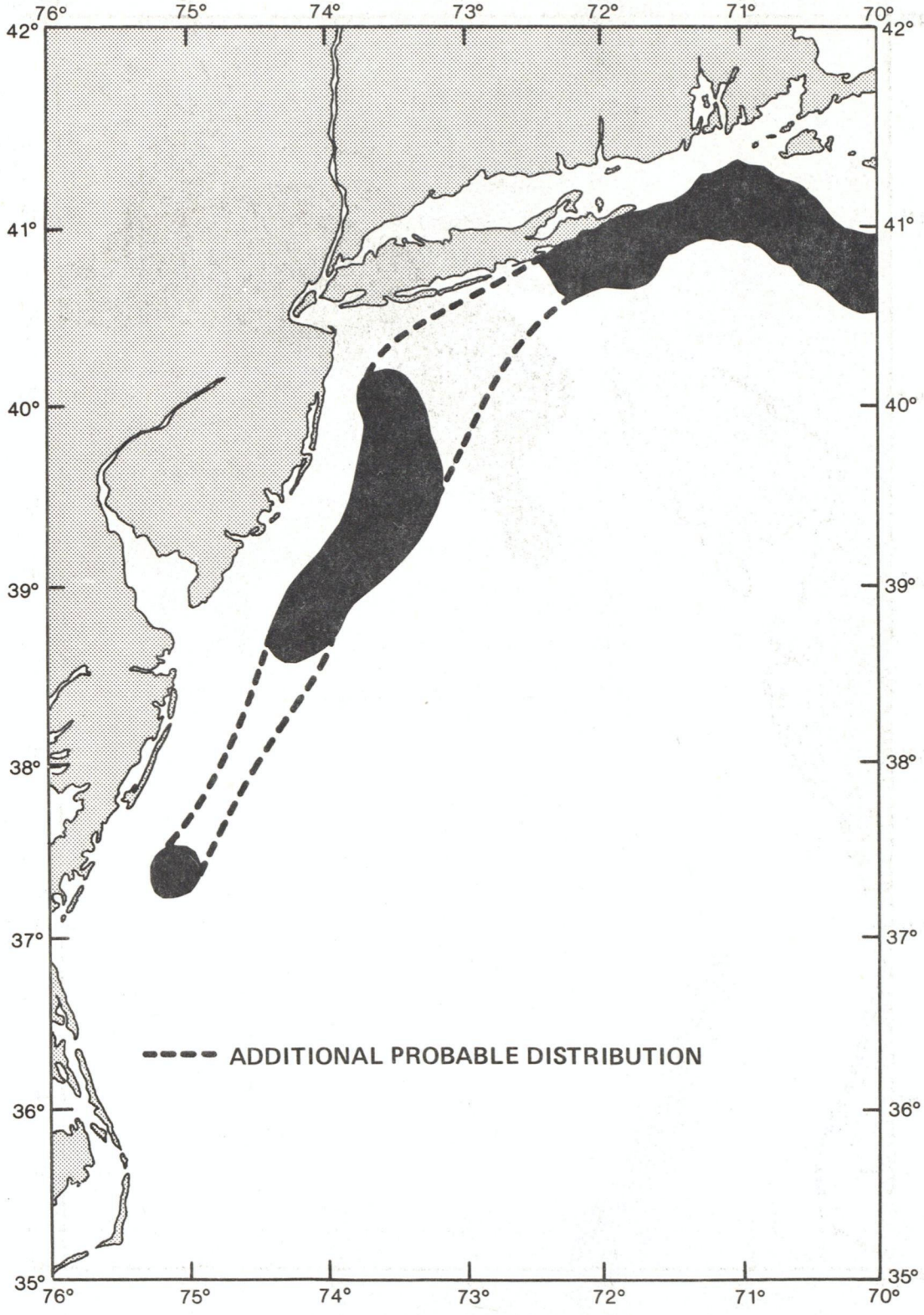

Figure 74.--Natural resource chart for winter flounder (spring) (after Gusey, 1976)

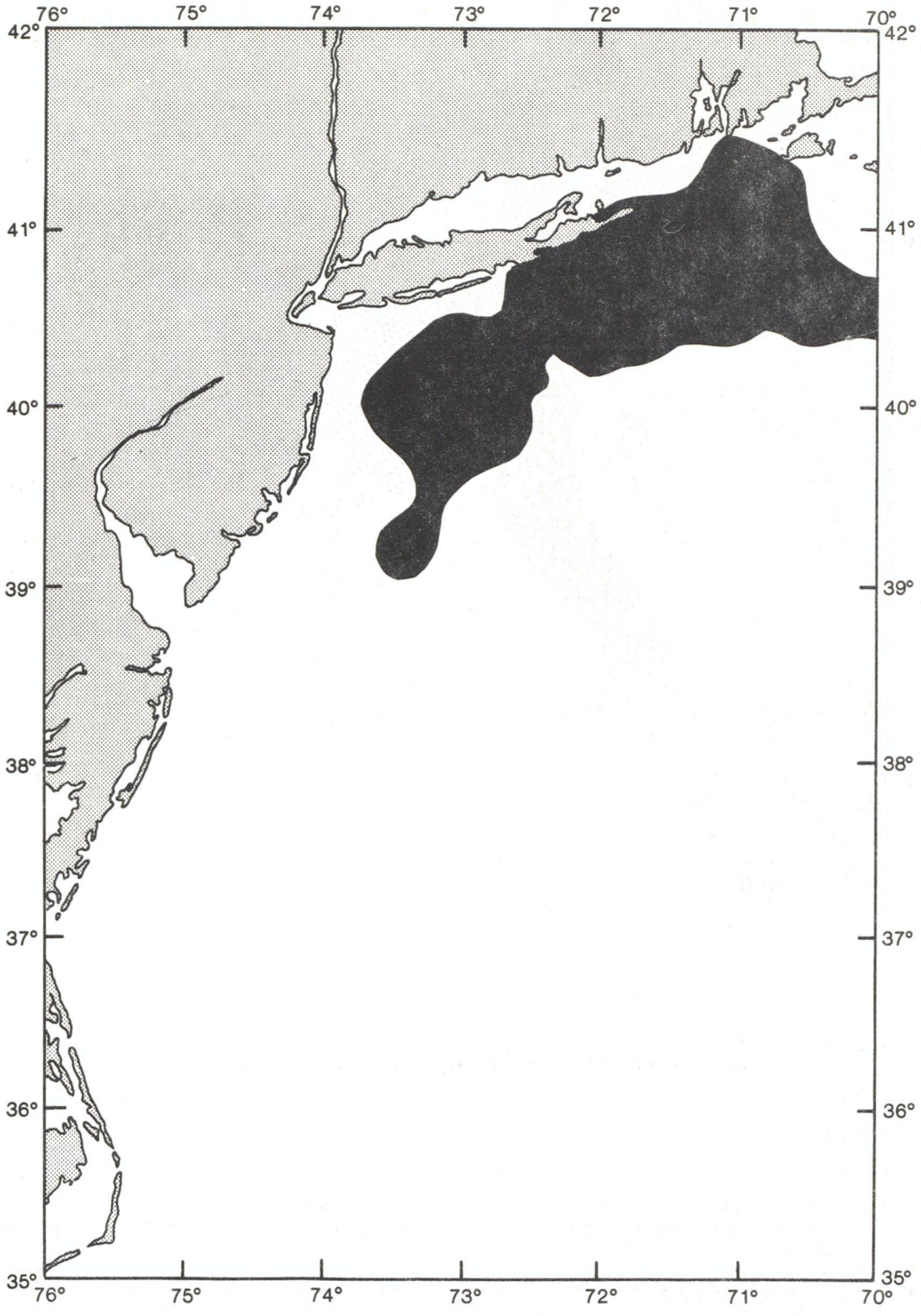

Figure 75.--Natural resource chart for yellowtail flounder (fall) (after Gusey, 1976)

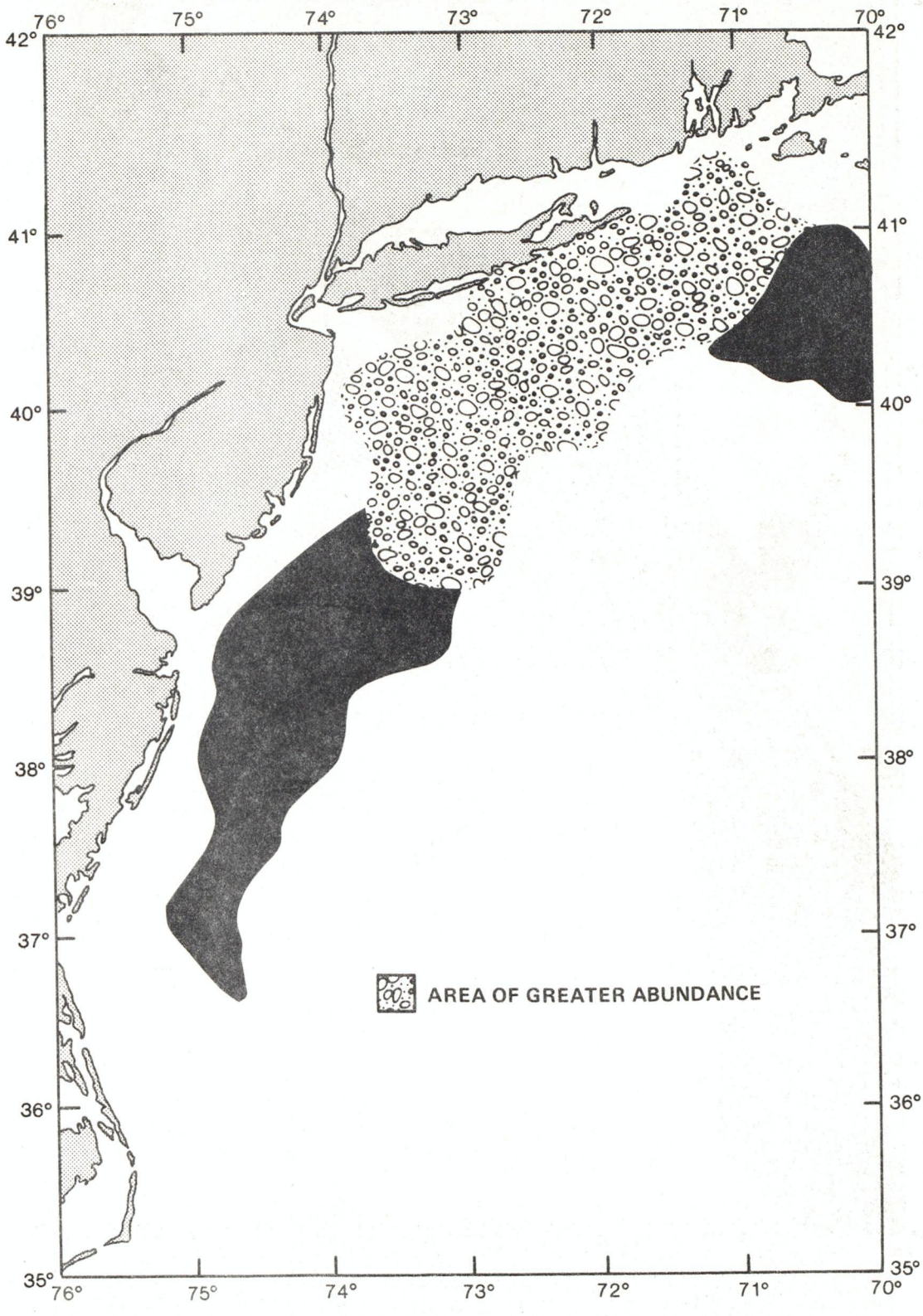

Figure 76.--Natural resource chart for yellowtail flounder (spring) (after Gusey, 1976)

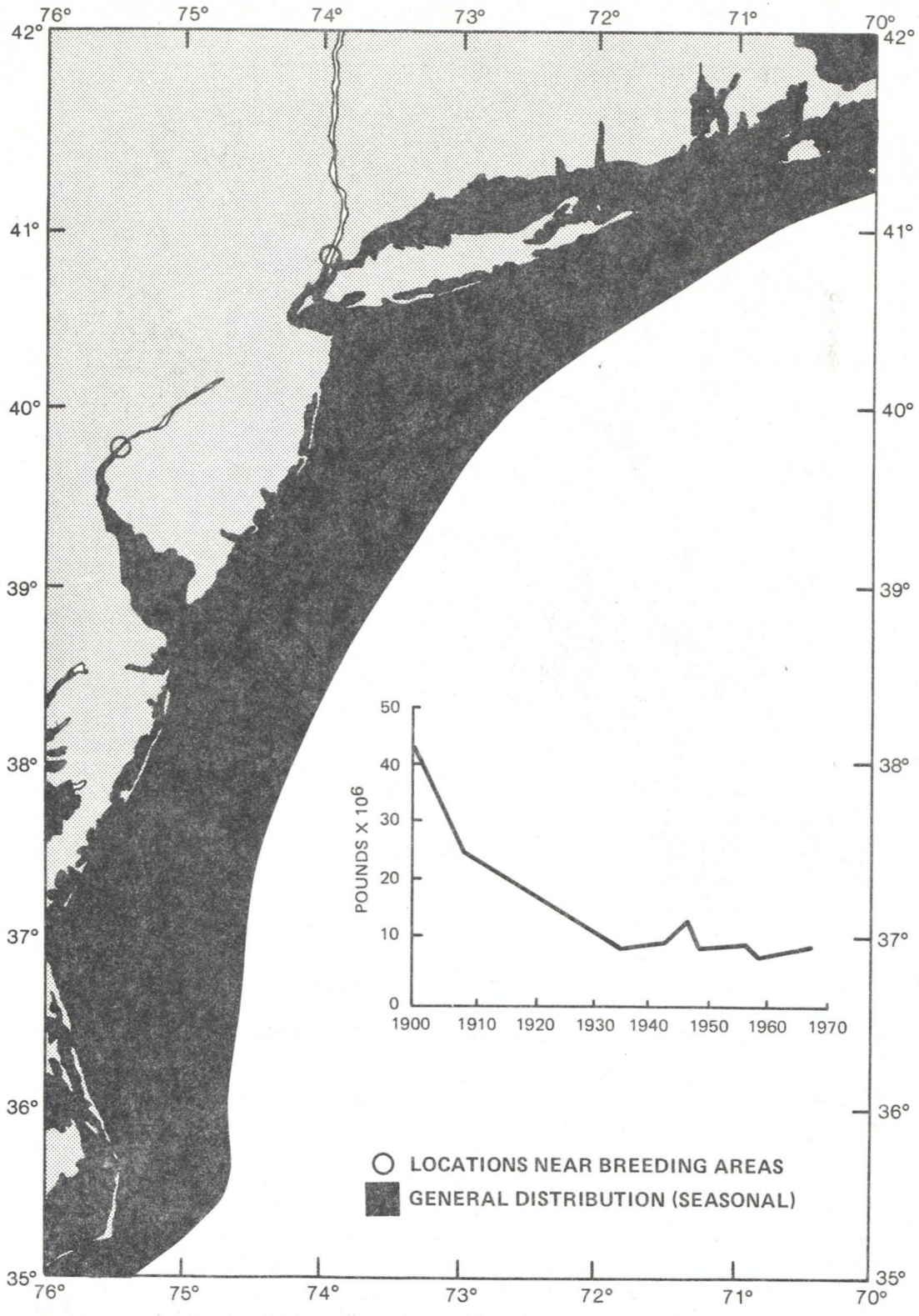

Figure 77.--Natural resource chart for American shad (after Marine Experimental Station, U.R.I., 1973)

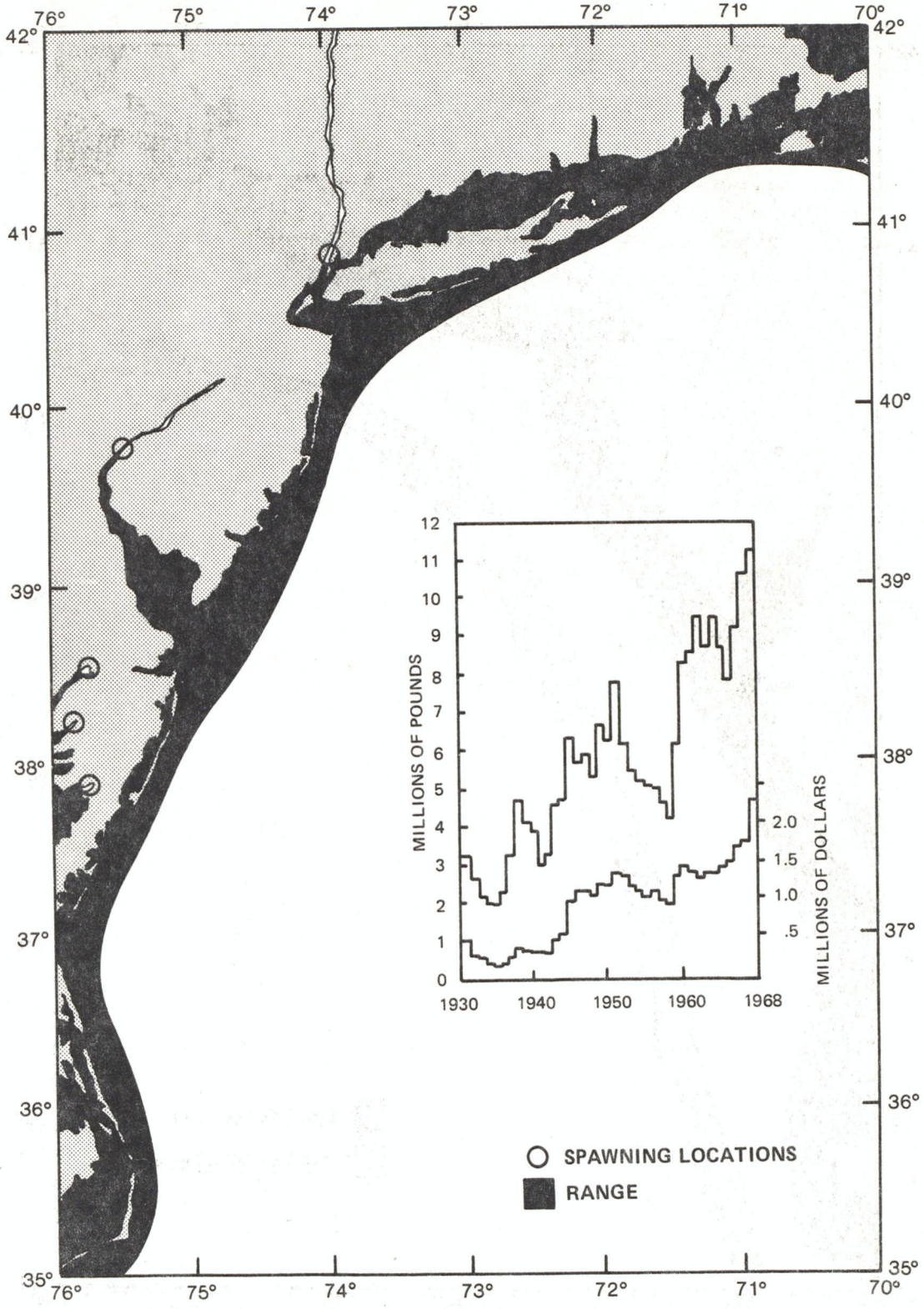

Figure 78.--Natural resource chart for striped bass (after Marine Experimental Station, U.R.I., 1973)

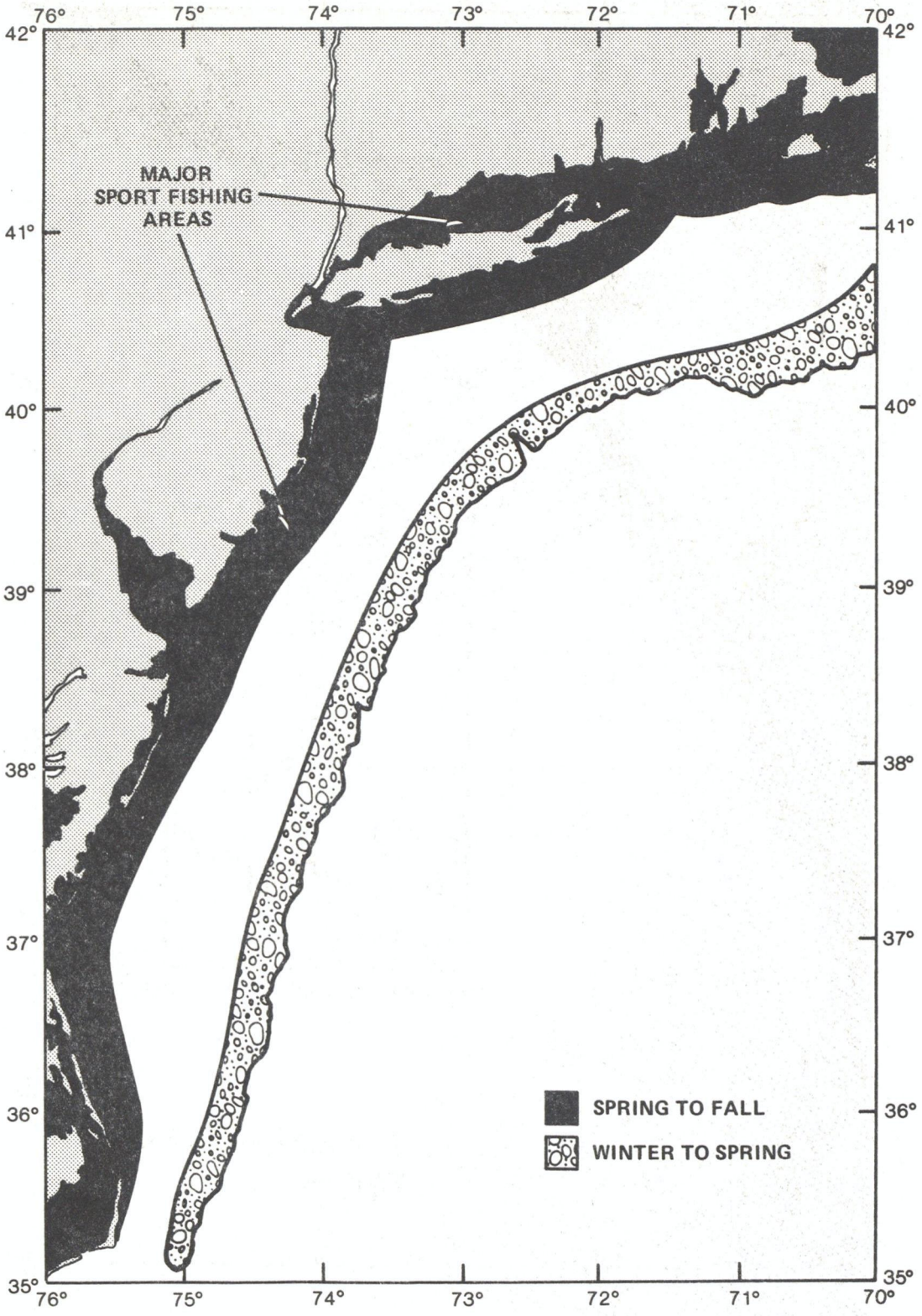

Figure 79.--Natural resource chart for summer flounder (after Marine Experimental Station, U.R.I., 1973)

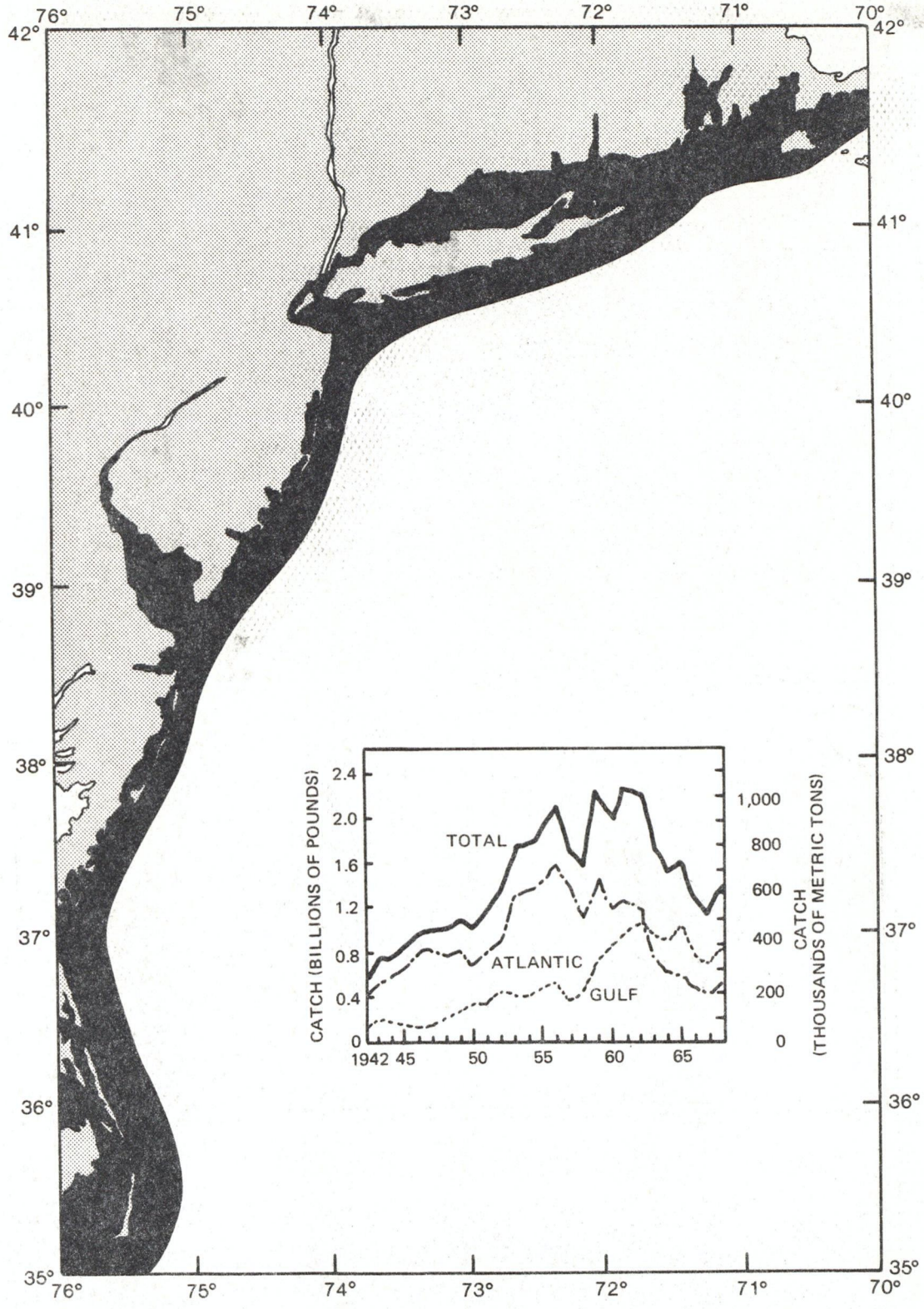

Figure 80.--Natural resource chart for menhaden (after Marine Experimental Station, U.R.I., 1973)

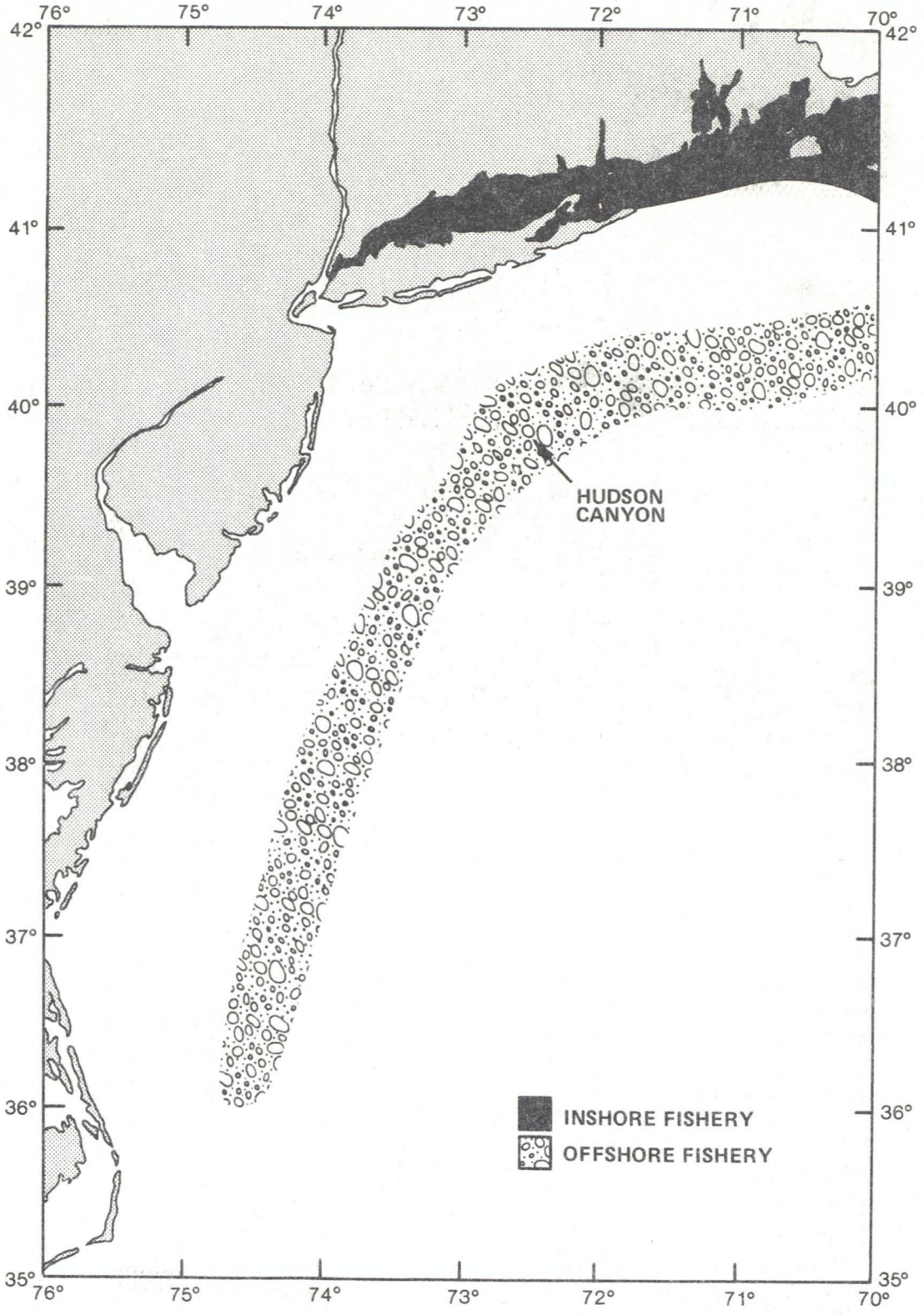

Figure 81.--Natural resource chart for lobster (after Marine Experimental Station, U.R.I., 1973)

Figure 82.--Natural resource chart for sea scallops and calico scallops (after Marine Experimental Station, U.R.I., 1973)

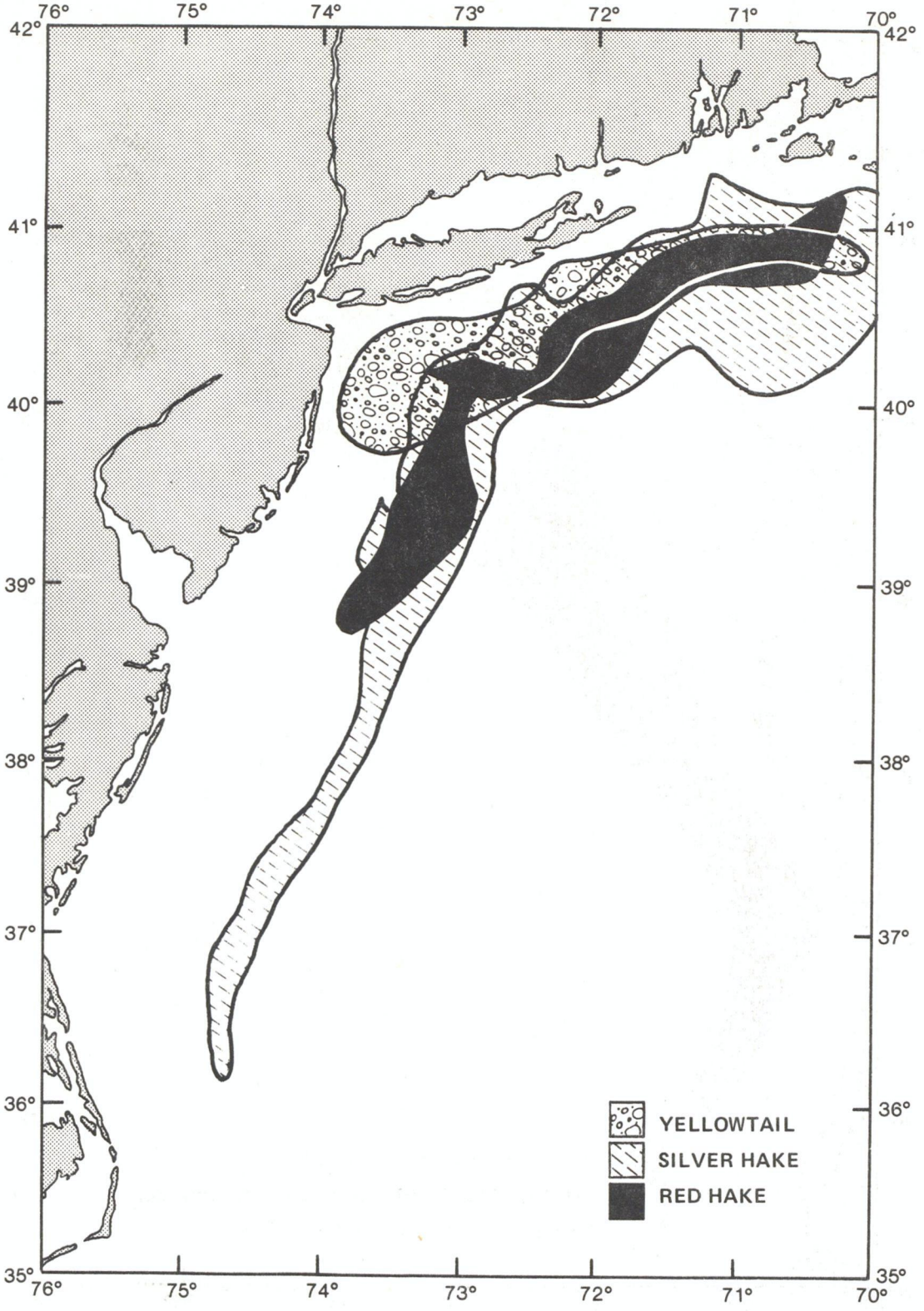

Figure 83.--Natural resource chart for yellow tail silver hake, and red hake (fall) (after Hennemuth, 1976)

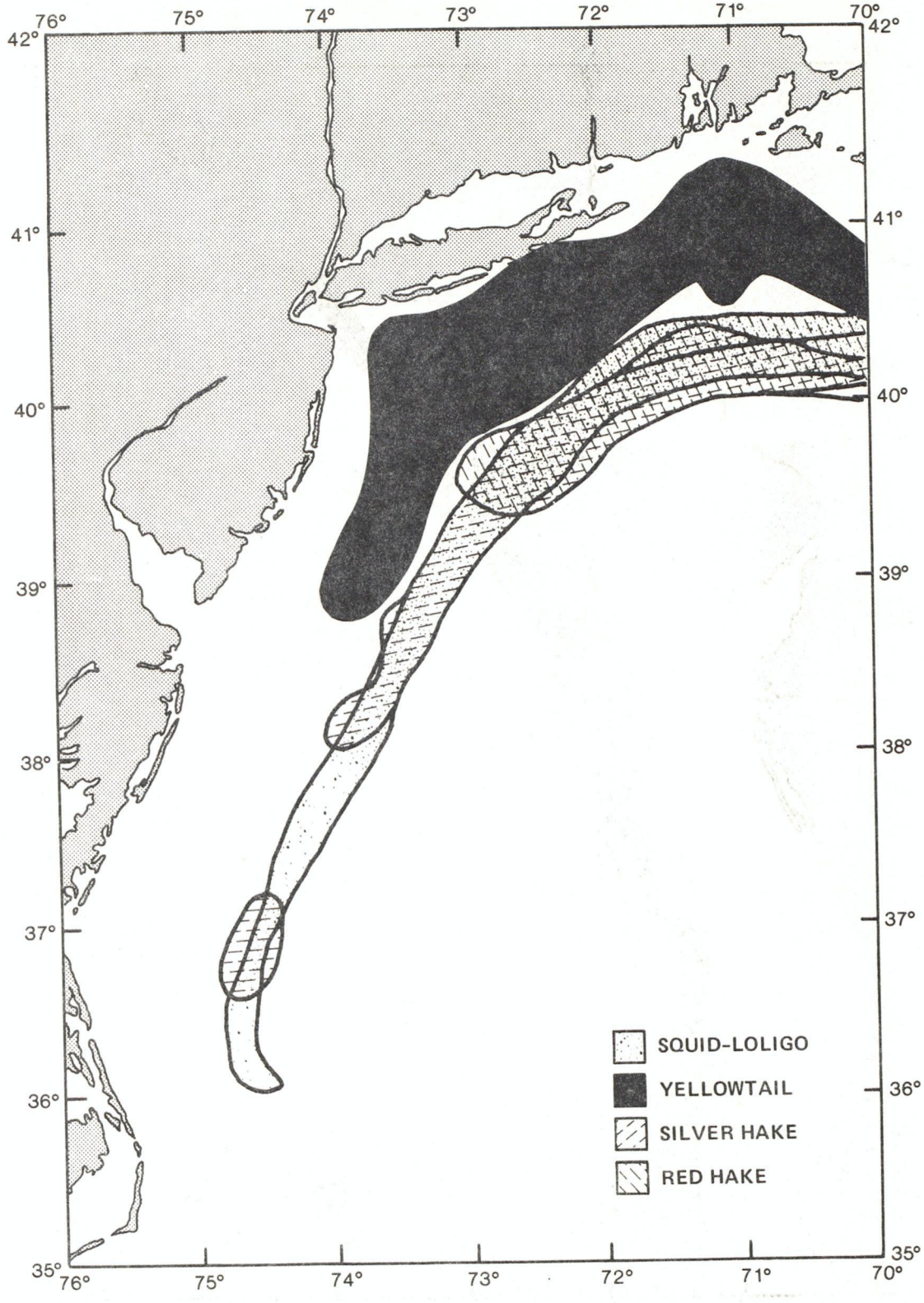

Figure 84.--Natural resource chart for squid, yellow tail, silver hake, and red hake (spring) (after Hennemuth, 1976)

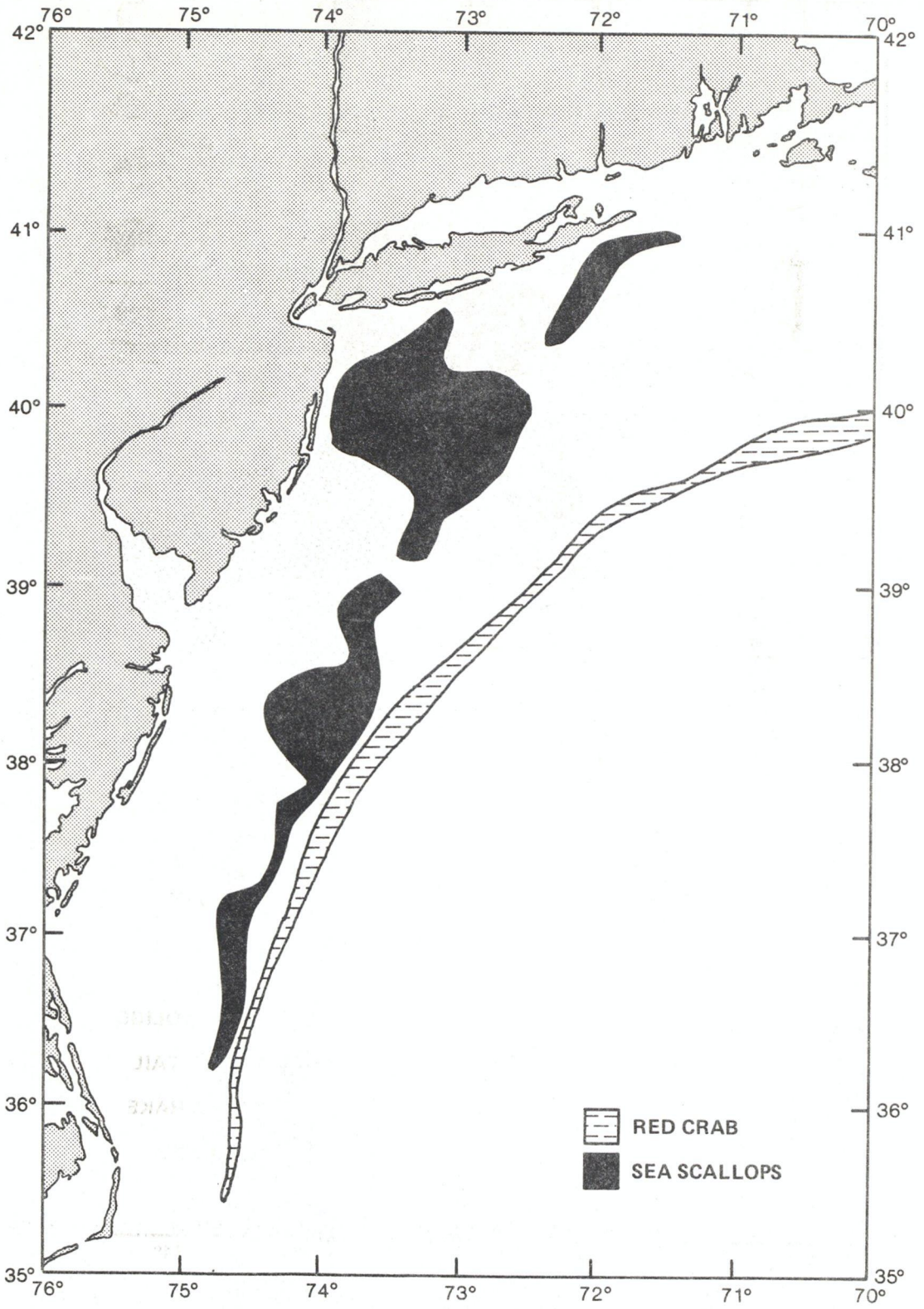

Figure 85.--Natural resource chart for sea scallops and red crab (after Hennemuth, 1976)

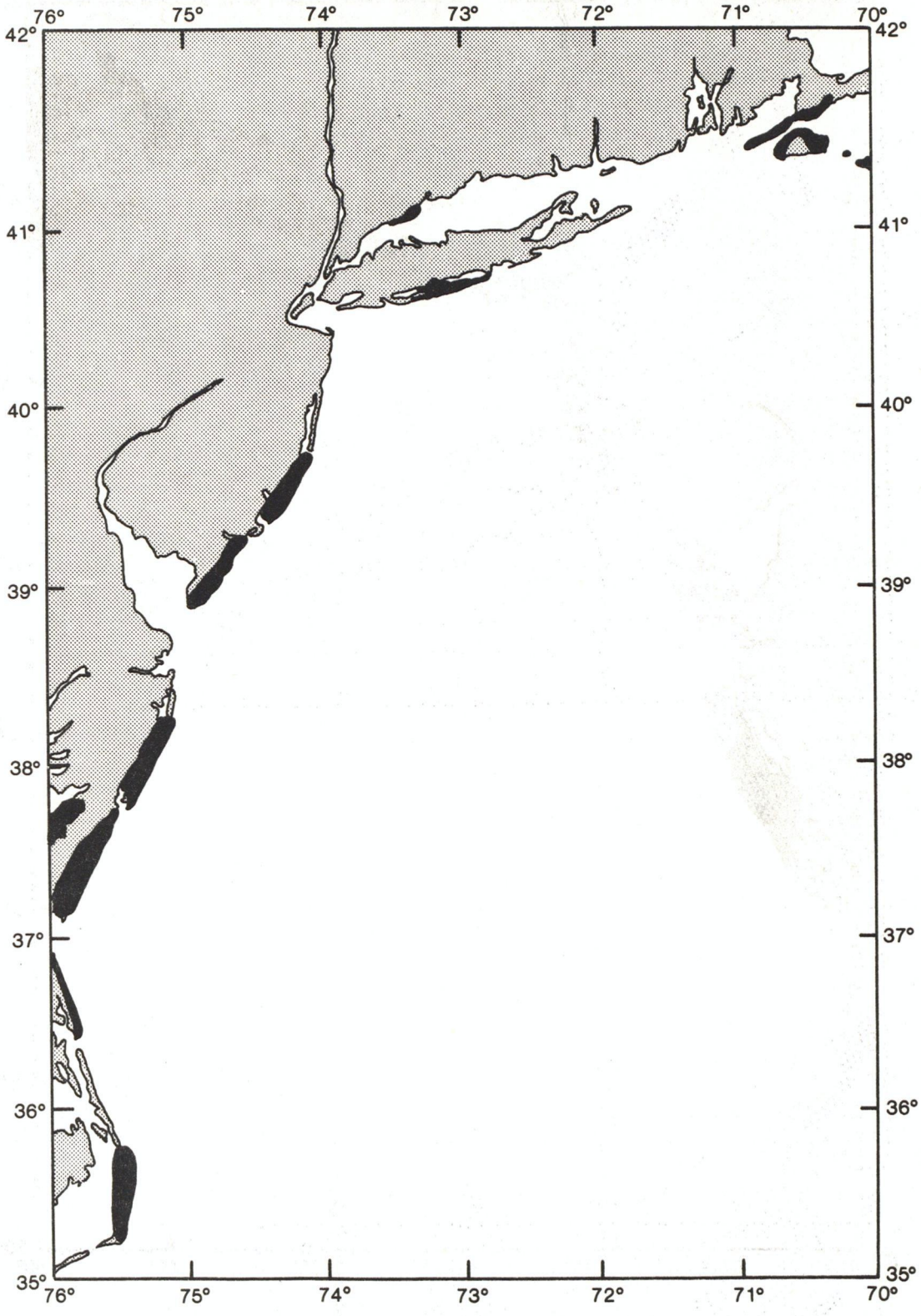

Figure 86.--Natural resource chart for wading birds (after Slack and Wyant, 1978)

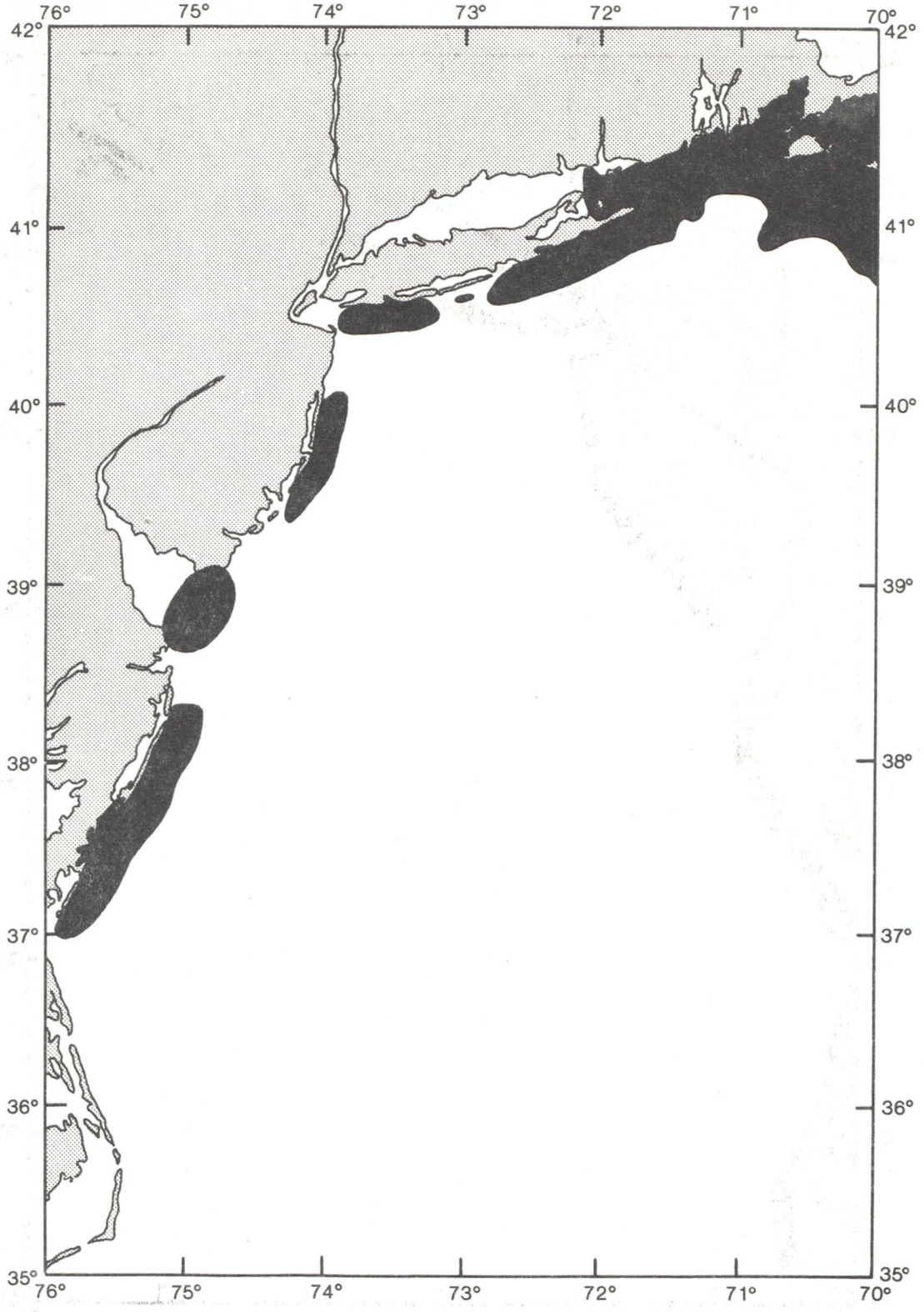

Figure 87.--Natural resource chart for sea ducks (after Slack and Wyant, 1978)

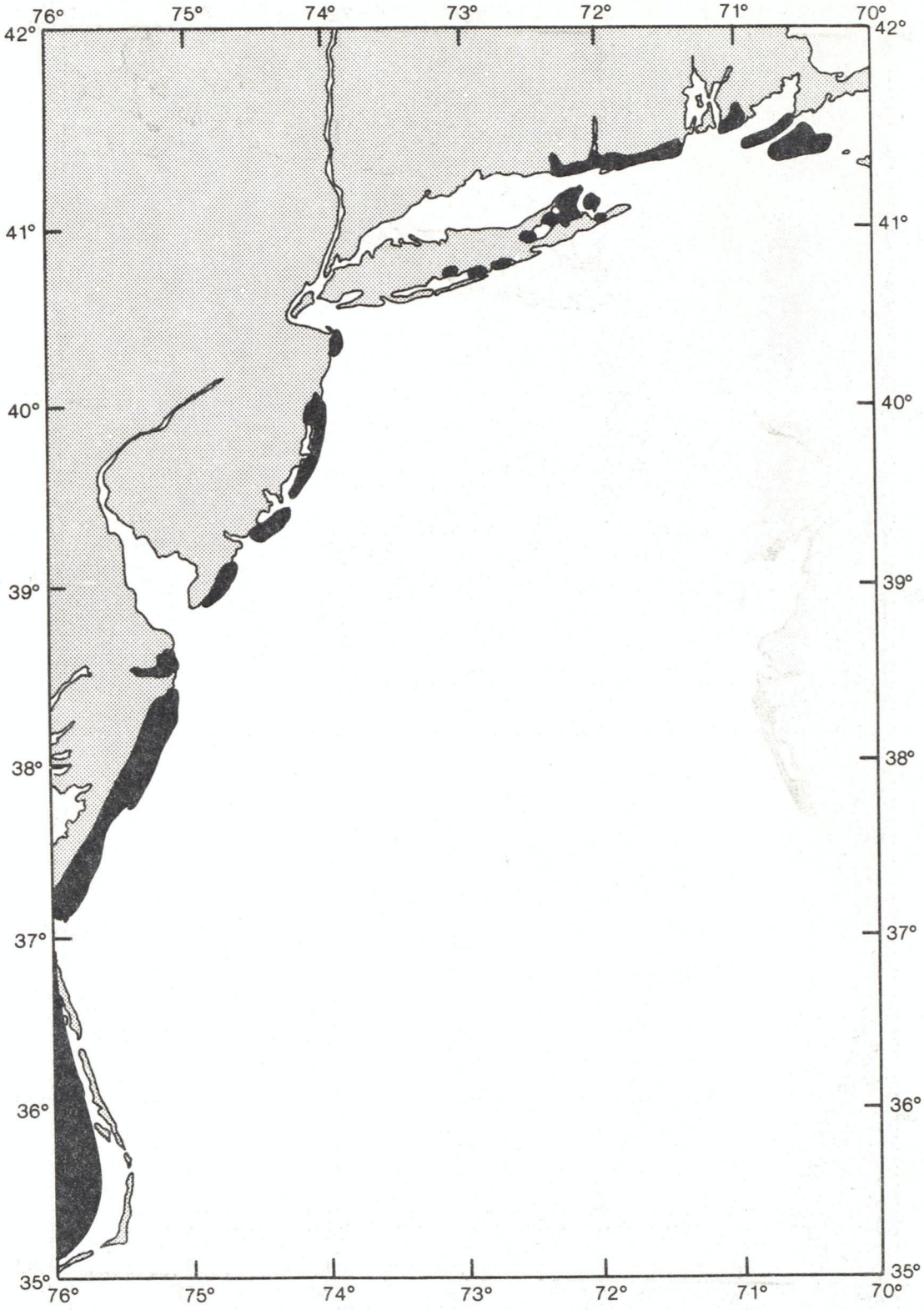

Figure 88.--Natural resource chart for osprey (after Slack and Wyant, 1978)

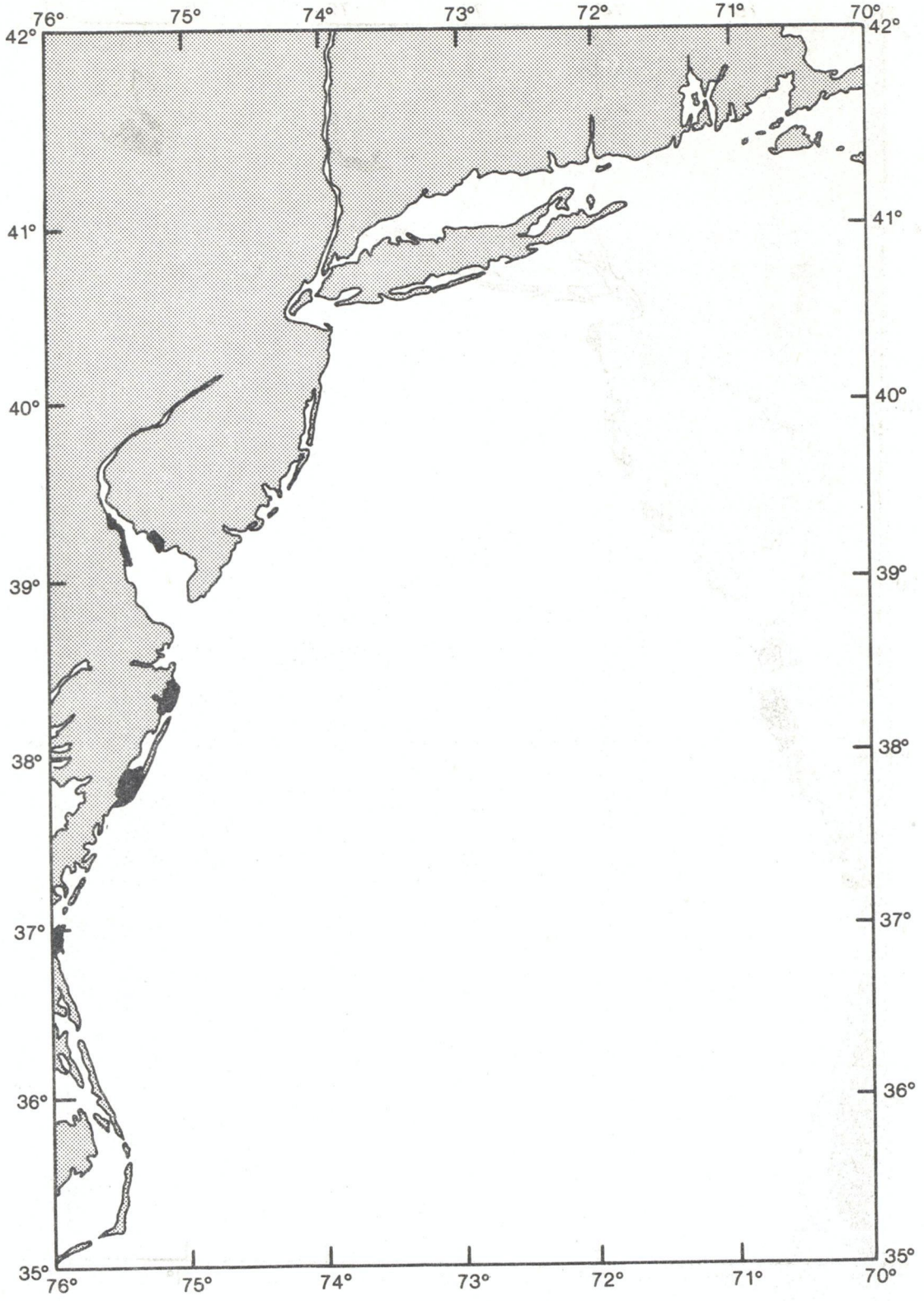

Figure 89.--Natural resource chart for the bald eagle (after Slack and Wyant, 1978)

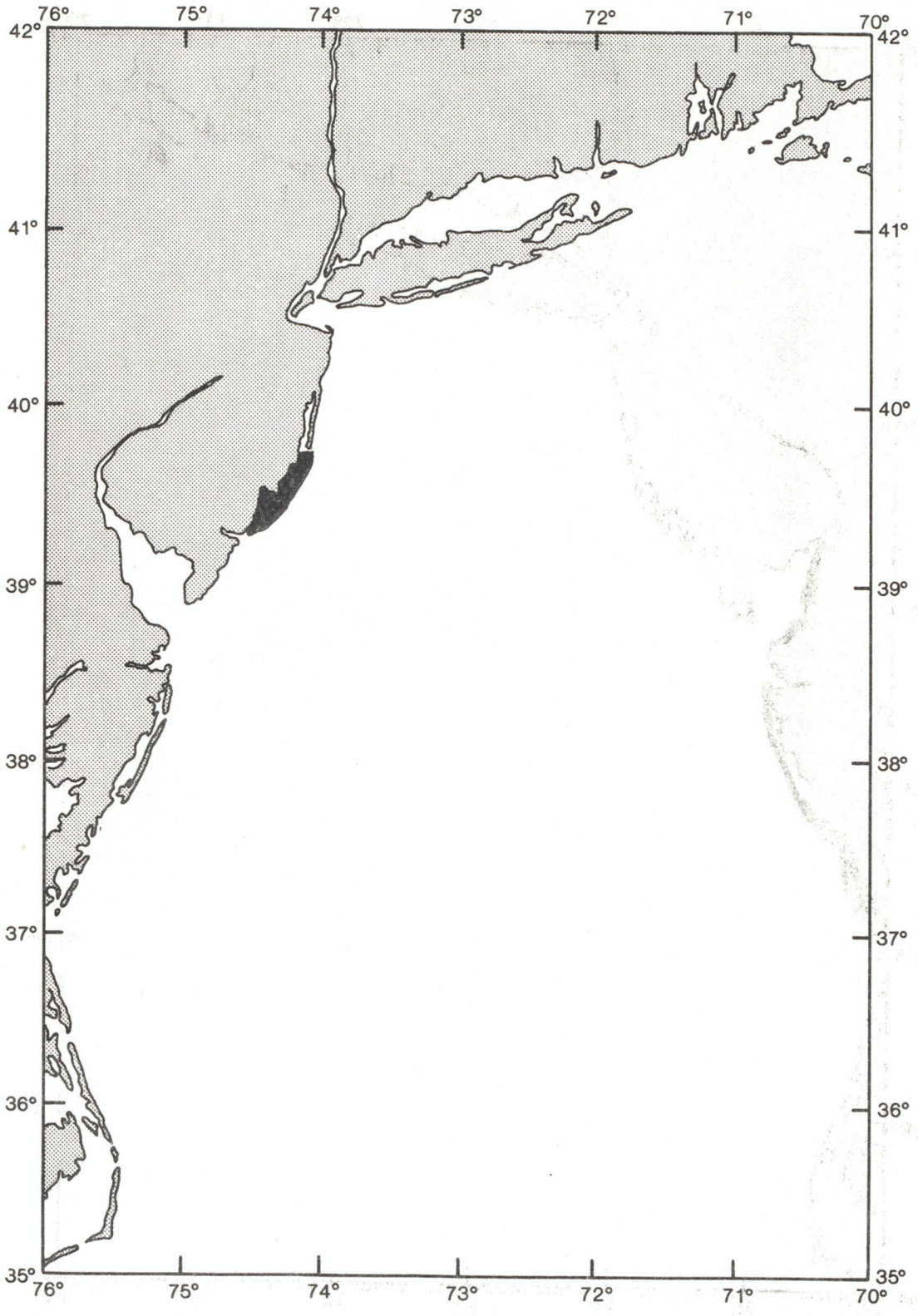

Figure 90.--Natural resource chart for peregrine falcon nesting areas (after Slack and Wyant, 1978)

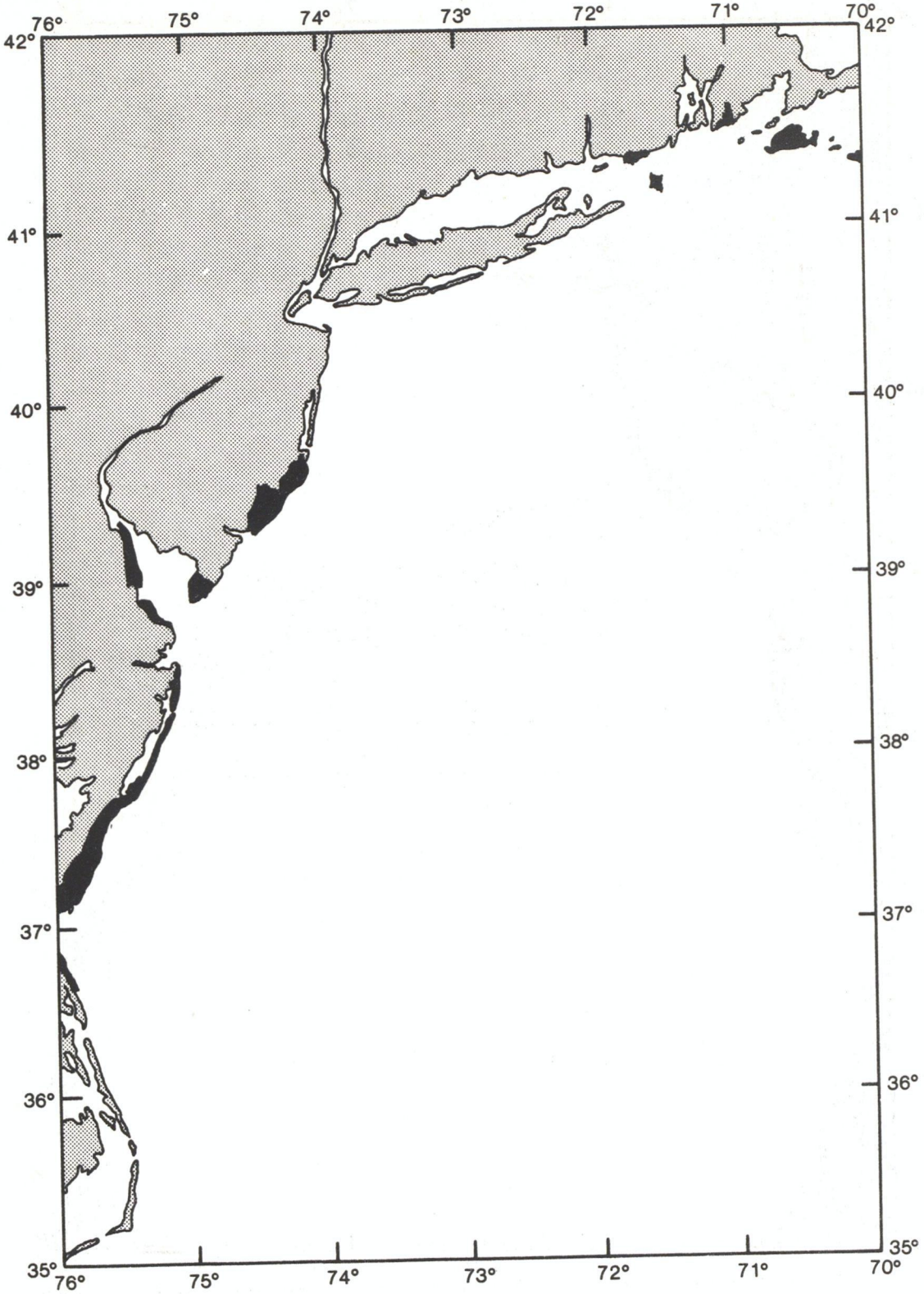

Figure 91.--Natural resource chart for peregrine falcon migratory points (after Slack and Wyant, 1978)

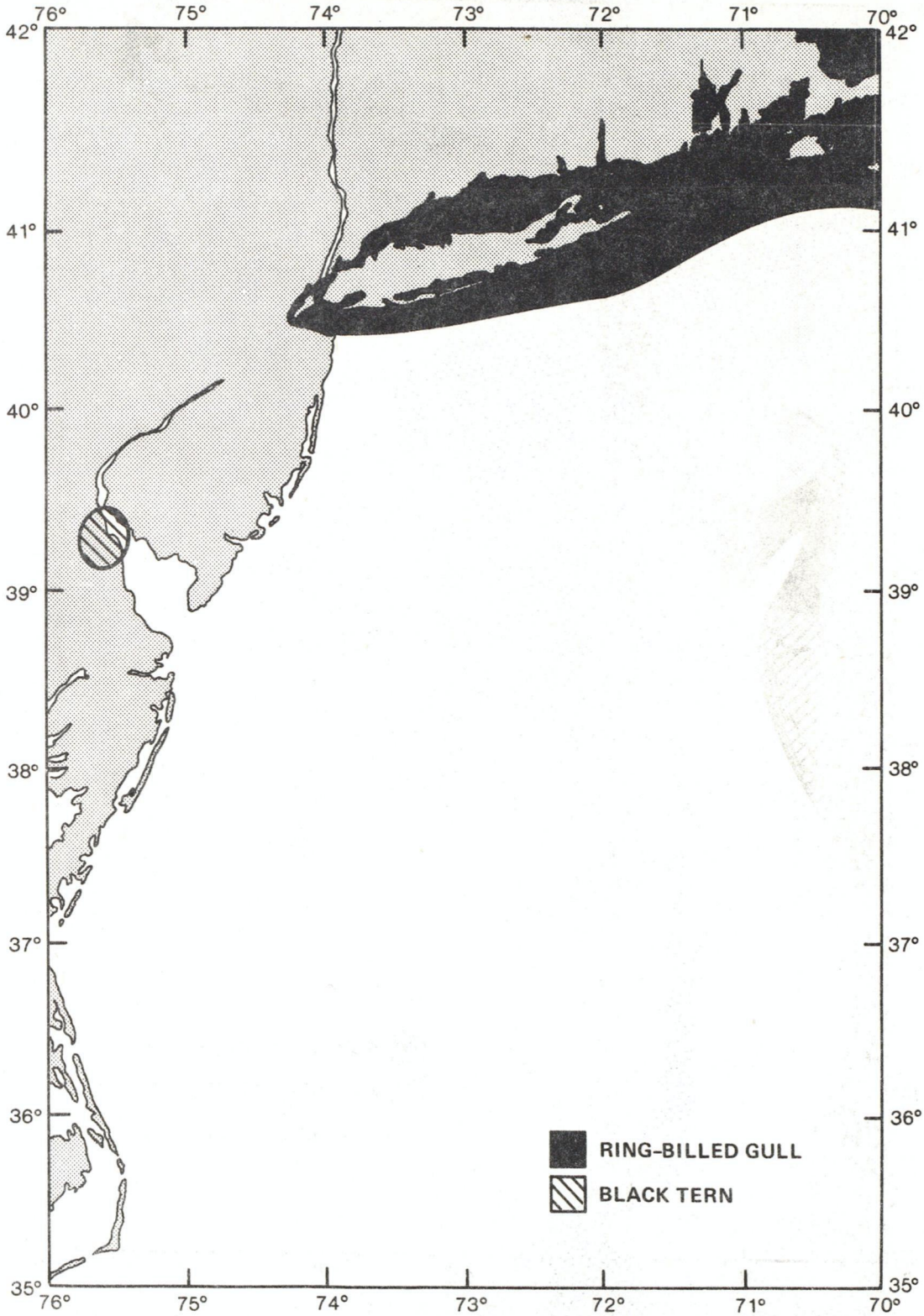

Figure 92.--Natural resource chart for birds with limited distribution (after Marine Experimental Station, U.R.I., 1973)

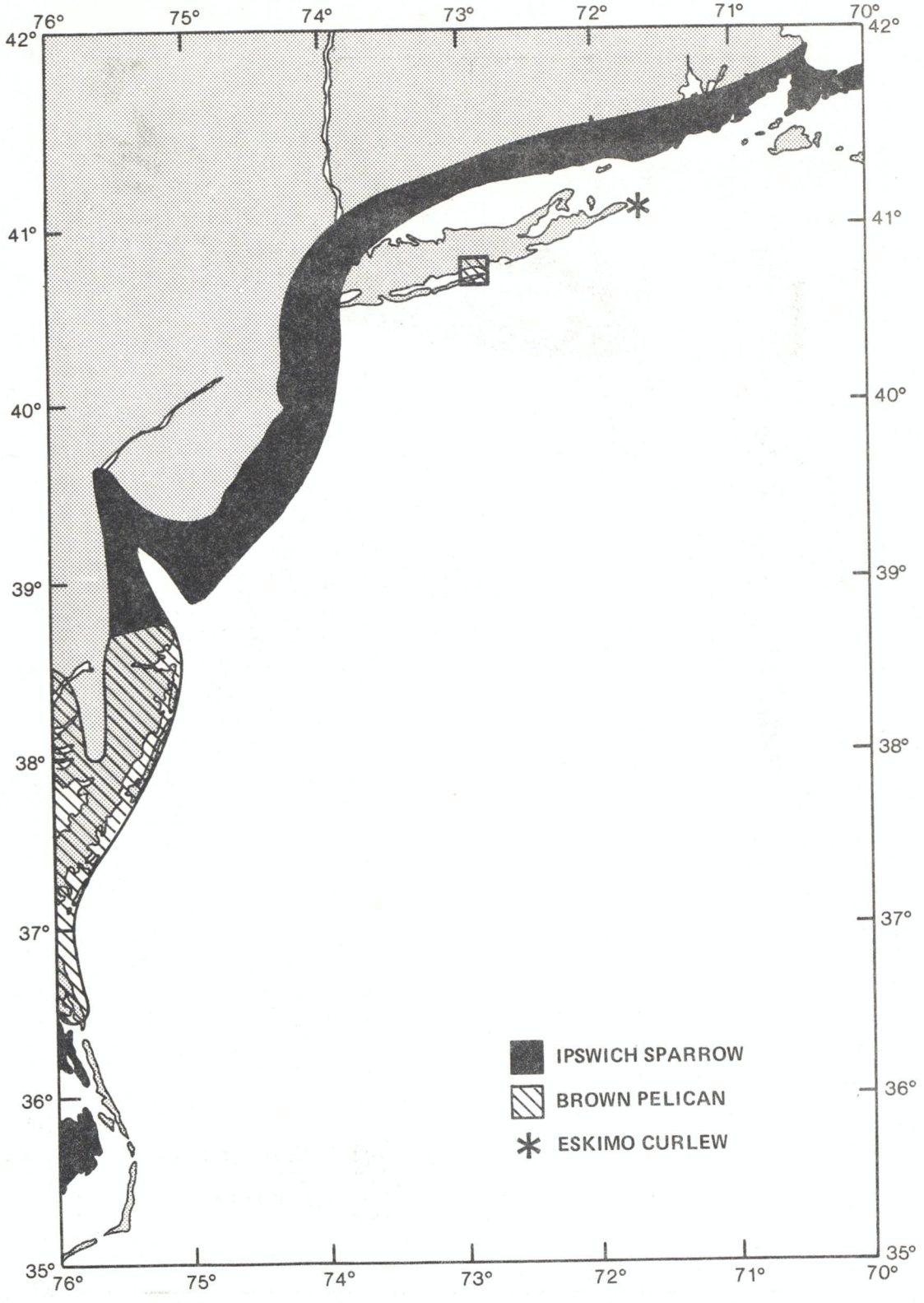

Figure 93.--Natural resource chart for birds with limited distribution (after Marine Experimental Station, U.R.I., 1973)

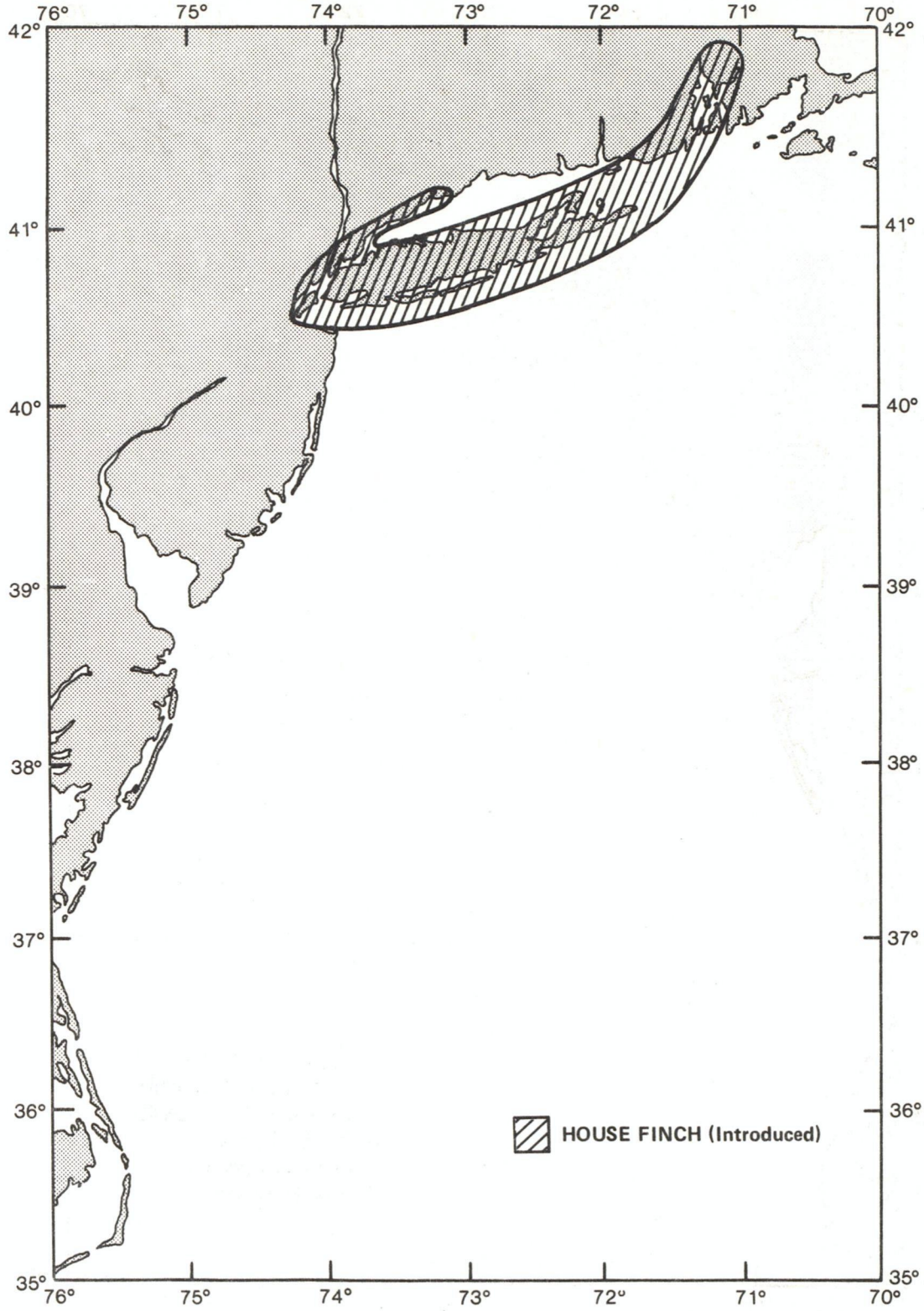

Figure 94.--Natural resource chart for birds with limited breeding distribution (after Marine Experimental Station, U.R.I., 1973)

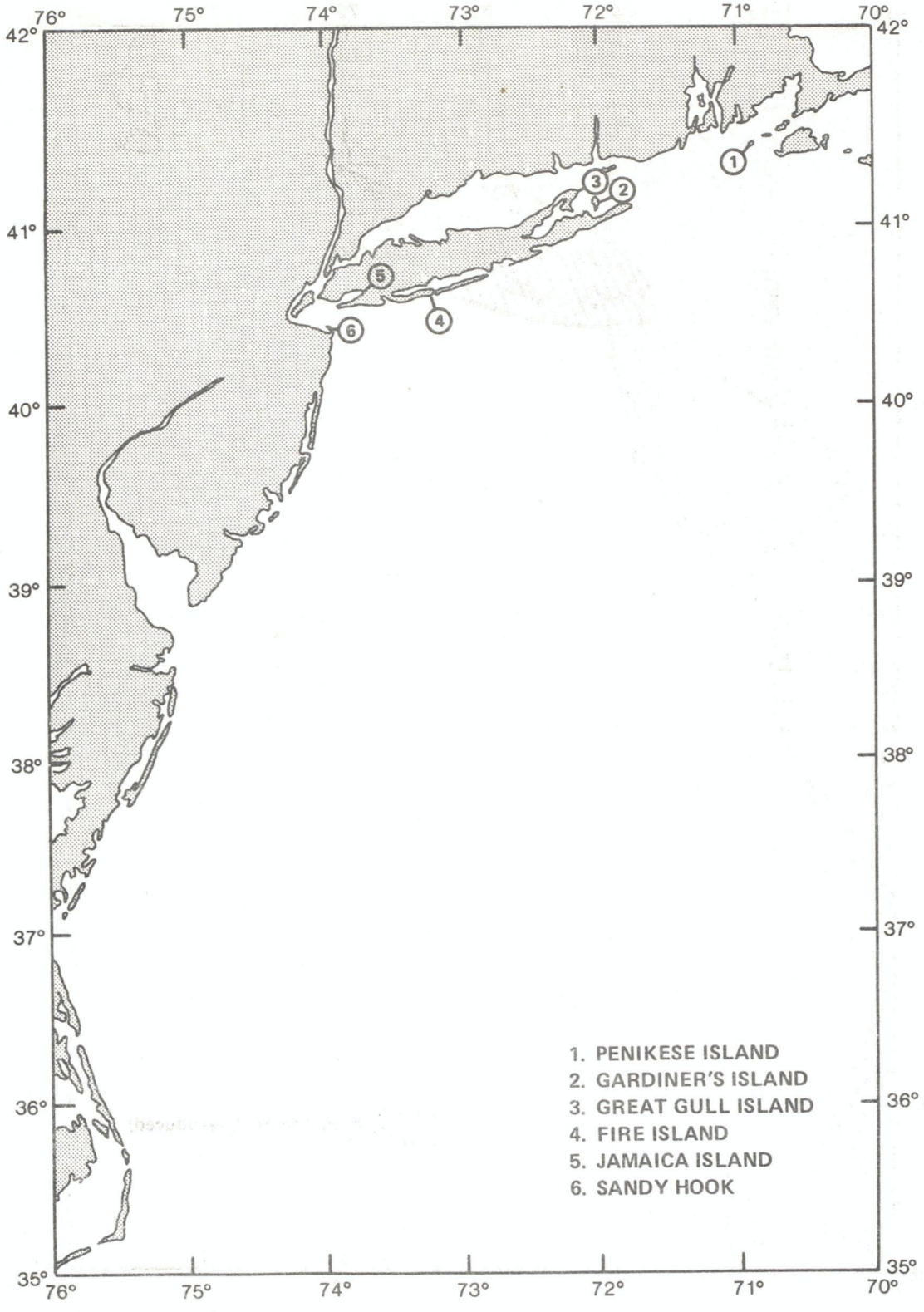

Figure 95.--Natural resource chart showing selected major breeding areas (after Marine Experimental Station, U.R.I., 1973)

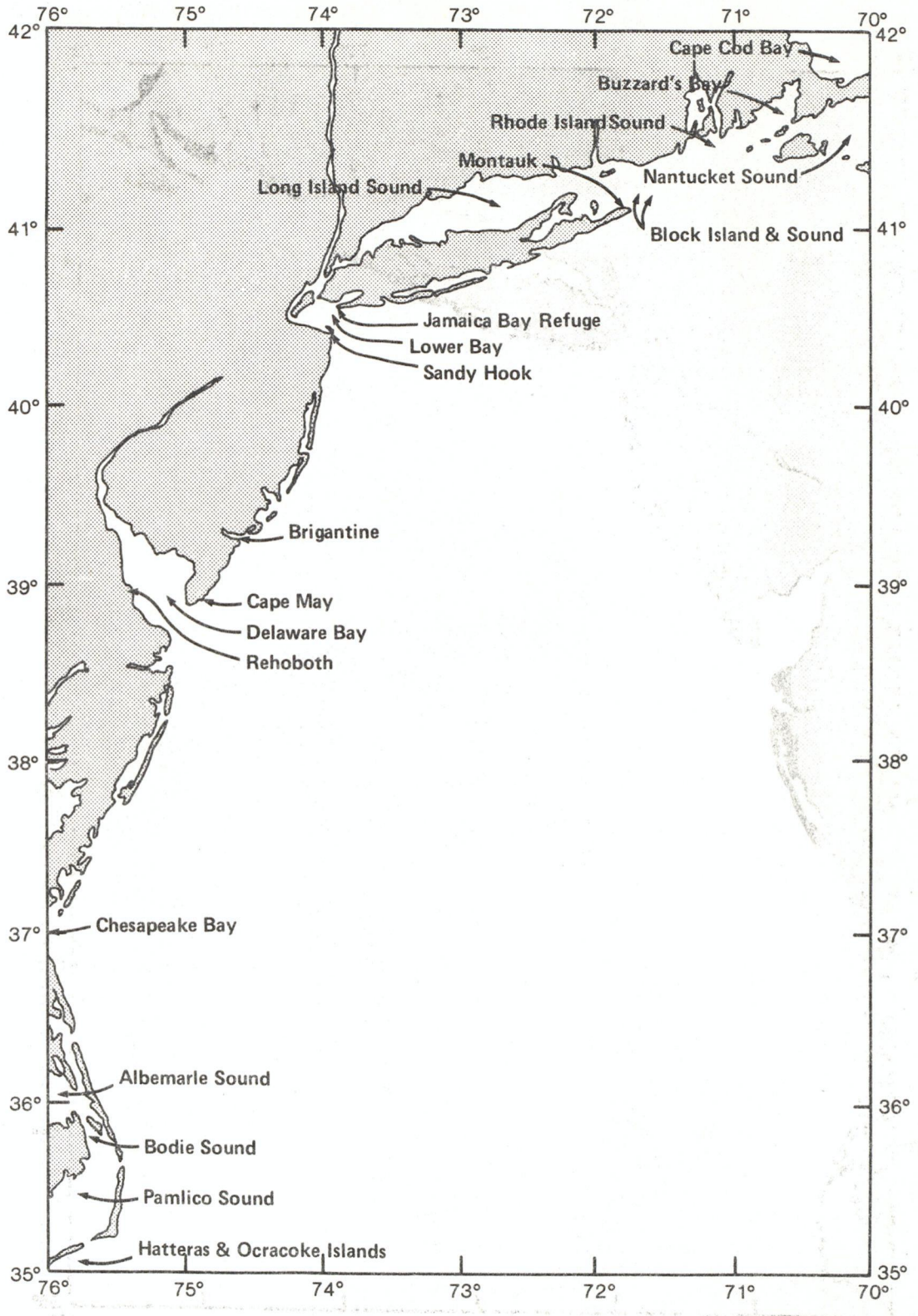

Figure 96.--Natural resource chart showing migration points (after Marine Experimental Station, U.R.I., 1973)

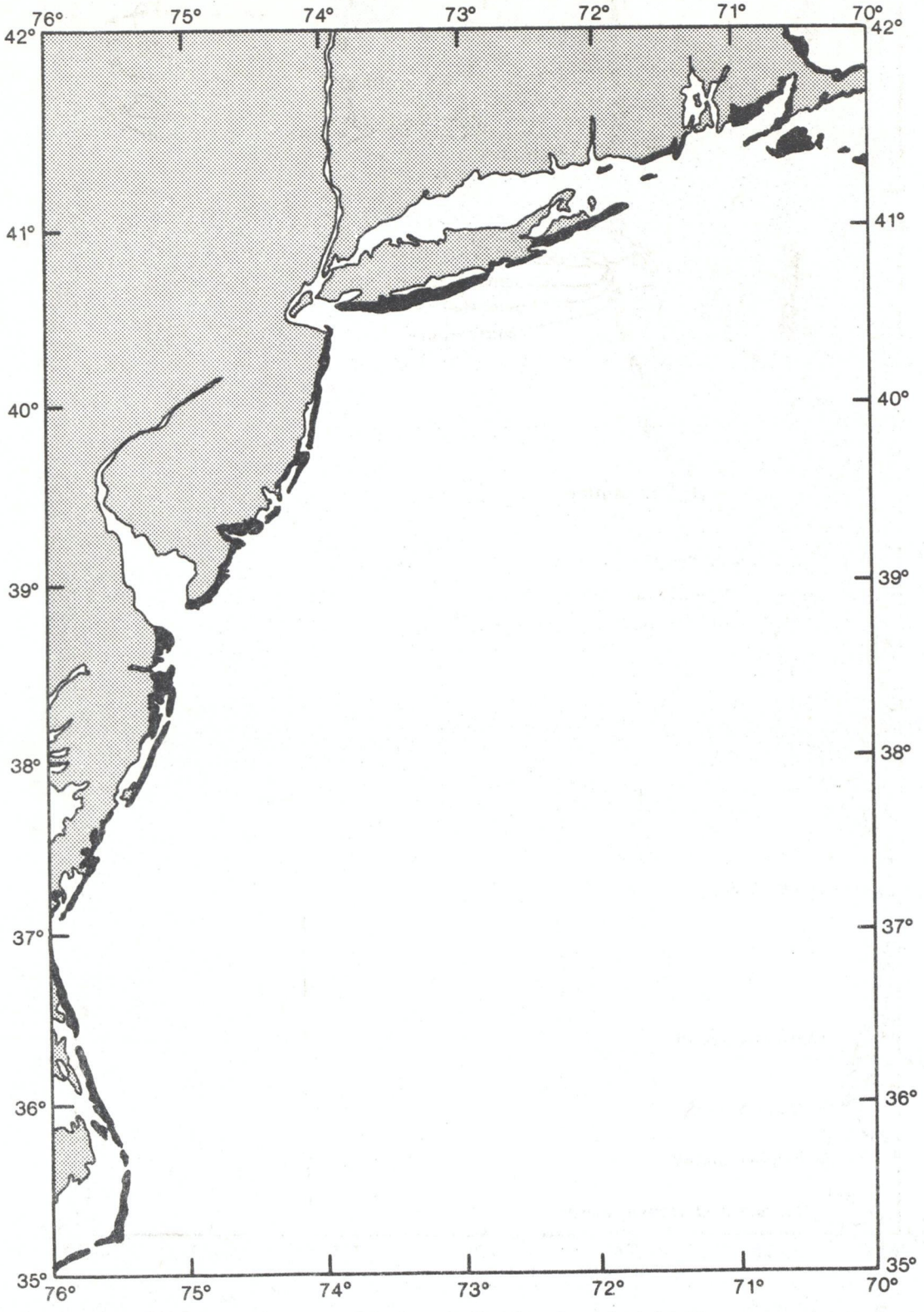

Figure 97.--Natural resource chart for sandy beaches (after Slack and Wyant, 1978)

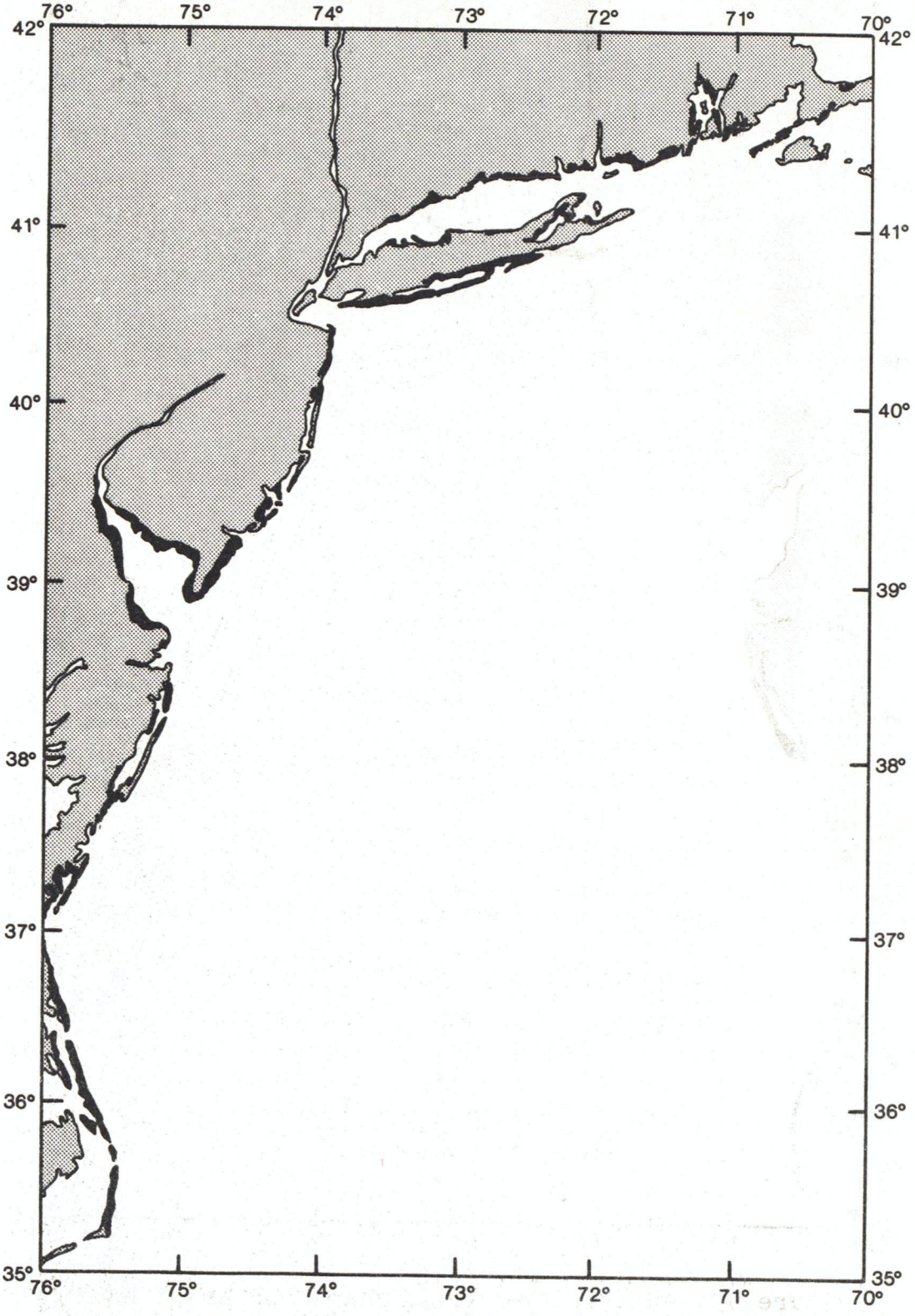

Figure 98.--Natural resource chart for coastal marshes (after Slack and Wyant, 1978)

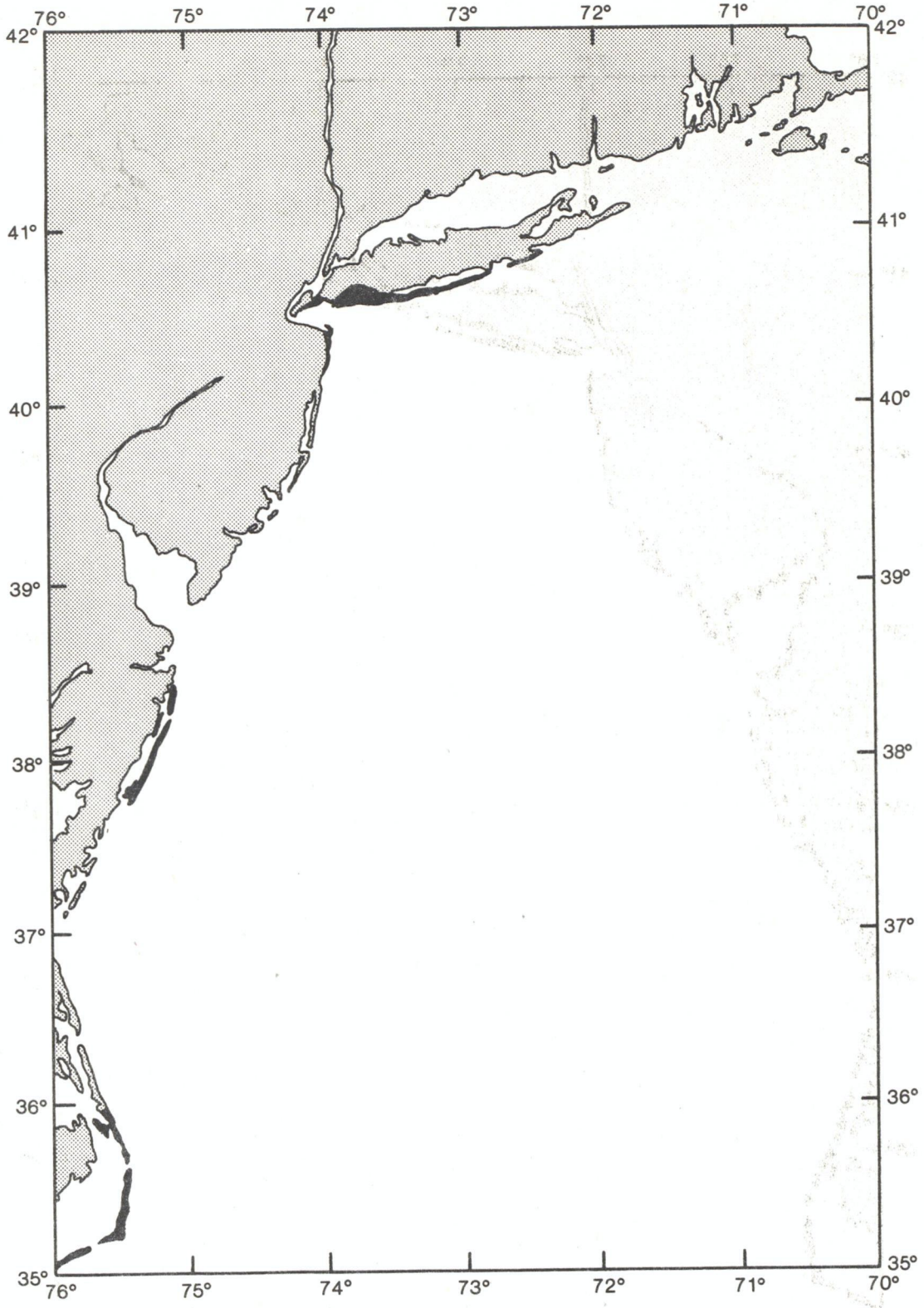

Figure 99.--Natural resource chart for areal extent of national parks, seashores, and recreation areas (after Slack and Wyant, 1978)

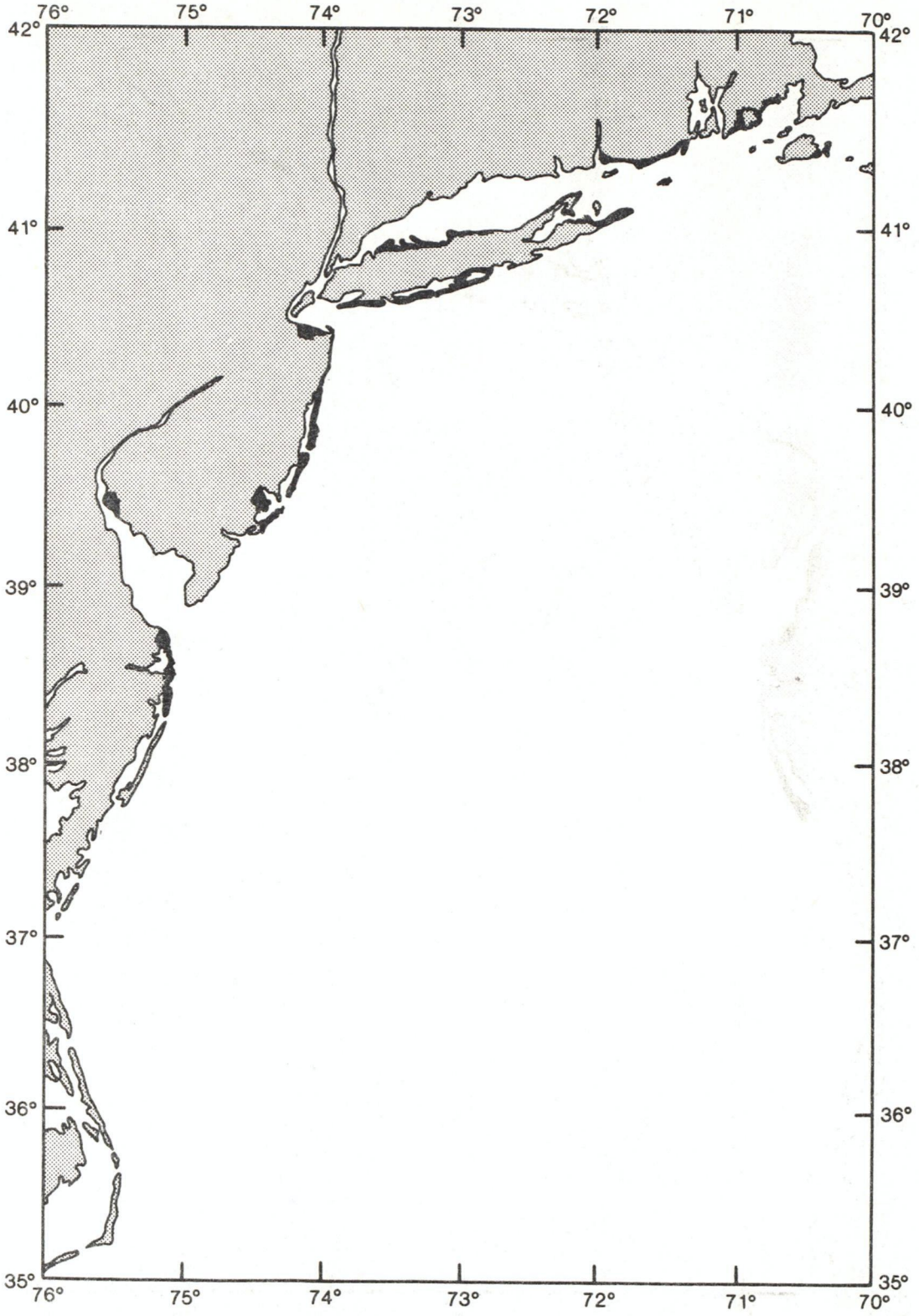

Figure 100.--Natural resource chart for areal extent of local and state parks and seashores (after Slack and Wyant, 1978)

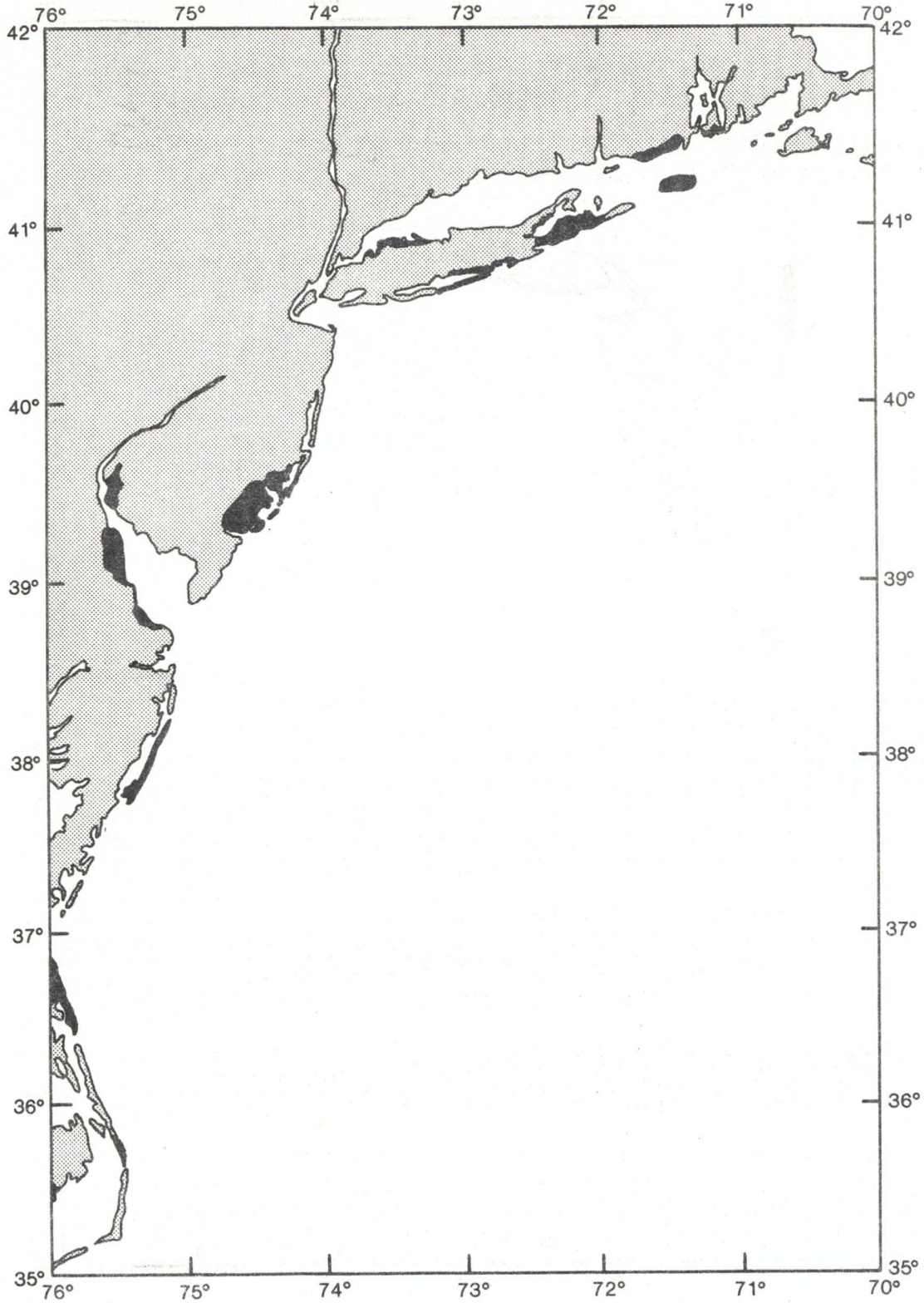

Figure 101.--Natural resource chart for areal extent of national wildlife refuges (after Slack and Wyant, 1978).

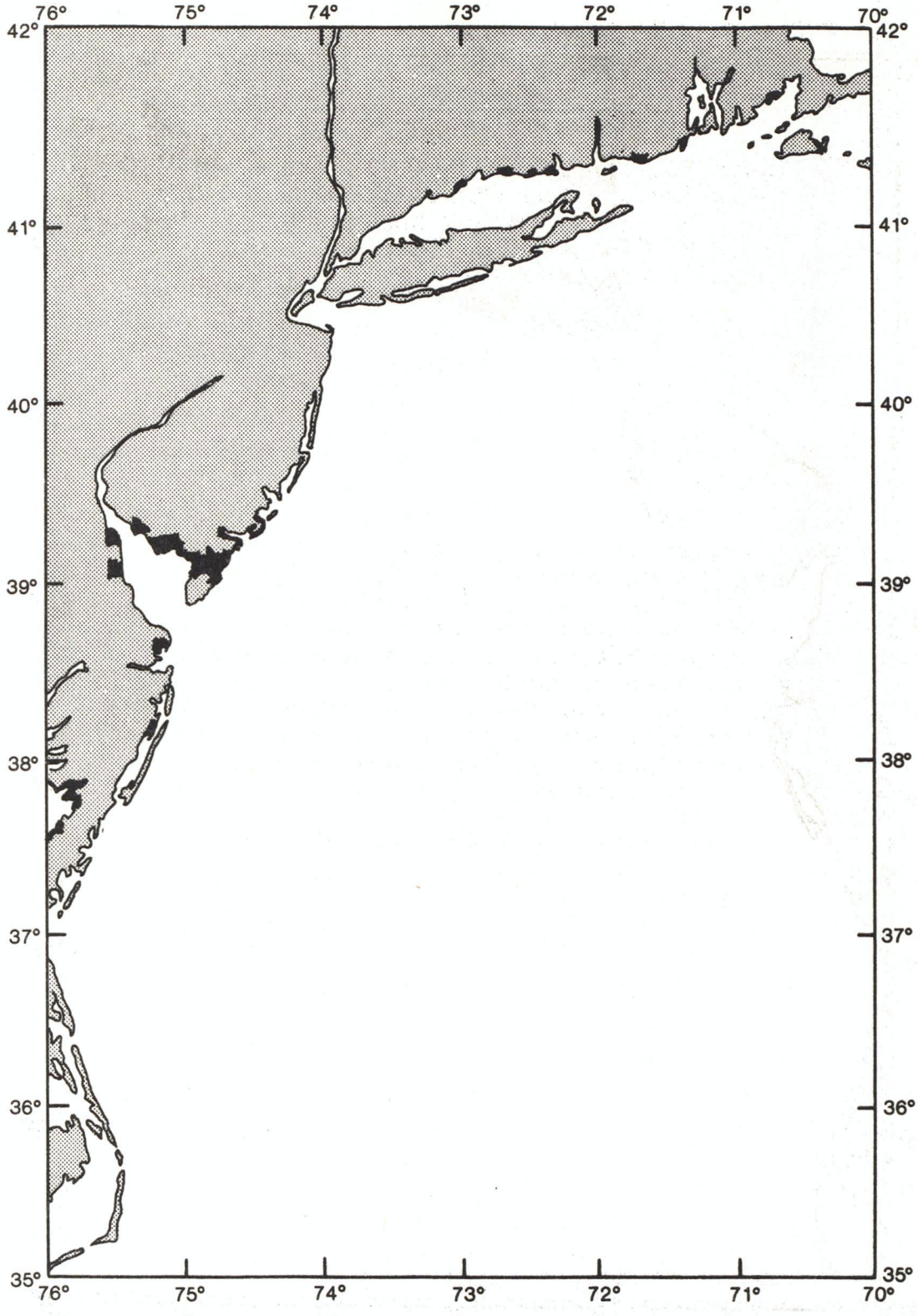

Figure 102.--Natural resource chart for areal extent of state wildlife and natural areas (after Slack and Wyant, 1978)

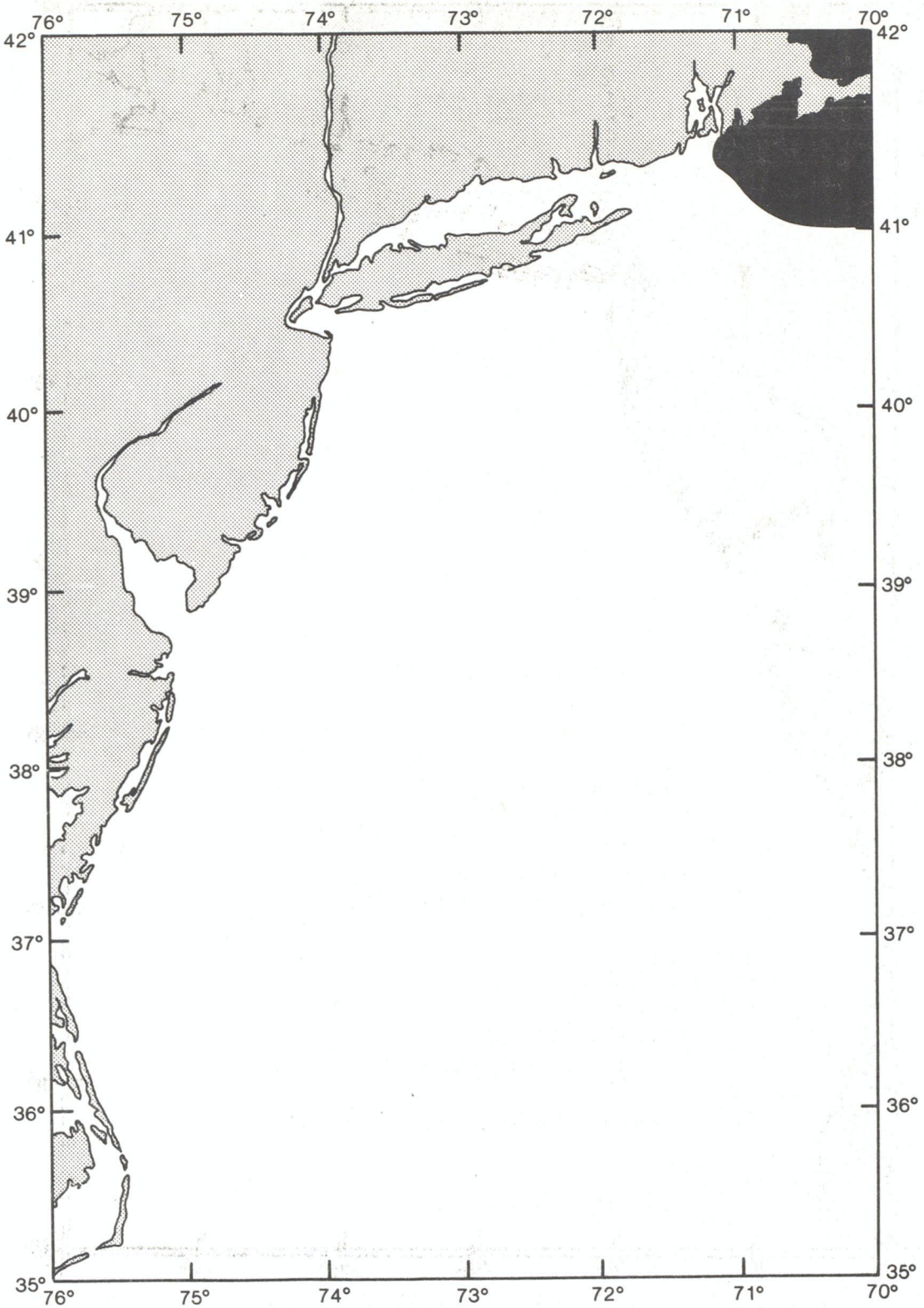

Figure 103.--Natural resource chart for areal extent of state marine sanctuaries (after Slack and Wyant, 1978)

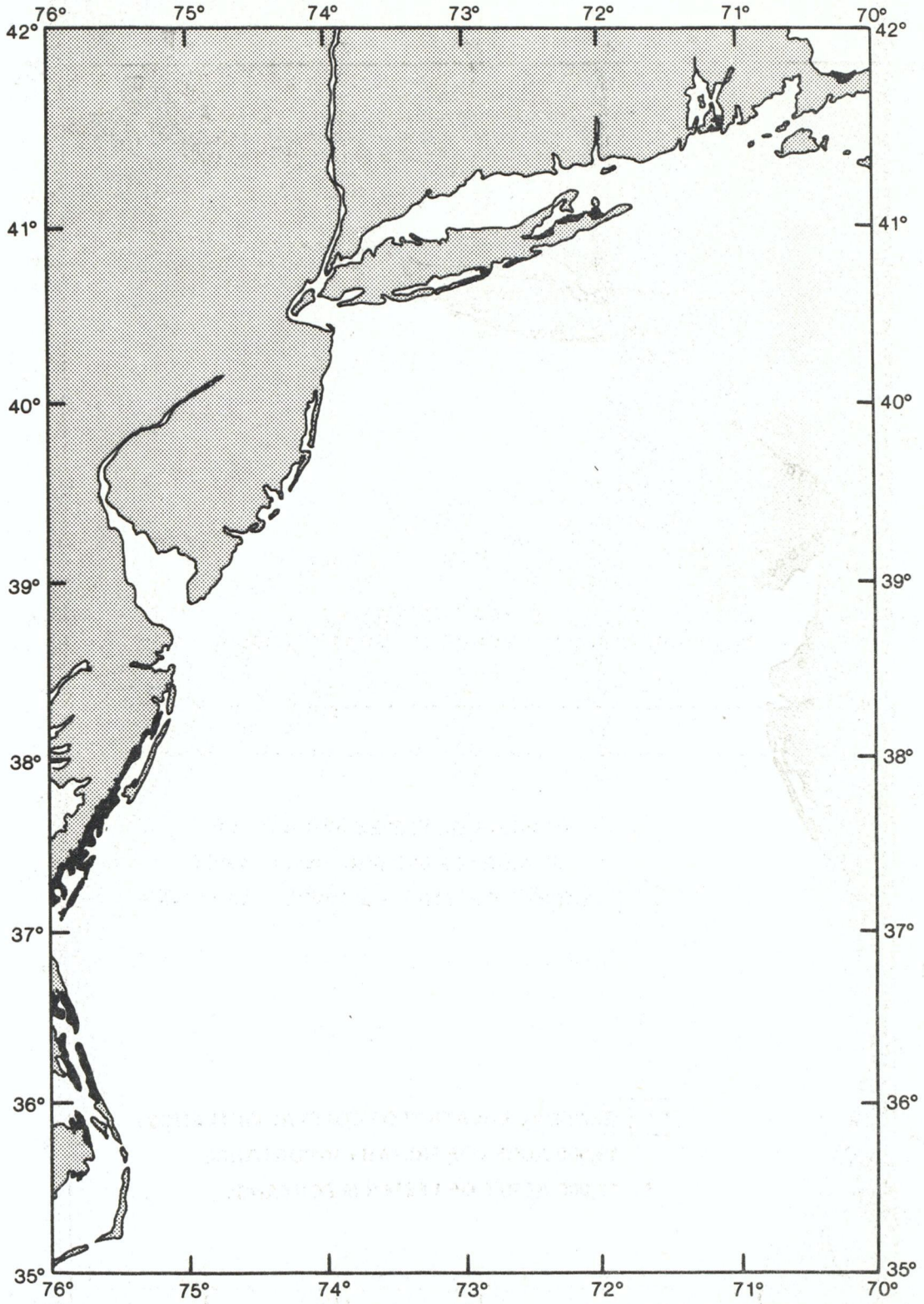

Figure 104.--Natural resource chart for areal extent of nongovernment wildlife and natural areas (after Slack and Wyant, 1978)

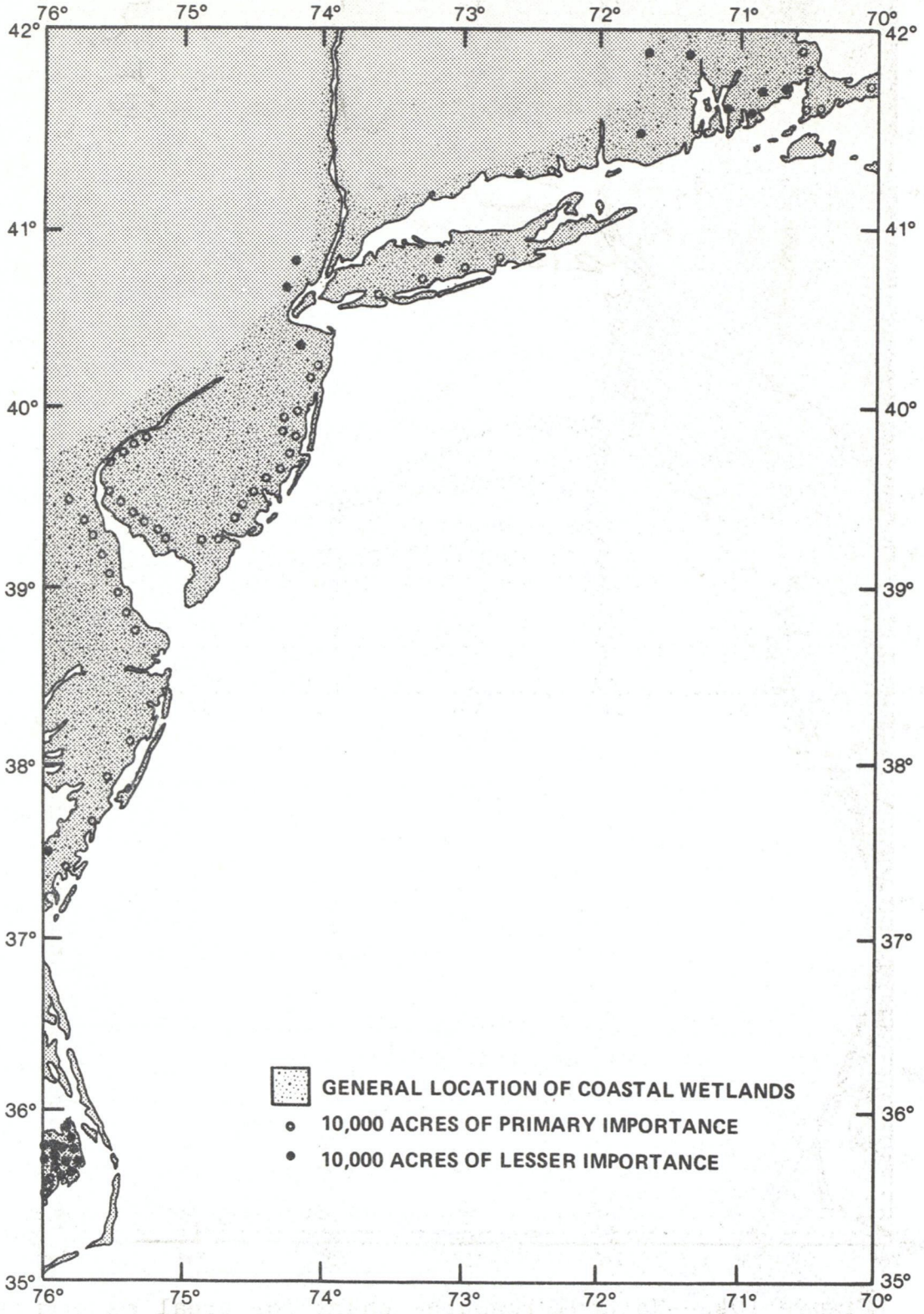

Figure 105.--Natural resource chart for wetlands (after Gusey, 1976)

4. DATA AND SUPPORT FOR ACTUAL SPILLS OR OIL SPILL PLANNING (NOAA)

a. Climatological Modeling
Chief, Marine Environmental Assessment Division
NOAA/EDIS/CEAS, D23
3300 Whitehaven St., N.W.
Washington, D.C. 20235
202/634-7381

b. Oceanographic Data Archives
Director, National Oceanographic Data Center
NOAA/EDIS/NODC, D7
2001 Wisconsin Avenue, N.W.
Washington, D.C. 20235
202/634-7232

c. Meteorological Data Archives
Director, National Climatic Center
NOAA/EDIS/NCC, D5
Federal Bldg.
Asheville, NC 28801
704/258-2850

d. Operational Marine Forecasts (including oil spills)
Director, Techniques Development Lab.
NOAA/NWS/TDL, W42
Gramax Building
8060 13th Street
Silver Spring, MD 20910
301/427-7613

e. Single Event Modeling, Advice and Forecasts
Chief, Oil Spill Scientific Support Team
7600 Sand Point Way, NE
Building 264 SW
Seattle, Washington 98115
(FTS) 399-5919

f. Marine Ocean Forecasts
Chief, Ocean Services Division
Gramax Building
8060 13th Street
Silver Spring, MD 20910
301/427-7778

5. ACKNOWLEDGEMENT

This report was conceived and written by Joseph M. Bishop, staff oceanographer, Marine Environmental Assessment Division Mr. Edward Ridley, Division Chief, Center for Environmental Assessment Services Dr. Kenneth Hadeen, Deputy Director, EDIS/NOAA. Thanks goes to Donna Harrigan for her detailed editing and technical assistance. The report was reviewed for technical merit by Dr. Dave Amstutz of the Department of Interior, Lt. Cdr. W. F. Holt U.S. Coast Guard, Drs. Dean Parsons and Neeland McNaulty of the National Marine Fisheries Service (NOAA) and Dr. Kurt Hess National Weather Service (NOAA).

6. REFERENCES

Amos, A. F., "The New York Bigh & Hydson Canyon in October 1974: Hydrography, Nepholometry, Bottom Photography, Currents, VEMA Cruise 32 Leg 1 Data," Prepared for the United States Energy Research and Development Administration under contract No. E (11-1)-2185, Lamont-Doherty Geological Observatory. Palisades New York, 1976, 192 pp.

Bearsley, R. C. & B. Butman, "Circulation on the New England Continental Shelf: Response to strong winter storms." Geophysical Research Letters, Vol 1 No. 4 1974 pp. 181-184.

Beardsley, R. C. & C. N. Flagg, "The Water Structure, Mean Currents, and Shelf-Water-Slope-Water Front on the New England Continental Shelf." Memoires de la Societe Royale des Sciences de Liege. Continental shelf dynamics, Seventh Liege Cologuium on Ocean Hydrodynamics, University of Liege, May 5-9, 1976, J. C. J. Nihoul, Ed., Siege de la societe: Universite Liege, Belgium, 1976, pp. 209-225.

Beardsley, R. C., W. C. Boicourt, and D. V. Hanson, "Physical Oceanography of the Middle Atlantic Bight," Proceedings of the Symposium, American Museum of Natural History, New York City, 3, 4, 5 November 1975, Special Symposia, Vol.2, M. Grant Gross, Ed., American Society of limnology and oceanogrpahy, Inc. Allen Press, Lawrence, Kansas, 1976, pp. 20-34.

Bisagn J. J., "Passage of Anticyclonic Gulf Stream Eddies through Deepwater Dumpsite 106 during 1974 and 1975," NOAA Dumpsite Evaluation Report 76-1, National Oceanic and Atmospheric Administration, U.S. Department of Commerce Washington, D.C. 1976, 39 pp.

Bishop, J., Surface Currents in the New York Bight as Related to a Simple Oil Trajectory Model. Conference of Coastal Meteorological Society, 1976.

Blumberg, Alan F., George L. Mellor and Sydney Levitus, The Middle Atlantic Bight: A Climatological Atlas of Oceanographic Properties. Fort Hancock, N.J.: Marine Sciences Consortium, August 1977.

Boicourt, W. C. and P. W. Hacker, "Circulation on the Atlantic Continental Shelf of the United States, Cape May to Cape Hatteras," Memoires de la Societe Royale de Sciences deliege, Vol. X. Continental Shelf Dynamics, Seventh Liege Coloquium on Ocean Hydrodynamics, University of Liege, May 5-9, 1975, J.C.S. Nihoul, Ed. Siege de la Societe, Universite Liege, Belgium, 1976 pp. 187-200.

Bowden, K. F., "Turbulence," Sec. VI, The Sea, M.N. Hill, Ed. Vol. I. Physical Oceanography, New York: Interscience Publishers, 1962 pp. 802-817.

Bowman, Malcolm J. and Lewis D. Wunderlick, Hydrographic Properties: MESA New York Bight Atlas, Monograph I. Albany N.Y.: New York Sea Grant Institute, February 1977.

Bumpus, D. F. and L. M. Lauzier, "Surface Circulation on the Continental Shelf Off Eastern North America Between New Foundland and Florida," Serial Atlas of the Marine Environment Folio 7. New York: American Geographical Society, 1965 pp. 4.

Christodoulou, George C., Jerome J. Connor, and Bryan R. Pearce, "Mathematical Modeling of Dispersion in Stratified Waters," Report No. MIT SC 76-14 Cambridge, Massachusetts: MIT Sea Grant Program, Massachusetts Institute of Technology, 1976 308 pp.

Fay, J., "The Spread of Oil Slicks on a Calm Sea," Oil on the Sea Hoult, D.P., Ed. New York: Plenum Press, 1969 pp. 53-63.

Goldsmith, V., W. D. Morris, R. J. Byrne, and C. H. Whitlock, "Wave Climate Model of the Mid-Atlantic Shelf and Shoreline (Virginia Sea), "NASA SP-358, Washington D.C.: National Aeronautics and Space Administration, 1974 144 pp.

Gusey, William F., The Fish and Wildlife Resources of the Middle Atlantic Bight. Houston, Texas: Shell Oil Company, January 1976.

Gutman, A. L., "Delineation of a Wave Climate for Dam Neck, Virginia Beach, Virginia" Special Report in Applied Marine Science and Ocean Engineering, No. 125. Gloucester Point, Virginia: Virginia Institute of Marine Science, 1976. 38 pp.

Hardy, C., G. Baylor, and P. Moskowitz, Sea Surface Circulation in the Northwest Apex of the New York Bight. Boulder, Colorado: Marine Ecosystems Analysis Program TM ERL MESA-13, 1976.

Harris, D. L., "Characteristics of Wave Records in the Coastal Zone," Waves on Beaches Meyer, C, Ed. New York: Academic Press, 1972.

Hennemuth, Richard C., Fisheries and Renewable Resources of the Northwest Atlantic Shelf, Woods Hole Ma: Northwest Fisheries Center, National Marine Fisheries Service, 1976.

Hesselbert, T., and H. U. Sverdrup, Die Stabilitat Sverhaltnisse bie Vertikalen Verschle bungen in der Atmosphare und in Meer" Bergens Museums Aarbok Nos. 14 and 15, Bergen, Norway: 1914.

Kinsman, G., Windwaves: Their Generation and Propagation at the Ocean Surface, Englewood Cliffs, New Jersey: Prentice-Hall, 1965.

Kolpack, Ronald L., and Noel B. Plutchak, "Elements of Mass Balance Relationships for Oil Released in the Marine Environment," Sources, Effects and Sinks of Hydrocarbons in the Aquatic Environment: Proceedings of the Symposium. American University Washington D.C. 9-11 August 1976 The American Institute of Biological Sciences, 1976.

Lettau, Bernhard, William A. Brower, Jr. and Robert G. Quayle, Marine Climatology: MESA New York Bight Atlas, Monography 7, Albany, New York: New York Sea Grant Institute, December, 1976.

Marine Experiment Station, University of Rhode Island, Coastal and Offshore Environmental Inventory: Cape Hatteras to Nantucket Shoals, Kingston R.I.: University of Rhode Island, 1973.

Marine Experiment Station, University of Rhode Island, Coastal and Offshore Environmental Inventory: Cape Hatteras to Nantucket Shoals, Complement Volume, Kingston R.I.: University of Rhode Island, 1974.

Naval Weather Service Detachment, Asheville North Carolina, Climatic Study of the Near Coastal Zone: East Coast of the United States, Asheville N.C.: Director, Naval Oceanography and Meteorology, June, 1976.

Neumann, G., and W. J. Pierson, Principles of Physical Oceanography Englewood Cliffs, New Jersey: Prentice-Hall, 1966.

Norcross, J. J., and E. M. Stanley, "Inferred Surface and Bottom Drift, June 1973 through October 1974" in "Circulation of Shelf Waters Off Chesapeake Bight," Professional Papers No. 3.

Environmental Science Services Administration Ed. Washington D.C. U.S. Department of Commerce, 1967 pp. 11-42.

Officer, Charles B., Physical Oceanography of Estuaries (and Associated Coastal Waters) New York: John Wiley & Sons, 1976.

Okubo, A., A Review of Theoretical Models of Turbulent Diffusion in the Sea TR 30 Maryland: Chesapeake Bay Institute Johns Hopkins University, 1962.

Pierson, W. J., "Visual Wave Observations," Miscellaneous Publication No. 5921, Washington D.C.: U.S. Navy Hydrographic Office, 1956.

Quayle, R. G., "A Climatic Comparison of Ocean Weather Stations and Transient Ship Records," Mariners' Weather Log, Vol. 18 No. 5 pp. 307-311.

Research Institute of the Gulf of Maine, the (TRIGOM) A Socio-Economic and Environmental Inventory of the North Atlantic Region: Sandy Hook to Bay of Fundy. Submitted to Bureau of Land Management (08550-CT3-8) South Portland, Maine; TRIGOM, November, 1974.

Saville Jr., T., "North Atlantic Coast Wave Statistics Hindcast by Bretshneider-Revised Sverdrup-Munk Method," Technical Memorandum NO. 55, Beach Erosion Board, Office of the Chief of Engineers, Department of the Army, Washington D.C.: Department of the Army, 1955.

Scott, J. T., and G. Csanady, "Near-Shore Currents Off Long Island," Journal of Geophysical Research, Vol. 81, 1976 pp. 181-184.

Shaw, Samual P. and G. C. Fredine, "Wetlands of the United States, Their Extent and Their Value to Water Fowl and Other Wildlife," Circular 39 Fish and Wildlife Service, Washington D.C.: U.S. Department of the Interior, 1956 (1971).

Shonting, D. H. "Rhode Island Sound Square Kilometer Study, 1967: Flow Patterns and Kinetic Energy Distribution," Journal of Geophysical Research. Vol. 74 No. 13, 1969 pp. 3386-3395.

Slack, James R. and Timothy Wyant, An Oil Spill Risk Analysis for the Mid-Atlantic (proposed sale 49) Outer Continental Shelf Lease Area. Reston, Virginia: U.S. Geological Survey, Water Resource Investigations 78-76, 1978.

Smith, Richard A., James R. Slack and Robert K. Davis. An Oil Spill Risk Analysis for the North Atlantic Outer Continental Shelf Lease Area. Reston Virginia: U.S. Geological Survey, 1976.

Stolzenback, K., O. Madsen, E. Adams, A. Pollack, and C. Cooper, "A Review and Evaluation of Basic Techniques for Predicting the Behavior of Surface Oil Slicks," Massachusetts Institute of Technology Department of Civil Engineering Report No. 222 Cambridge Ma.: Massachusetts Institute of Technology, 1977.

U.S. Department of Commerce, Marine Surface Observations," Weather Service Observing Handbook No.1. Silver Spring Md.: 1974.

Voorhis, A. D., D. C. Webb, and R. C. Millard, "Current Structure and Mixing in the Shelf Slope Water Front South of New England" Journal of Geophysical Research Vol. 81 No. 21, 1976 pp. 3695-3708.

Williams, Robert and Fred A. Godshall, Summarization and Interpretation of Historical Physical Oceanographic and Meteorological information for the Mid-Atlantic Region. Final Report to the Bureau of Land Management (AA 550-IAC-12) Washington D.C.: U.S. Department of Commerce NOAA/EDIS, 1976.

*U.S. GOVERNMENT PRINTING OFFICE: 1980 311-046/386 1-3

NOAA--S/T 79-294